Isolation, Characterization and Synthesis of a Phenyl-substituted Pyrrole Isolated from the Flavonoid Fraction of Mānuka Honey

A thesis submitted in partial fulfilment of

the requirements for the degree

of

Master of Science in Chemistry

at

The University of Waikato

by

Ching Wan Chan

THE UNIVERSITY OF
WAIKATO
Te Whare Wānanga o Waikato

The University of Waikato

2011

Abstract

Compound **1**, which occurs in the flavonoid fraction of mānuka honey and showed a statistical correlation with the non-peroxide antibacterial activity of the honeys, was extracted from fifteen kilograms of mānuka honey using Amberlite XAD-2 resin and liquid-liquid extraction, and isolated by a combination of Sephadex-LH20 column chromatography and HPLC. Characterization of **1** was achieved by one and 2D- ^{1}H and ^{13}C NMR spectroscopy and GC-MS and **1** was identified as 2-formyl-5-(2-methoxyphenyl)-pyrrole.

In addition to **1**, two other non-flavonoids were isolated from the flavonoid fraction and their identities confirmed as caffeic acid and *p*-coumaric acid.

Synthesis of **9** (3-hydroxy-1-(2-methoxyphenyl)-3-(oxazol-4-yl) propan-1-one), an intermediate in the route to **1**, gave a yield of 67.5% as a pale yellow crystals after crystallization from CH_2Cl_2/hexane. Synthesis of **1** from **9** only resulted in barely traceable amount of **1**. The dominant product after recrystallization from CH_2Cl_2/hexane was **10** ((*E*)-1-(2-methoxyphenyl)-3-(oxazol-4-yl)prop-2-en-1-one) which was the dehydrated analogue of **9**.

The synthesis of **1** was repeated. The product mixture was fractionated on a silica gel column, followed by two cycles of preparative layer chromatography applied to the fractions which contained **1** and yield 0.36 mg of **1** (0.00179 mmol, 0.2%).

Acknowledgements

My heartfelt gratitude goes to my supervisor Prof. Alistair Wilkins, who provided me the training on GC-MS, NMR, the packing of silica gel column, and the application of the Chromatotron. Without his expertise experience and knowledge in NMR, I would not have been able to complete my research. My deepest gratitude and appreciation go to my other supervisor, Assoc. Prof. Merilyn Manley-Harris, who gave me the opportunity to work under her supervision and provided me all the necessary guidance that I needed to complete this research.

I should like to thank Prof. Brian Nicholson who guided me in the synthesis of the compound **1** using Schlenk techniques, and also Mrs. Pat Gread for acquiring HRMS data for me.

To Mr. Ben Deadman, who initiated this project by exploration of the flavonoids of mānuka honey so that I could take further steps and finish it with conclusive results.

Lastly I wish to thank my family for their endless support throughout the time that I have been in New Zealand

Table of contents

List of figures

List of tables

List of abbreviations

^{13}C	Carbon -13
1D	One dimensional
^{1}H	Proton
2D	Two dimensional
AGEs	Advanced glycation endproducts
ATP	Adenosine triphosphate
AU	Absorbance units
a_w	Water activity
C18	18 carbon chain
$CDCl_3$	Chloroform-d_1
cGMP	Cyclic guanosine monophosphate
COSY	Homonuclear correlated spectroscopy
d	Doublet
Da	Daltons
dd	Doublet of doublets
ddd	Doublet of doublets of doublets
DHA	Dihydroxyacetone
DIBALH	Diisobutylaluminium hydride
DMSO	Dimethyl sulfoxide
DMSO-d_6	Hexadeuteriodimethyl sulfoxide
DNA	Deoxyribonucleic acid
ECM	Extra cellular matrix
ESI-MS	Electrospray mass spectrometry
GC-MS	Gas chromatography with mass spectrometry
h-ALR2	Human Aldose Reductase
HIV	Human immunodeficiency virus
HMBC	Heteronuclear multiple bond coherence
HOD	Hydrogen deuterium oxide
HRMS	High resolution mass spectrometry
HSQC	Heteronuclear single quantum coherence
Hz	Hertz
J	Coupling constant

LDA	Lithium diisopropylamide
MCV	Molluscum contagiosum virus
MGO	Methylglyoxal
Mpt	Melting point
MRSR	Methicillin-resistant *Staphylococcus aureus*
MsCl	Methane sulphonyl chloride
msec	Millisecond
MΩcm	Mega Ohm centimetres
nmr	Nuclear magnetic resonance
R^2	Regression squared
RP18	Reversed phase with an 18 carbon chain
s	Singlet
SELNOESY	1D-selective Nuclear Overhauser effect spectroscopy
td	Triplet of doublets
THF	Tetrahydrofuran
TMS	Tetramethylsilane
UMF^{TM}	Unique mānuka factor
λ_{max}	Wavelength of maximum absorption

Introduction

1.1. Mānuka honey

Honey is a natural substance produced by honeybees. Nectar or honeydew is collected by honeybees and taken back to the hive, where it is processed into honey, which serves as a food for larvae.[1] The use of honey and production by humans can be traced back to 10,000 years ago.[2]

Mānuka honey is derived from the nectar of the mānuka tree (*Leptospermum scoparium*), a native of New Zealand. The flowers of the mānuka tree are generally white and 10 to 12 mm in diameter. Black, sooty mould may grow on the bark giving it a dark colouring as mānuka is often colonised by scale insects which feed off the phloem of the tree and excrete honeydew.[3] Honeybees have been observed harvesting this honeydew from scale insects on mānuka trees for the production of honey.[4]

1.2. Antibacterial properties of honey

Honey is used as a wound dressing because of its antibacterial activity against a large number of pathogenic bacteria and fungi.[5] Common wound infecting bacteria such as methicillin-resistant *Staphylococcus aureus* (MRSA), *Pseudomonas aeruginosa* and vancomycin-resistant enterococci bacterial strains show resistance to a range of antibiotics. However, clinical studies have found that honey, especially mānuka honey is very effective as an antibiotic against these resistant strains.[6]

Honey assists wound healing by creation of a physical barrier between the wound and outside sources of infection. Apart from this, hydrogen peroxide is released by the action of the enzyme glucose oxidase, which is present in honey, and which transforms glucose to gluconic acid. Low levels of hydrogen peroxide help to stimulate the growth of blood vessels (angiogenesis), fibroblasts and epithelial cells, assisting the repair of tissue damage.[7] Moreover, the osmotic pressure of the honey dressing helps to move lymph through tissue and provides a

moist healing environment with increased oxygenation and nutrient supply to promote healing.[8]

In vitro honey can activate B-lymphocytes, T-lymphocytes, and phagocytes, and can stimulates the release of tumour necrosis factor α, interleukin 1 and 6 cytokines and these cytokines convey signals in the immune system. This suggests honey assists in wound healing by increasing immunity and stimulating the immune response.[9]

1.3. Factors which contribute to the antibacterial activity of honey

The factors that contribute to the antibacterial activity of honey of all origins are osmotic pressure, acidity and hydrogen peroxide. However, mānuka honeys have an additional antibacterial factor, which is known as non-peroxide activity.

1.3.1. Osmotic pressure

Honey is predominantly sugar (>80%) and its strong interaction with water molecules leads to supersaturated solutions. Honey has an average of 17.2% water content and ranges from 13.4% - 22.9%.[10] The percentage of free water molecules is measured as the water activity (a_w) which in honey ranges from 0.47 to 0.70 a_w. Although inhibition is dependent on the species of bacteria, most species of bacteria are inhibited by conditions where a_w is below 0.94.[11] However *Staphylococcus aureus* has a high tolerance of low a_w and complete inhibition is achieved only when the a_w is less than or equal to 0.86.[5a]

1.3.2. Acidity

An equilibrium between gluconic acid and gluconolactone makes the pH of honey average 3.91 and range from 3.42 - 6.10.[12] Honeybee secretions contain enzyme glucose oxidase that converts glucose to gluconic acid,[13] which, via intramolecular esterification, forms gluconolactone. The optimum pH for the growth of many pathogenic bacteria is between 7.2 and 7.4 and therefore some honeys are likely to be sufficiently acidic to cause the inhibition of many bacteria.

1.3.3. Hydrogen peroxide

Hydrogen peroxide has been identified as the major antibacterial agent in honey and accounts for all of the observed antibacterial activity in most honeys.[14] Hydrogen peroxide is formed when the enzyme glucose oxidase converts glucose to gluconic acid in honey (**Fig. 1.1**). Together, with acidity caused by gluconic acid, hydrogen peroxide acts as a preservative of the honey while it ripens.[12b]

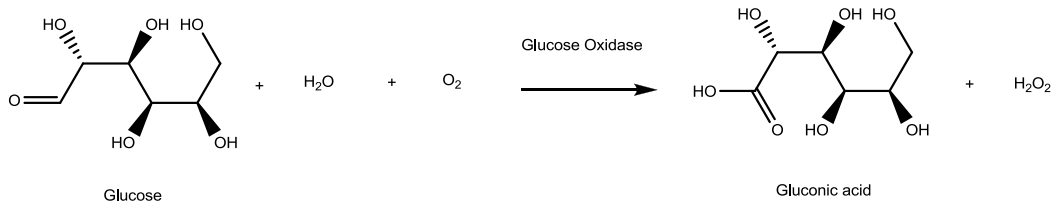

Fig. 1.1: Formation of hydrogen peroxide during the conversion of glucose to gluconic acid.

Full strength honey does not give a significant therapeutic effect as the concentration of hydrogen peroxide is negligible due to the fact that the enzyme glucose oxidase is deactivated by the acidity of gluconic acid. The therapeutic effect only shows when honey is diluted.[5a]

High levels of hydrogen peroxide are known to cause DNA damage leading to cell injury and death[15] but this is not an issue when honey is used as an antibacterial agent because the glucose oxidase enzyme will only activate when honey is diluted. This allows honey to supply controlled levels of hydrogen peroxide continuously over time to provide effective antibacterial activity without the tissue damage usually caused by applying hydrogen peroxide solution directly as an antibiotic.[7]

1.3.4. Non-peroxide antibacterial properties of mānuka honey

It is widely accepted that some New Zealand mānuka honeys exhibit significant non-peroxide antibacterial activity,[16] known as UMF™ (Unique Mānuka Factor). This is rated as the non-hydrogen peroxide activity using phenol as reference point. Mānuka honey that demonstrates an antibacterial activity

equivalent to a 5% solution of phenol is classified as UMF™ 5+ and honey can be rated up to UMF™ 30+ which is the equivalent of a 30% phenol solution. However, not all mānuka honeys possess non-peroxide activity. A survey of 26 different types of monofloral New Zealand honeys found that non-peroxide activity was only present in 38% of mānuka honeys.[17] High UMF™ activity honey are generally produced in Northland, Coromandel, East Cape and Marlborough.[18] Common wound infecting bacteria such as *Escherichia coli, Proteus mirabilis, Pseudomonas aeruginosa, Salmonella typhimurium, Serratia marcescens, Staphylococcus aureus* and *Streptococcus pyogenes* were found to be inhibited by active mānuka honey.[19]

The non-peroxide activity observed in mānuka honeys was a mystery before Adams *et al.*[20] established a positive relationship between the level of methylglyoxal (MGO) and the antibacterial activities of the honeys by using the *o*-phenylenediamine derivatisation to form its quinoxaline derivative to determine the MGO levels of 49 mānuka and 34 non-mānuka honey samples which varied from 38 to 828 mg/kg, together with isolation and identification of the active fraction of mānuka honey.

A similar study by Mavric*et al.*[21] identified high levels of MGO in mānuka honey and suggested it was responsible for the non-peroxide activity observed in mānuka honeys. MGO was detected as its quinoxaline derivative of *o*-phenylenediamine at levels ranging from 38 to 761 mg/kg in six mānuka honeys by high performance liquid chromatography. These levels were significantly higher than those observed in 50 samples of other honey types, which had an average of 3.1 mg/kg and ranged between undetectable to 5.7 mg/kg. Of the 6 mānuka honeys, which exhibited antibacterial activity against *Escherichia coli* and *Staphylococcus aureus* at minimum concentrations of 15-30% (v/v with water), correspond to MGO concentrations of 1.1 to 1.8 mM. The minimum concentration of MGO needed to inhibit these bacteria is 1.1 mM, suggesting that the high levels of MGO found in mānuka honey were responsible for its non-peroxide activity. Moreover, an inactive forest honey with addition of 1.9 mM MGO gave it an antibacterial activity comparable to that of a UMF™

20+mānuka honey containing a natural MGO level of 1.9 mM. This indicated MGO was responsible for the non-peroxide activity observed in mānuka honeys.

In a subsequent study, Donarski *et al.*[22] found out that the level of MGO in 6 mānuka honeys varied from 338 to 817 mg/kg by quantitative NMR spectroscopy and Stephens *et al.*[23] found out that the level of MGO in 19 mānuka honeys varied from 102 to 1490 mg/kg by using the *o*-phenylenediamine derivatisation to form its quinoxaline derivative.

All the above studies indicate that MGO is primarily responsible for the non-peroxide activity observed in mānuka honeys

1.3.5. Methylglyoxal (MGO)

Methylglyoxal is a naturally occurring dicarbonyl compound, formed during the caramelisation of carbohydrates and during the Maillard reaction between carbohydrates and amino acids.[20] It is present in a wide range of food such as wine, beer, coffee, dairy products, soy sauce and juices.[24] The interest in concentration of MGO in food is due to concerns over the toxicity of MGO.

1.3.5.1. Speciation of MGO

The speciation of MGO is temperature and matrix dependant.[25] In aqueous solutions an equilibrium forms between the methylglyoxal monohydrate and methylglyoxal dihydrate (**Fig. 1.2**).

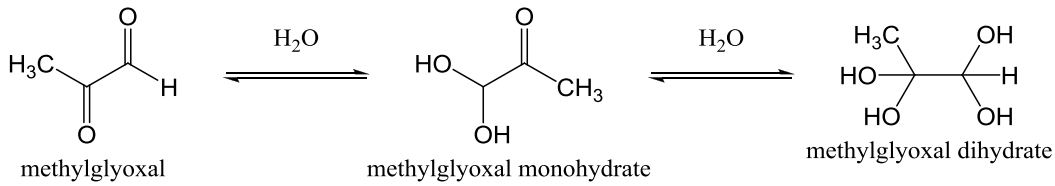

methylglyoxal — methylglyoxal monohydrate — methylglyoxal dihydrate

Fig. 1.2: Formation of methylglyoxal monohydrate and methylglyoxal dihydrate from MGO in aqueous solutions.

1.3.5.2. Toxicity of MGO

The toxicity of methylglyoxal has been the subject of a large number of *in vivo* and *in vitro* studies. It was found that 2 g/kg of body weight of MGO had no adverse effects when applied orally, subcutaneously or intravenously to mice and rats. Chronic doses of up to 1 g/kg body weight per day were also given orally, subcutaneously or intravenously to mouse, rats and dogs, which also showed no adverse effects after observation for 90 days.[26] However, a review by Kalapos[27] identified a number of studies reporting that methylglyoxalwas toxic and lethal to mice within 4 hours when 800 mg/kg of body weight of MGO was given intraperitoneally.

MGO can be mutagenic as the reaction of MGO with guanine residues in DNA can cause cancer and this effect is enhanced in the presence of hydrogen peroxide.[28] However, its cytotoxicity can also exert an anti-cancer effect.[26-27]

Apart from this, MGO can disrupt extra cellular matrix (ECM) interactions of endothelial cells and cause anoikis of endothelial cells and decreased angiogenesis.[29]

The reaction of MGO with amino groups of proteins form advanced glycation endproducts (AGEs)[30] and these accumulate during the process of wound healing. AGEs have demonstrated the ability to regulate a variety of inflammatory cell responses and growth-promoting events during wound healing. However, excessive AGEs could impair normal cellular functions and wound tissue remodelling through promotion of oxidative stress.[31]

1.3.5.3. Source of MGO in honey

In 2009, Adams *et al*.[32] found out that the presence of MGO in mānuka honey was attributed to the non-enzymatic conversion of dihydroxyacetone (DHA) in *Leptospermum scoparium* nectar to MGO in maturing mānuka honey. The nectar washed from *Leptospermum scoparium* flowers contained estimated level of DHA up to 13,600 mg/kg, which is many times that found in fresh mānuka honey. The disappearance of DHA and the appearance of MGO in freshly

produced honeys with time of storage at 37 ºC indicated that the source of MGO was the non-enzymatic conversion of DHA.

1.3.5.4. Detection of MGO in honey

The reactivity of MGO, low molecular mass and lack of ultraviolet (UV) chromophore have made direct detection of MGO in honey not feasible by using conventional analytical detection systems. The detection of MGO has normally been performed by using *o*-phenylenediamine derivatisation to form its quinoxaline derivative.[20-21, 23] However, the derivatisation step is subject to the Maillard reaction which can lead to overestimates of concentration.[33]

Two methods for the direct quantification of methylglyoxal in mānuka honey have been successfully demonstrated. Adams *et al*.[20] used an HPLC system with mixed mode size exclusion/ligand exchange columns connected in series couple with refractive index (RI) and UV detection while quantitative NMR spectroscopy (qNMR) was used by Donarski *et al.*[22]

1.4. Flavonoids

Flavonoids are plant pigments that are ubiquitous to photosynthesising cells and are highly diversified.[34] They are a large and diverse group of phenolics, with a basic C_6-C_3-C_6 structure in common. The two C_6 aromatic rings are designated ring A and ring B with the C_3 unit bridging them (**Fig. 1.3**), and based on the oxidation state of the C_3 bridging unit they can be subdivided into a number of classes.[35] The classes of flavonoids are aurones, isoflavones, chalcones, flavanones, flavones, flavonols, flavanon-3-ols, anthocyanidins, flavan-3-ols, proanthocyanidins, flavans, flavan-3,4-diols and dihydrochalcones. The structures of the main classes are shown in **Fig. 1.4**.[36] Individual compounds are classified according to the way they differ in the number and positions of substituents on the aromatic rings of these classes. The substituents are usually hydroxy-groups which may also be methylated or glycosylated.[35]

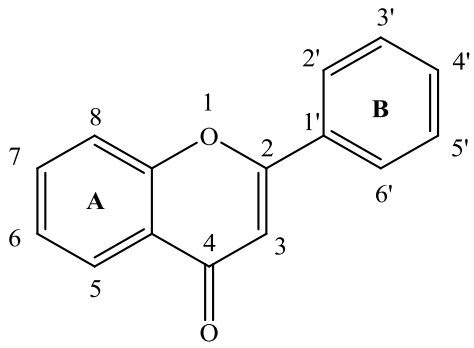

Flavone

Fig. 1.3: The structure of flavone.[35]

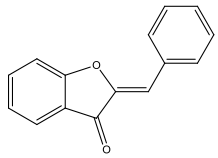

Aurone

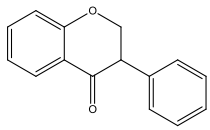

Isoflavone

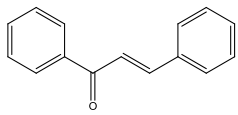

Chalcone

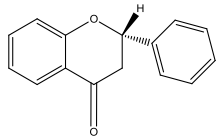

Flavanone

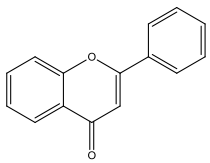

Flavone

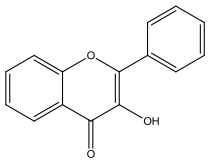

Flavonol

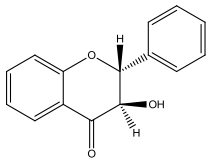

Flavanon-3-ol

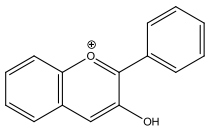

Anthocyanidin

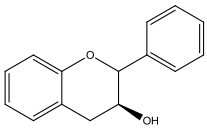

Flavan-3-ol

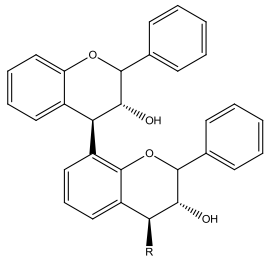

Proanthocyanidin

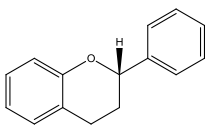

Flavan

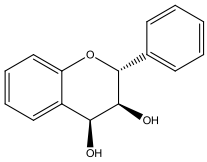

Flavan-3,4-diol

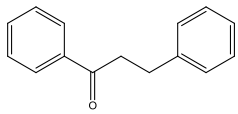

Dihydrochalcone

Fig. 1.4: The basic structures of the main class of flavonoids (proanthocyanidins occur as dimers, trimers, tetramers and pentamers; R = 0, 1, 2 or 3 flavan-3-ol structures).[36]

1.4.1. Biosynthesis of flavonoids

Biosynthesis of flavonoids is almost exclusively limited to the higher plants and uses an estimated 2% of the total carbon fixed by photosynthesis in plants. The biosynthetic origin of the C_6-C_3-C_6 unit lies in both the polyketide and shikimate biosynthetic pathways. Ring A is the result of condensation of three acetate units in the polyketide pathway while ring B and the linking C_3 unit are formed via the shikimic acid pathway.[35]

1.4.2. Biological roles of flavonoids

Flavonoids occur in all parts of plants including the roots, stems, leaves, flowers, pollen, fruit, seeds, wood and bark. The main role of flavonoids is to act as pigments and provide colour to the plant's flowers to attract pollinators. They strongly absorb light in the ultra-violet region and are used as protection against harmful UV-B radiation.[36]

Flavonoids can act as protective agents against a number of attacking organisms including viruses, bacteria, fungi (through production of flavonoid phytoalexins which are antibiotic), and encroaching plants (through production of allelopathic flavonoids which inhibit germination and growth). [35-37]

Another role of flavonoids is to act as messengers. Flavonoids secreted by the roots of the host plant such as legumes are taken up by nitrogen fixing bacteria, which have a symbiotic relationship with the host plant, and trigger the secretion of *nod* factors. The host plant responds to the *nod* factors and nitrogen fixing bacteria are incorporated into the root structure. [34, 37]

1.4.3. Medicinal properties of flavonoids

The average human is estimated to ingest 0.5 - 2 g of flavonoids per day in a normal diet which leads to extensive research on the effects of flavonoids on animal and human physiology.[34]

Flavonoids have been reported to be anti-inflammatory, oestrogenic, enzyme inhibitory, antimicrobial, antiallergic, antioxidant, antiviral,

antithrombotic, anaesthetic and cytotoxic antitumour, all of which give the potential to prevent or treat cancers, cardiovascular disease, hypertension, allergies, vascular fragility, duodenal ulcers, gastric ulcers, diabetes, and bacterial and viral infections.[38]

The antimicrobial activity of propolis (bee glue) is attributed to its high flavonoid content, and high concentrations of flavonoids have been found to possess antimicrobial activity against a variety of bacterial species including methicillin resistant *Staphylococcus aureus.*[36, 38b]

Another useful medicinal property of the flavonoids is the ability to scavenge free radicals. Free radicals are produced during important physiological processes such as respiration and the immune response and can cause extensive cellular damage; flavonoids, can by scavenging, reduce them to non-reactive species.[38b]

1.4.4. Identification of flavonoids

Traditional methods for the identification of flavonoids involved the use of colour reactions with reagents such as aqueous sodium hydroxide, concentrated sulphuric acid, magnesium-hydrochloric acid and sodium amalgam with acid and also involved the use of degradative studies.[39] However, these methods have now been replaced by spectroscopic techniques such as ultraviolet and visible absorption (UV-Vis) and nuclear magnetic resonance (NMR) spectroscopy which require much less material for characterisation and these new methods can also yield structural information.[37]

1.4.4.1. Ultraviolet-visible absorption spectroscopy

Flavonoids have a large degree of conjugated unsaturation, which cause them to absorb strongly in the ultraviolet and visible regions of the electromagnetic spectrum.[35] They typically exhibit two major absorption peaks in the region of 240 to 400 nm. These peaks are commonly referred to as Band I (usually 300-380 nm) and Band II (usually 240-285 nm). Band I is associated

with absorption due to the B-ring cinnamoyl system, while Band II is the result of absorption involving the A-ring benzoyl system (**see Fig. 1.5**).[37, 40]

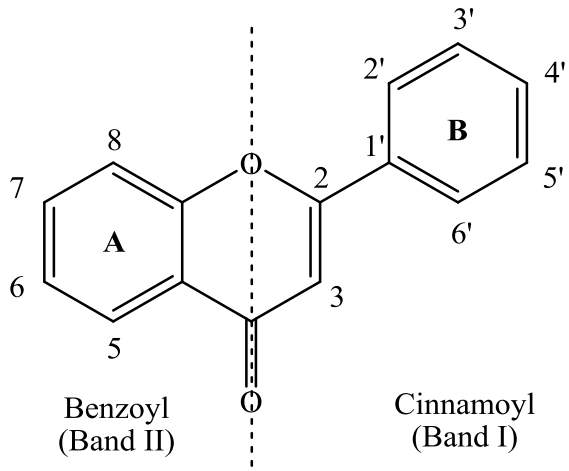

Fig. 1.5: The conjugated systems responsible for the major ultraviolet-visible absorption peaks of flavonoids.[40]

1.4.4.2. Nuclear magnetic resonance (NMR) spectroscopy

One and 2D-NMR spectroscopy are a useful techniques for the characterisation of all flavonoids. Most flavonoids are sufficiently soluble in hexadeuteriodimethyl sulfoxide (DMSO-d_6) to allow direct NMR analysis. However there are down sides. The high boiling point of DMSO-d_6 makes the recovery of flavonoids difficult. Some flavonoids are known to decompose in DMSO-d_6, and the tendency of this solvent to absorb moisture can be problematic.[40a, 40c]

The combination of chemical shift and multiplicity of the proton NMR of flavonoids can yield significant information about oxygenation and substitution patterns, along with other signals such as methoxyl or glucosyl protons.[37, 40a, 40c]

1.5. Isolation of flavonoids from honey

There has been a long development history of isolation techniques for flavonoids, such as thin-layer chromatography, high-performance thin-layer chromatography, centrifugal thin-layer chromatography, column chromatography, droplet counter-current chromatography, gas-liquid chromatography and HPLC.

Among these methods, HPLC has proved to be one of the most powerful methods for quantitative determinations of plant phenolics.[41] HPLC systems are usually binary in which an acidified aqueous solvent gradually changes to an organic solvent such as methanol over the duration of the HPLC run with detection by UV absorbance. This coupled with electrospray mass spectrometry (ESI-MS) gives additional information about the structure of flavonoids from fractionation patterns without the need to isolate them.[38a]

Direct use of HPLC for quantitative analysis of flavonoids in honey is hard to achieve due to the high sugar content of the honey. Firstly, it interferes with the direct and complete extraction of flavonoids,[42] and secondly, it forms inconvenient interphases in liquid-liquid extractions, which prevents complete recovery of flavonoids.[42a]

The use of the non-ionic polymeric resin Amberlite XAD-2 allows the sugars and polar compounds to be removed, leaving a fraction containing flavonoids and other phenolic compounds.[42] However, other UV-absorbing compounds such as phenolic acid derivatives interfere with the analysis of flavonoids.[42a] This leads to the use of column chromatography through Sephadex LH-20 to separate flavonoids from other phenolics. Under 360nm UV light, the phenolic acid derivatives elute first as a blue fraction. The flavonoids elute later as a dark purple fraction.[42a]

Liquid-liquid extraction with diethyl ether is another method to remove the flavonoids (recovery >95% after three extractions) from an aqueous solution of the phenolic fraction, leaving the majority of the phenolic acid derivatives and any remaining polar compounds in the aqueous layer.[42b]

1.6. Flavonoids in mānuka honey

Weston *et al.*[43] reported that the flavonoid profile of 19 mānuka honeys of varying UMF ratings from throughout the North Island of New Zealand was similar to that of most European honeys, containing pinobanksin, pinocembrin, chrysin and galangin at a total average level of 14.9 μg/100g of honey. There was

no difference in the flavonoid profile of mānuka honey from different geographical regions and no correlation between the flavonoid content with UMF rating of the honeys.

Yao *et al.*[44] in a later study found significantly higher levels of flavonoids in two New Zealand mānuka (*Leptospermum scoparium*) honey which had an average flavonoid content of 3060 μg/l00g of honey, a value considerably higher than the level of 14.9 μg/100g reported by Weston *et al.*[43a] The difference in these results was attributed to insufficient XAD-2 resin for the mass of honey analysed by Weston *et al.*[43a] Yao *et al.*[44] also found a range of flavonoids, which were not reported by Weston *et al*. The flavonoids found in mānuka honey include myricetin, tricetin, pinobanksin, quercetin, luteolin, quercetin 3-methyl ether, kaempferol, 8-methoxykaempferol, pinocembrin, quercetin 3,3′-dimethyl ether, isorhamnetin, chrysin and two unidentified flavonoids. Quercetin (13.8%), isorhamnetin (12.9%), chrysin (12.6%), luteolin (12.6%) and one of the unknown flavonoids (12.7%) together they represented 64.6% of the total flavonoid content.

Deadman[45] reported that in 31 samples of varying UMF ratings New Zealand mānuka (*Leptospermum scoparium*) honey, the total flavonoid content of mānuka honey was found to range between 590-2240 μg /100g of honey, with an average of 1160 μg/100g. The main constituents were pinobanksin (23.1%), pinocembrin (15.1%), luteolin (11.8%) and chrysin (11.4%), and these made up 61.4% of the total flavonoid content.

Deadman also reported the presence of an unknown compound which showed a weak positive correlation ($R^2 = 0.36$) with non-peroxide anti-bacterial activity. This compound was found to elute with the flavonoids at high levels (13.6% of total flavonoids by integration based on the assumption that it showed a similar UV response to that determined for quercetin.) in mānuka honey but the UV absorption spectrum indicated that it was not a flavonoid.[45] Isolation and characterization of this compound, **1**, was the topic of the this thesis. Compound **1** unexpectedly proved to be a phenyl substituted pyrrole derivative rather than a flavonoid.

1.7. Pyrroles

The planar, electron rich, five-membered heteroaromatic pyrrole ring (**Fig. 1.5**) was found in coal tar by Runge and identified by Baeyer.[46] The capacity to form hydrogen bonds, coordinate metals, and provide stacking interactions make it a key constituent of the bicyclic indole side chain of L-tryptophan residues in proteins and the tetrapyrroles such as heme *b* (**Fig. 1.6**), vitamin B12 (**Fig. 1.7**) and chlorophyll α (**Fig. 1.8**) with iron, cobalt, or magnesium atoms chelated in the equatorial plane of the macrocycles.[47] In addition, it is present in a wide range of natural products and this has lead to extensive research on synthesis and chemical behaviours of pyrroles.

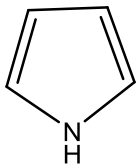

Fig. 1.6: Structure of pyrrole.[48]

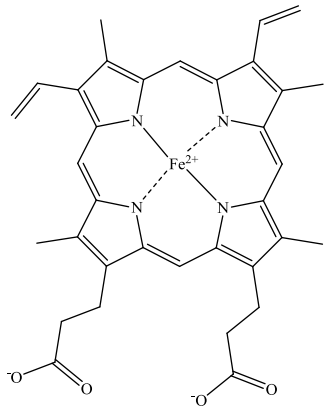

Fig. 1.7: Structure of heme *b*.

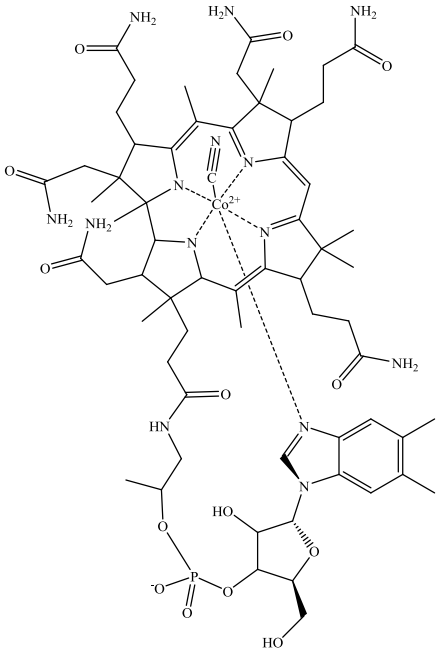

Fig. 1.8: Structure of vitamin B12.

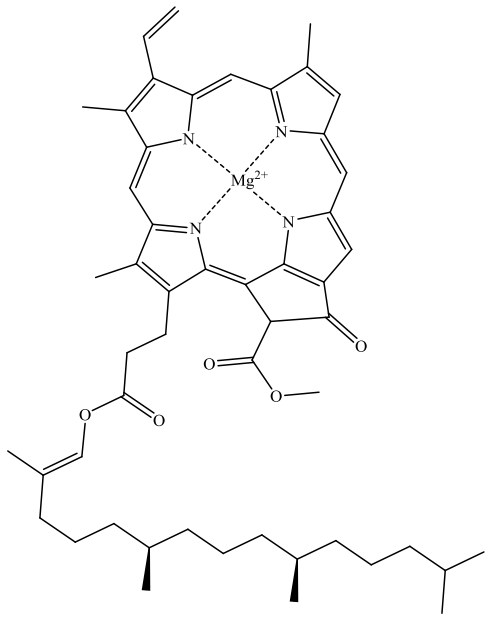

Fig. 1.9: Structure of chlorophyll α.

1.7.1. Pyrrole in natural products

Pyrrole-containing natural products, include the well-known tetrapyrrolic, prodiginine family for example prodigiosin (**Fig. 1.10**), are produced by *Serratia marcescens*, where three pyrrole rings are present with two directly coupled in tandem array. They have been reported to have antibacterial, antifungal, antiprotozoal, antimalarial, immunosuppressive and anticancer properties.[49] A structurally related species roseophilin (**Fig. 1.11**) which was isolated from *Streptomyces griscovirides* has been shown to have antitumor activity.[50]

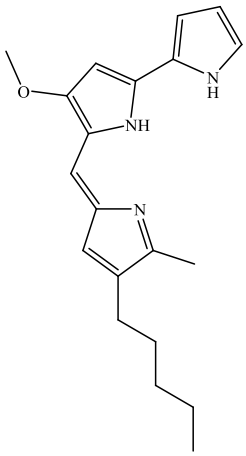

Fig. 1.10: Structure of prodigiosin.

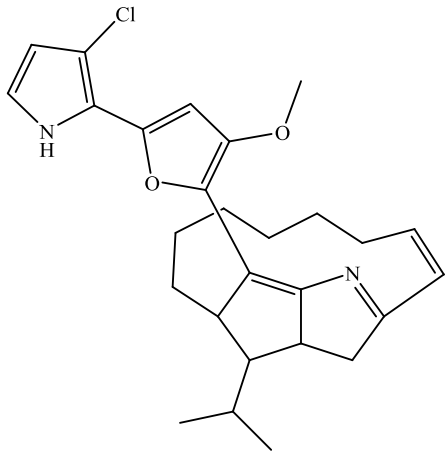

Fig. 1.11: Structure of roseophilin.

The tambjamines family is a 2,2'-bipyrrolic class of cytotoxic alkaloids, isolated from bacteria and marine invertebrates with diverse aliphatic termini. Members of this family show wide range of bioactivity, for example, tambjamines D (**Fig. 1.12**) and E (**Fig.1.13**) have been correlated with antitumor properties through DNA intercalation and oxidative cleavage of single-strand DNA.[51]

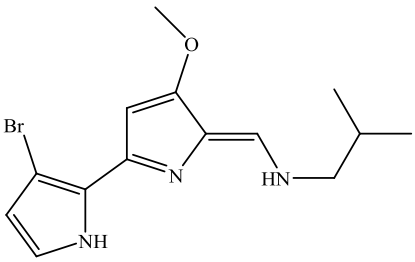

Fig. 1.12: Structure of tambjamines D.

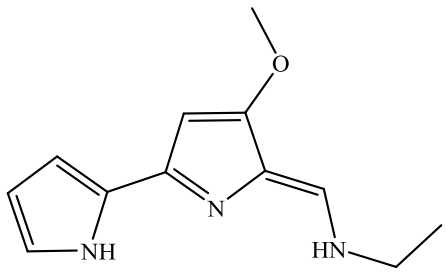

Fig. 1.13: Structure of tambjamines E.

Rebeccamycin (**Fig. 1.14**), isolated from *Saccharotrix aerocologines*[52] and staurosporine **(Fig. 1.15**), isolated from *Streptomyces*,[53] have a somewhat similar aglycone but differ by the sugar structure linked to the indole nitrogen(s). Rebeccamycin is known to inhibit topoisomerase I while staurosporine is known to be a non-selective kinase inhibitor without activity against topoisomerases.[54, 55]

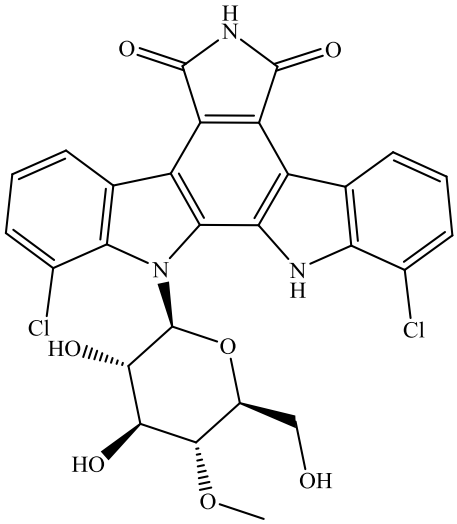

Fig. 1.14: Structure of rebeccamycin.

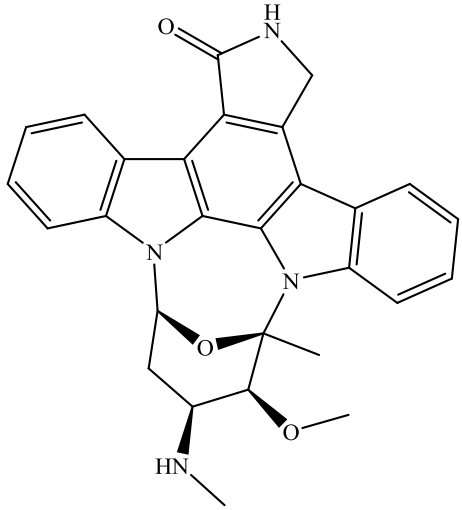

Fig. 1.15: Structure of staurosporine.

Monopyrrolic natural products are being discovered in increasing numbers in various sources such as insects, sponges, plants, fungi and bacteria.[56] Batrachotoxin (**Fig. 1.13**), is isolated from skin extracts from a Colombian poison-dart frog (family Dendrobatidae),[57] and is one of the most toxic substances known to man. Clorobiocin (**Fig. 1.14**) is an antibiotic that acts by an inhibition of the DNA Gyrase enzyme involved in the cell division in bacteria and is derived from *Streptomyces* species.[58]

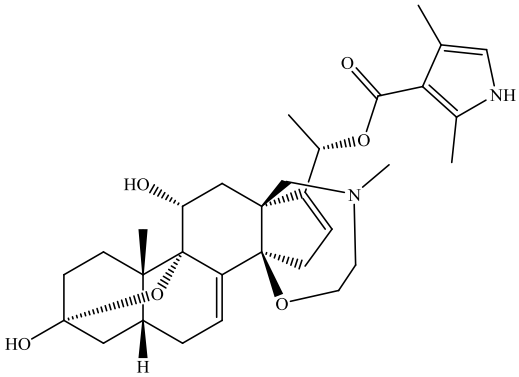

Fig. 1.16: Structure of batrachotoxin.[57b]

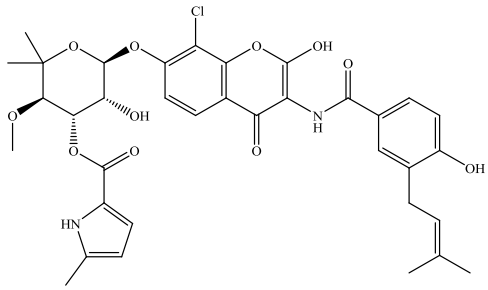

Fig. 1.17: Structure of clorobiocin.[58]

1.7.2. Pyrroles in honey

Pyrroles can arise from Maillard reactions or from the pyrolysis of amino acids when heated.[59] 1*H*-Pyrrole was found in *Robinia pseudoacacia L*., *Castanea sativa L*. and *Salvia officinalis L.*[59-60] 1*H*-pyrrole-2-carboxylic acid was found in *Paliurus spina-christi* honey.[61] 2-acetylpyrrole was found in *abbamelen*, a honey-based Sardinian product[62] and 1*H*-pyrrole-3,4-diacetic acid was found in Pine honey (*Pinus brutia Ten*).[63]

1.7.3. Phenyl substituted pyrroles

1.7.3.1. Natural occurrence

The Lamellarin family (**Fig. 1.18**) are 3,4-diarylated pyrroles which were isolated first in 1985 from a prosobranch mollusc of the genus *Lamellaria*.[64] The family has shown cytotoxicity and antitumor activity, multidrug resistance reversal activity, inhibition of HIV-1 Integrase and MCV topoisomerase, antibiotic and antibacterial activity, inhibition of ATP-Citrate Lyase and Human Aldose Reductase (h-ALR2), cell division inhibition and immunomodulatory activity, antioxidant activity and feeding deterrence.[65]

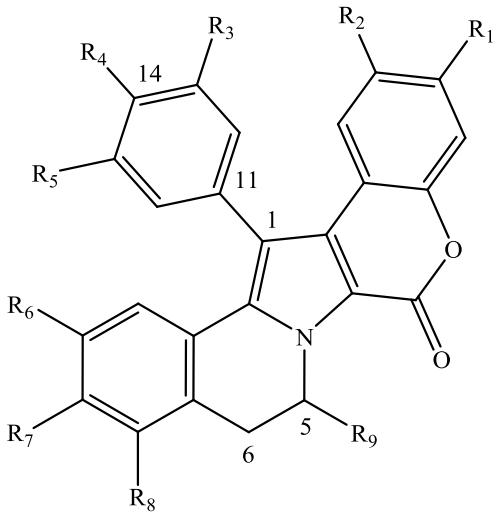

Fig. 1.18: General structure of lamellarin where a single or a double bond is present between C_5 and C_6 depending upon the particular example.

Pyrrolnitrin (**Fig. 1.19**) is a tryptophan-derived antifungal and antibiotic isolated from *Pseudomonas pyrrocinia*.[66] Both pentabromopseudilin (**Fig. 1.20**), produced by *P. bromoutilis*, and pentachloropseudilin (**Fig. 1.21**), produced by an *Actinoplanes* sp. strain, are strongly active against Gram-positive bacteria. Pentabromopseudilin is also known to inhibit a number of different enzyme systems and has high *in vitro* activity against leukemia and melanoma cell lines.[66]

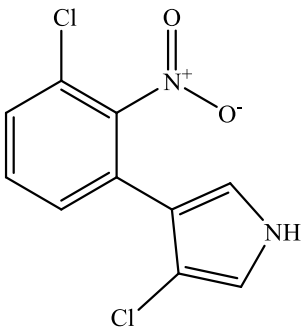

Fig. 1.19: Structure of pyrrolnitrin.

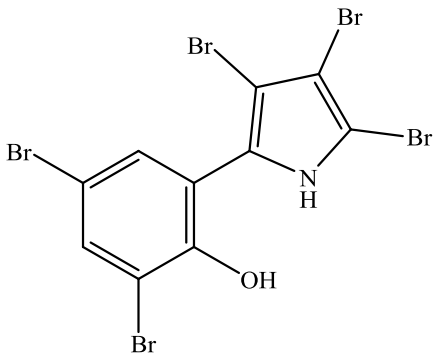

Fig. 1.20: Structure of pentabromopseudilin.

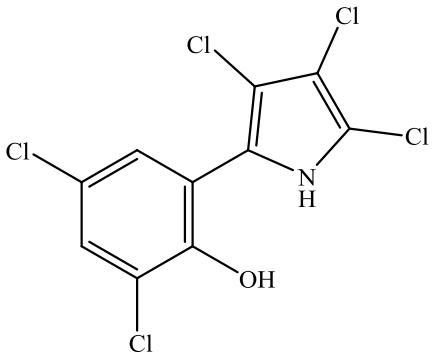

Fig. 1.21: Structure of pentachloropseudilin.

1.7.3.2. As intermediate and synthesis targets

2-Chloro-6-(1*H*-pyrrol-3-yl)aniline (**Fig. 1.22**) acts as an intermediate for synthesis of pyrrolnitrin.[67] 3-(3,5-dichloro-2-methoxyphenyl)-1*H*-pyrrole (**Fig. 1.23**) acts as an intermediate for the synthesis of pentachloropseudilin and 3-(2-methoxyphenyl)-1*H*-pyrrole (**Fig. 1.24**) acts as an intermediate for the synthesis of pentabromopseudilin.[68]

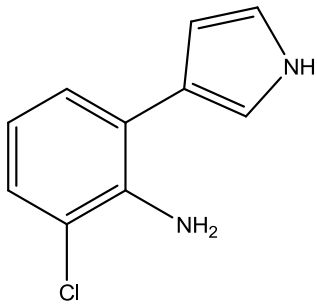

Fig. 1.22: 2-Chloro-6-(1*H*-pyrrol-3-yl)aniline.

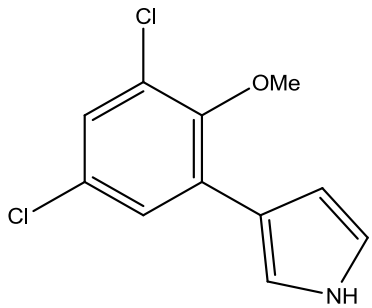

Fig. 1.23: 3-(3,5-Dichloro-2-methoxyphenyl)-1*H*-pyrrole.

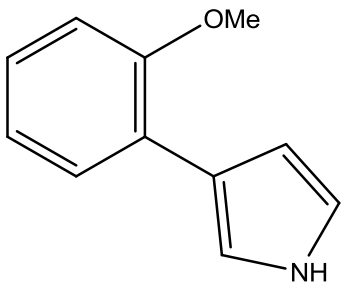

Fig. 1.24: 3-(2-Methoxyphenyl)-1*H*-pyrrole.

Phenyl substituted 2-formylpyrroles are used to prepare a pyrrolo[1,2-a] quinoxaline analogue,[69] which shows biological activity. For example, 1-(5-bromopyridin-2-yl)-3-(2-(6-fluoro-4-oxopyrrolo[1,2-a]quinoxalin-5(4*H*)-yl)ethyl) thiourea**(Fig. 1.25**) which is anti-HIV agent.[70]

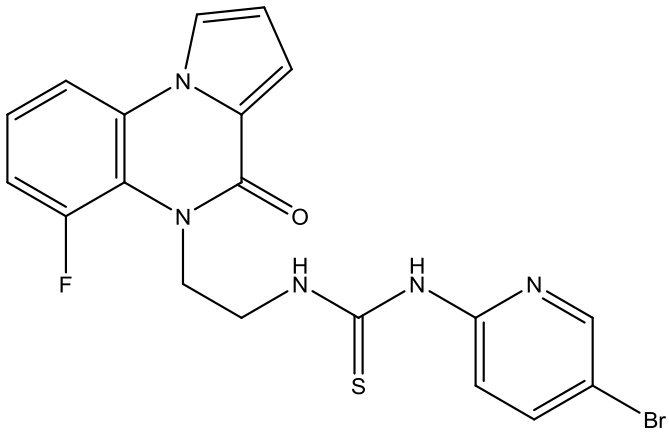

Fig. 1.25: 1-(5-Bromopyridin-2-yl)-3-(2-(6-fluoro-4-oxopyrrolo[1,2-a]quinoxalin-5(4*H*)-yl)ethyl)thiourea.

2-(4-Fluorophenyl)-3-(4-pyridinyl)-5-substituted pyrrole analogues (**Fig. 1.26**) have been shown to be inhibitors of *Eimeria tenella* cGMP-dependent protein kinase and active in *in vivo* anticoccidial assays.[71]

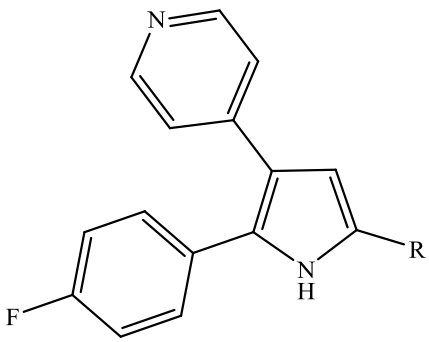

Fig. 1.26: General structure of 2-(4-fluorophenyl)-3-(4-pyridinyl)-5-substituted pyrroles.

Phenyl substituted pyrrole derivatives continue to attract the attention of synthetic organic chemists, due to their inherent biological activity.

1.8 Aim

The aim of this thesis was the isolation, characterization and synthesis of **1** which had been shown to be weakly correlated with non-peroxide anti-bacterial activity ($R^2 = 0.36$).[45]

Materials and Method

2.1. Materials

Fifteen kilograms of mānuka honey were sourced from Natures Country Gold (Hamilton, New Zealand) for use in the isolation of flavonoids. Honeys were stored in a cold room (5 - 8 ºC) when not being used.

Solvents used in this study were methanol, water, dimethyl sulfoxide, diethyl ether, hexanes, dichloromethane, tetrahydrofuran, concentrated hydrochloric acid and sodium hydroxide. Methanol used in the extraction of flavonoids was redistilled from drum grade while the methanol used for HPLC was of HPLC grade supplied by Scharlau.

Water used in the extraction of flavonoids was deionised and obtained from a Crystal Pure Ultra Pure Water System. Higher grade Milli-Q water was used as a solvent in the HPLC system and was obtained from a Barnstead E-pure system (18.2 MΩcm). Dried and purified diethyl ether, hexanes, tetrahydrofuran and dichloromethane were obtained from a Pure Solvent Purification System (Model: PS-SD-5) as needed and used promptly.

The dimethyl sulfoxide used for the cleaning of HPLC systems was of spectrophotometric grade supplied by Aldrich Chemical Company. Deuterated dimethyl sulfoxide-d_6 (99.9 atom % D containing 0.03% v/v TMS or 99.5 atom % D) and deuterated chloroform (99.8 atom% D), both obtained from Sigma-Aldrich, were used as the solvent for NMR analysis.

Concentrated hydrochloric acid was obtained from Ajax Finechem and sodium hydroxide was obtained from Merck.

Lithium diisopropylamide (LDA), ethyl 4-oxazolecarboxylate and 4-formyloxazole were obtained from Sigma-Aldrich Inc. Diisobutylaluminium hydride (DIBALH), triethylamine (Et_3N), *p*-coumaric acid and caffeic acid were obtained from Aldrich Chemical Company, Inc. Methane sulphonyl chloride (MsCl) was obtained from Riedel-de Haën.

2.2. Methods

2.2.1. Evaporation

Large volumes of liquid were reduced using rotary evaporators comprised of a Büchi Rotavapor R-200, Büchi Heating Bath B-490 and a Büchi Vac® V-500 vacuum pump with the water bath set to 40ºC unless specified.

Once liquid volumes had been reduced enough to fit in a sample vial, further evaporation was achieved using a blow down block which consisted of a Pierce Reacti-Therm Heating Module set to heat samples to 40ºC and a Pierce Reacti-Vap Evaporating Unit which blew nitrogen gas over the samples.

2.2.2. Melting point

Melting points were measured on a Reichart Thermopan melting point apparatus and are uncorrected.

2.2.3. High performance liquid chromatography (HPLC)

2.2.3.1. HPLC conditions

1 was isolated with a binary HPLC system operated using Waters Empower Pro software (Waters Empower 2, build number 2154). Two Waters 515 HPLC pumps were operated remotely with their flows being combined through a mixer (Grace Binary Large Volume Mixer SS Housing with 350 µL Mixer Cartridge). This mixer setup was required to suppress noise generated by the mixing of eluents at high pressure.

Samples were injected manually using a Rheodyne 7725i injector system fitted with a Rheodyne loop (50 µL). Separation of extracts was achieved using a Waters Symmetry Shield™ octadecylsilane HPLC column (RP18, 5 µm, 3.0 x 250 mm). A matching guard column (Waters Universal Sentry™ Guard

SymmetryShield™ Column in a Waters Universal Sentry™ Guard Column Holder) was fitted to protect the analytical column.

Binary gradients were operated on this system. Solvent A was Milli-Q water and methanol (5% v/v) to prevent microbial growth, acidified with acetic acid (0.075% v/v). Solvent A was prepared in batches (1 L) which were sonicated (20 minutes) to assist removal of dissolved gases prior to using in the HPLC. Solvent B was methanol. A degasser (Waters In-Line Degasser AF) was also utilised in the HPLC system to further remove dissolved gases. Detection was achieved using a Waters 996 Photodiode Array Detector (240.0 - 400.0 nm).

Gradient system 1 shown in **Table 2.1** was run at a constant combined flow rate (0.3 mL/minutes) and used for the isolation of flavonoid extracts.

Table 2.1: Gradient system 1 used for the analytical HPLC analysis of flavonoid extracts

Time (minutes)	Solvent A %[1]	Solvent B %[2]
0	70	30
15	70	30
20	40	60
60	0	100
70	0	100
73	70	30
78	70	30

[1] Acetic acid (0.075% v/v) and methanol (5% v/v) in Milli-Q water

[2]Methanol

Gradient method 2 shown in **Table 2.2** was run at a constant combined flow rate (0.3 mL/minutes) and used to purify the peak obtained using gradient method 1

Table 2.2: Gradient system 2 used to purify the peak obtained from using gradient method 1

Time (minutes)	Solvent A %[1]	Solvent B %[2]
0	70	30
5	70	30
10	55	45
50	20	80
52	0	100
60	0	100
63	70	30
68	70	30

[1] Acetic acid (0.075% v/v) and methanol (5% v/v) in Milli-Q water

[2]Methanol

2.2.3.2. Cleaning the HPLC column

It was found that certain components of honey persistently stayed in the HPLC column and could contaminate the column so that the chromatogram peaks became broadened and resolution was reduced. Multiple injections of dimethyl sulfoxide (ca. 50 μL) with a constant flow of methanol was applied to restore the column.

2.2.4. Gas chromatography with mass spectrometry (GC-MS)

GC-MS was carried out on a HP 6890 series GC fitted with a Phenomenex ZB-5 95% methyl siloxane column (30 m x .25 mm x .25 μm) interfaced to a HP 5973 Mass selective detector. Conditions used were 120°C (0.75 minutes), 50°C/minutes up to 200°C, and 10 °C/minutes up to 295°C (held 15 minutes). The mass spectrometer was set with either full ion monitoring (all compounds) or a selected ion monitoring *m/z* 201 ($M^{+\cdot}$), *m/z* 158 and *m/z* 130 ions (in the case of **1**).

2.2.5. Nuclear magnetic resonance spectroscopy

One and 2D- ^{1}H and ^{13}C NMR spectra of samples were obtained using a Bruker Avance DRX-400 spectrometer (upgraded to AVIII-400 status during the

latter stages of the investigations reported in this thesis) equipped with a superconducting magnet (52 mm). ^{1}H and ^{13}C experiments were carried out at 400 and 100 MHz respectively using a 5 mm inverse $^{13}C/^{1}H$ probe head except for the determination of ^{13}C spectra of **1,** which was acquired using a 5 mm dual $^{13}C/^{1}H$ probe head. Samples were dissolved in dimethyl sulfoxide-d_6 for NMR analysis. Operation of the NMR spectrometer and processing of spectra were performed using standard Bruker Topspin software 1.3 (DRX-400) or 3.0 (AVIII-400). Coupling constants *J* are reported in Hz, accurate to 0.1-0.2 Hz.

2.2.6. High resolution mass spectrometry (HRMS)

Mass spectra were recorded in positive-ion mode on a Bruker MicrOTOF mass spectrometer with electrospray interface and MeOH as mobile phase. Assignment of major peaks was confirmed by recording the high-resolution isotope pattern of the ions and comparing with the theoretical pattern obtained using the Isotope program.

2.2.7. Isolation of honey flavonoids

The method used to extract flavonoids from honey is a variation of that developed by Ferreres *et. al.*[42a]

2.2.7.1. Cleaning and swelling of the Amberlite XAD-2 resin

Dry Amberlite XAD-2 resin was left to soak overnight in a 50% solution of methanol and water to allow the resin to swell to its working volume. It was kept covered in solvent at all times (except when filtering on the Büchner funnel to remove excess solvent) and reused without having to swell the resin overnight.

The resin was cleaned by soaking in methanol overnight. This was considered sufficient to absorb any contaminants which could later elute into the flavonoid fraction. Removal of the resin from solvents was achieved by filtering it on a Büchner funnel. While this would not completely dry the resin, it was considered sufficient to remove excess solvent.

2.2.7.2. Extraction of phenolics using Amberlite XAD-2 resin

Unknown compounds were isolated from 15 kg of mānuka honey. Batches of honey (ca. 1 kg) were dissolved in acid water (pH 2 with HCl, ca. 3 L) and stirred until homogenous. Clean and swelled Amberlite XAD-2 resin (500 g) was added to the honey solution and stirred (1 hour) by a magnetic stirrer. The resin and honey solution slurry was then poured into a glass column (4 cm x 120 cm) and the honey solution drained out. The resin was washed with acid water (2 L) and deionised water (1 L) to remove the sugars and other polar compounds. All the aqueous washings and the honey solution were collected and later subjected to a second extraction on XAD-2 resin.

The phenolics were eluted from the resin by washing with distilled methanol (600 mL) and then deionised water (1 L). The column was inverted and deionised water flushed through to wash the resin out of the column. The resin was then partially dried on a Büchner funnel and added back to the aqueous washings to increase the recovery of flavonoids by extracting those compounds not recovered during the first treatment. The phenolic extracts were combined and concentrated under vacuum at 40ºC until the extract reached a syrupy consistency.

2.2.7.3. Liquid-liquid extraction and cleanup of the extract

The combined phenolic extract obtained from the XAD-2 resin extraction was resuspended in Milli-Q water (150 mL). The extract was then filtered through cotton wool to remove solids which had not dissolved. The filtrate was then subjected to eight extractions with diethyl ether (150 mL). The ether extracts were combined and concentrated to dryness under vacuum at 40ºC.

2.2.7.4. Sephadex LH-20 separation of the phenolic extract

The flavonoids were separated from the phenolic acids by chromatography on a Sephadex LH-20 column according to the method described by Bohm.[37]

The extract was dissolved in distilled methanol (40 mL) and poured into a column of Sephadex LH-20 (4 cm x 30 cm) which had been pre-soaked in 30% (v/v) distilled methanol in water. The phenolics were then eluted and collected

using increasing strength methanol solutions as shown in **Table 2.3**. The flow rate was increased by applying a light head pressure with N_2 gas.

Table 2.3 The solvents used in Sephadex LH-20 chromatography of phenolic extract and the fractions collected.

Fraction number	Solvent (% methanol v/v in water)	Volume used (mL)
1	30	250
2	30	250
3	60	250
4	60	250
5	80	250
6	80	250
7	100	250
8	100	250
9	100	250

2.2.8. Synthesis of 1

The method used to synthesise **1** is a variation of that developed by Reeves *et al.*[72] All reactions were carried out under dry, high purity nitrogen using standard Schlenk techniques, unless otherwise stated.

2.2.8.1. Synthesis of 6

A solution of ethyl 4-oxazolecarboxylate (1.00 g, 7.78 mmol) in CH_2Cl_2 (20 mL) was treated at -84^oC with DIBALH (16 mL, 16 mmol) for 1 hour. The reaction mixture was quenched with MeOH (10 mL), warmed to room temperature, and poured into 2 M aq HCl (20 mL). The layers were separated and the aqueous phase extracted with CH_2Cl_2 (2 x 20 mL). The combined organic phases were dried ($MgSO_4$), filtered through a short pad of SiO_2 and concentrated on a rotary evaporator at a bath temperature of 0^oC to give crude product. The product was recrystallized from CH_2Cl_2/hexanes.

2.2.8.2. Synthesis of 9

To THF (20 mL) at -84^{o}C was added LDA (2.5 ml, 5.5 mmol). The resultant solution of LDA was added dropwise to a solution of *o*-methoxyacetophenone (0.6 mL, 4.5 mmol). The reaction mixture was stirred at -84^{o}C for 30 minutes. A solution of 6 (0.5 g, 5.5 mmol) in a minimal amount of THF was added dropwise at -84^{o}C. The reaction mixture was stirred for 30 minutes at -84^{o}C, quenched with saturated aqueous NH_4Cl (20 mL) and allowed to warm to room temperature. The layers were allowed to separate, and the aqueous layer was extracted with EtOAc (2 x 20 mL). The combined organic layers were dried ($MgSO_4$), filtered and concentrated. The product was recrystallized from CH_2Cl_2/hexanes.

2.2.8.3. Synthesis of 1

A solution of **9** (0.40 g, 1.6 mmol) in THF (7 mL) was treated at 0^{o}C with Et_3N (0.7 mL) followed by dropwise addition of MsCl (0.2 mL). The reaction mixture was stirred at 0^{o}C for 1 hour. The reaction was then treated with aqueous 2M NaOH (10 mL) and the reaction mixture was heated at 70^{o}C for 16 hours. After cooling to room temperature, a GC-MS was run and showed the existence of a very small amount of product. The reaction mixture was heated at 70^{o}C for another 48 hours. After cooling to room temperature, the reaction mixture was diluted with saturated aqueous $NaHCO_3$ solution, extracted with EtOAc (2 x 20 mL) and the organic layer was dried ($MgSO_4$), filtered and concentrated. The product was recrystallized from CH_2Cl_2/hexanes.

2.2.8.4. Repeated synthesis of 1 for bioassay

A solution of **9** (0.23 g, 0.9 mmol) in THF (4 mL) was treated at 0^{o}C with Et_3N (0.4 mL) followed by dropwise addition of MsCl (0.1 mL). The reaction mixture was stirred at 0^{o}C for 1 hour. The reaction was then treated with aqueous 2 M NaOH (6 mL) and the reaction mixture was heated at 70^{o}C for 72 hours. After cooling to room temperature, the reaction mixture was diluted with saturated aqueous $NaHCO_3$ solution, extracted with EtOAc (2 x 20 mL) and the organic layer was dried ($MgSO_4$), filtered and concentrated.

The product was purified by chromatography on an SiO_2 column (4 cm x 30 cm) equilibrated in hexane. The column was eluted with EtOAc – hexane (1:9→1:0) in a stepwise gradient using 100 mL aliquots of solvent with 10% increase in EtOAc and collecting fractions of 100 mL. The individual fractions were examined by GC-MS. The fraction containing **1** was concentrated and further purified via preparative layer chromatography.

Preparative layer chromatography was performed using a circular plate (220 mm diameter, 2 mm silica layer: Merck PF245) installed on a Chromatotron (Harrison Research). The circular plate was reactivated at 100^{o}C for 1 hour and cooled to room temperature for 1 hour prior to use.

For initial bulk separation, the plate was eluted with successive 100 mL aliquots of hexane-diethyl ether (4:1, 7:3, 3:2) and collecting fractions of 15 mL followed by 100 mL of ethanol-diethyl ether (4:1) (purging eluent). The individual fractions were examined by GC-MS.

For final purification for bioassay, the plate was eluted with successive 50 mL aliquots of hexane-diethyl ether (4:1, 2:3, 4:1) and collecting fractions of 15 mL followed by 50 mL of ethanol-diethyl ether (4:1) (purging eluent). The individual fractions were examined by GC-MS.

Results and Discussion

3.1. Isolation and identification of caffeic acid and *p*-coumaric acid from the flavonoid fraction

The flavonoid fraction of New Zealand mānuka honey (fraction 5) showed the presence of a complex series of peaks when examined by HPLC (See **Fig. 3.1**). This fraction was initially believed to be composed of only flavonoids, however, a systematic evaluation of the peaks present in that fraction showed the presence of several non-flavonoid compounds including **1** which eluted at 35.0 minutes (see Section **2.2.7.1**) The two predominant non-flavonoid components of fraction 5 were identified as caffeic acid and *p*-coumaric acid (see **Figs. 3.2** and **3.3**).

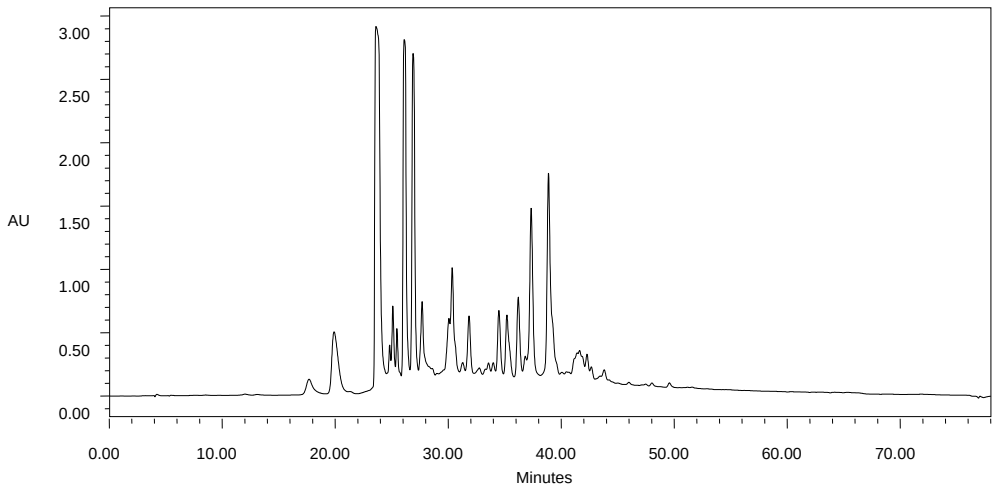

Fig. 3.1: HPLC Chromatogram of the flavonoid fraction 5 (UV wavelength 340 nm, gradient method 1).

Caffeic acid was identified as the peak eluting between 22.5 – 24.0 minutes using the chromatographic conditions (gradient method 1) described in **Section 2.2.3.1** (**Fig. 3.2**). ^{1}H NMR data determined for the isolated specimen was identical to that determined for an authentic specimen. Sample ^{1}H NMR (DMSO-d_6): δ 9.63 (broad s, 1H), 7.40 (d, 1H, J = 16.0 Hz), 7.01 (d, 1H, J = 2.0 Hz), 6.95 (dd, 1H, J = 8.0, 2.0 Hz) 6.75 (d, 1H, J = 16.0 Hz). Standard ^{1}H NMR (DMSO-d_6): δ 9.35 (broad s, 1H), 7.40 (d, 1H, J = 16.0 Hz), 7.01 (d, 1H, J = 2.0 Hz), 6.95 (dd, 1H, J = 8.0, 2.0 Hz) 6.75 (d, 1H, J = 16.0 Hz).

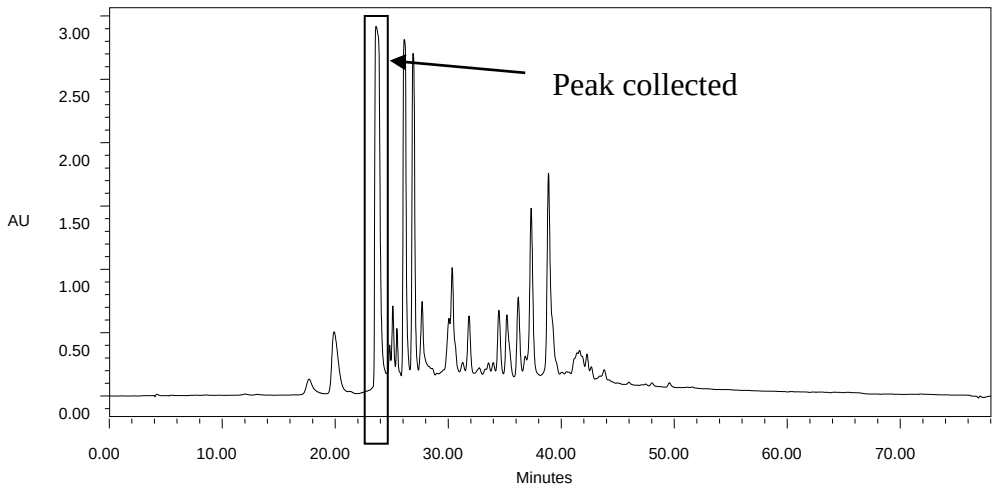

Fig. 3.2: HPLC Chromatogram of the flavonoid fraction showing the non-flavonoid peak (caffeic acid) which was collected (UV wavelength 340 nm, gradient method 1).

p-Coumaric acid was identified as the peak eluting between 26.1 – 26.9 minutes using the chromatographic conditions (gradient method 1) described in **Section 2.2.3.1** (**Fig. 3.3**). ^{1}H NMR data determined for the isolated specimen was identical to that determined for an authentic specimen.Sample ^{1}H NMR (DMSO-d_6): δ 11.70 (broad s, 1H), 9.98 (broad s, 1H), 7.50 (d, 2H, J = 8.4 Hz), 7.48 (d, 1H, J = 16.0 Hz), 6.79 (d, 2H, J = 8.4 Hz), 6.27 (d, 1H, J = 16.0 Hz). Standard ^{1}H NMR (DMSO-d_6): δ 12.11 (broad s, 1H), 9.95 (broad s, 1H), 7.52 (d, 2H, J = 8.4 Hz), 7.50 (d, 1H, J = 16.0 Hz), 6.78 (d, 2H, J = 8.4 Hz), 6.29 (d, 1H, J = 16.0 Hz).

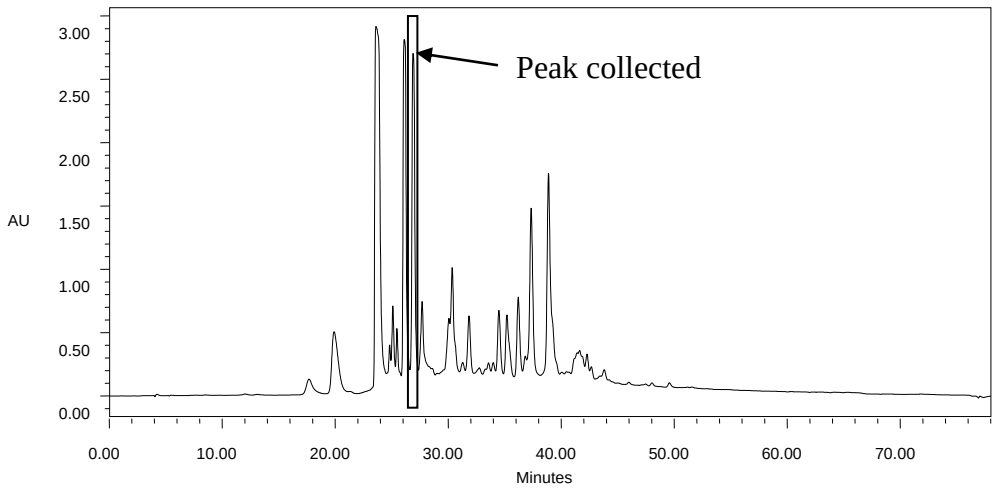

Fig. 3.3: HPLC Chromatogram of the flavonoid fraction showing the non-flavonoid peak (*p*-coumaric acid) which was collected (UV wavelength 340 nm, gradient method 1).

Although both caffeic acid and *p*-coumaric acid were found to be present in all of the 31 mānuka samples after reviewing HPLC chromatograms from Deadman's results,[45] quantification of the level of these compounds was not feasible. During the isolation of the flavonoid fraction from honey, one of the steps uses liquid-liquid extraction with diethyl ether (see **Section 2.2.7.3**) which removes the flavonoids from an aqueous solution of the phenolic fraction, leaving the majority of the phenolic acid derivatives and any remaining polar compounds in the aqueous layer. Hence the recovered diethyl ether extracts will typically contain less than the actual amount of caffeic acid and *p*-coumaric acid present in the honey.

3.2. Isolation of 1

1, which had a UV maximum at 340 nm (**Fig. 3.4**) was obtained from the flavonoid fraction of New Zealand mānuka honey by collecting the peak eluting between 35.0 - 35.5 minutes (**Fig. 3.5**) using the chromatographic conditions (gradient method 1) described in **Section 2.2.3.1**.

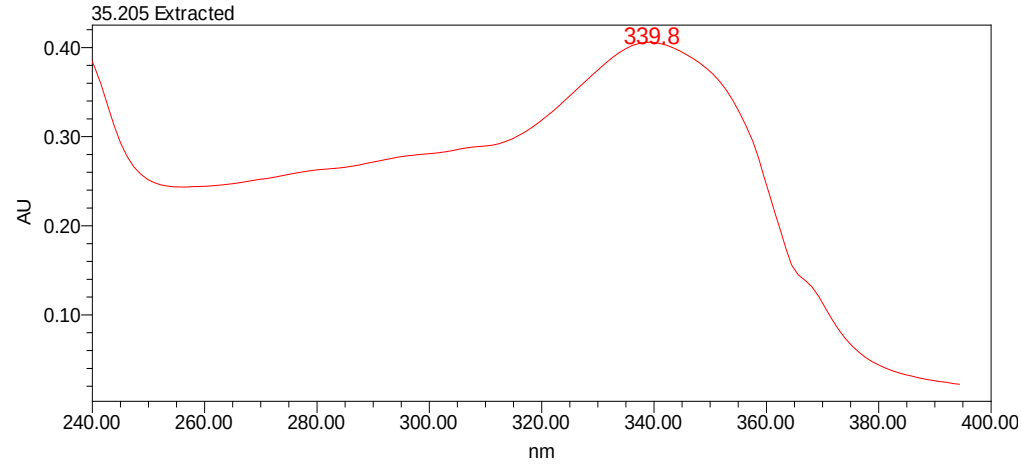

Fig. 3.4: UV Absorption spectrum of the peak which eluted at 35.2 minutes.

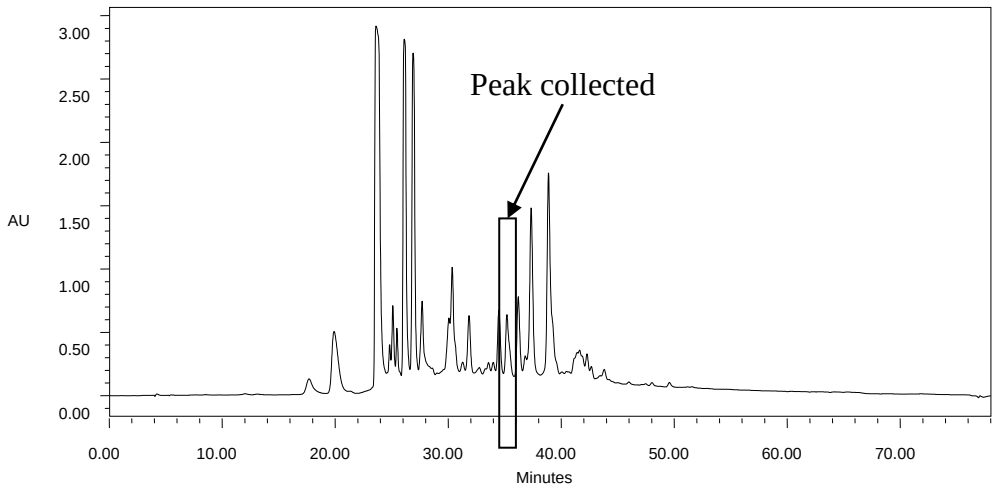

Fig. 3.5: HPLC Chromatogram of the flavonoid fraction showing peak collected (UV wavelength 340 nm, gradient method 1).

The collected fraction was further purified using gradient method 2 (**see Section 2.2.3.1**) and the peak eluting between 38 - 38.5 minutes was collected (**Fig. 3.6)**. The HPLC chromatogram of purified **1** is shown in **Fig. 3.7**.

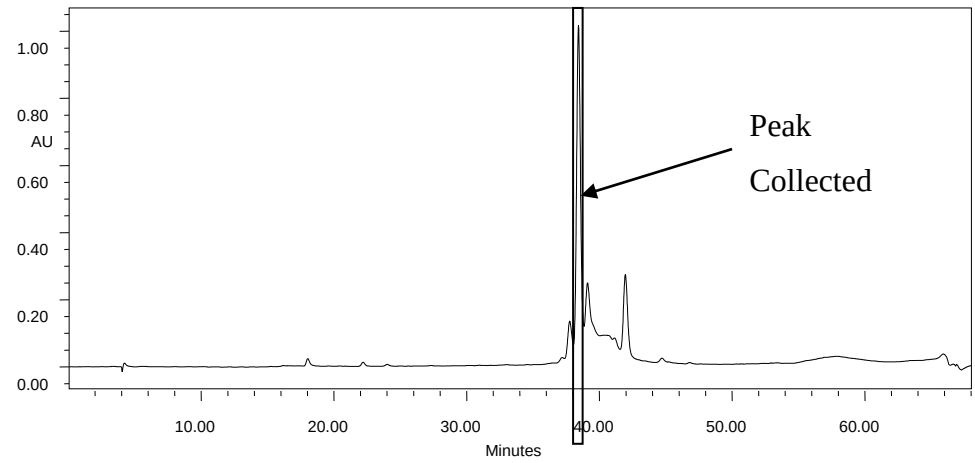

Fig. 3.6: HPLC Chromatogram of peak collected from flavonoid fraction (UV wavelength 340 nm, gradient method 2).

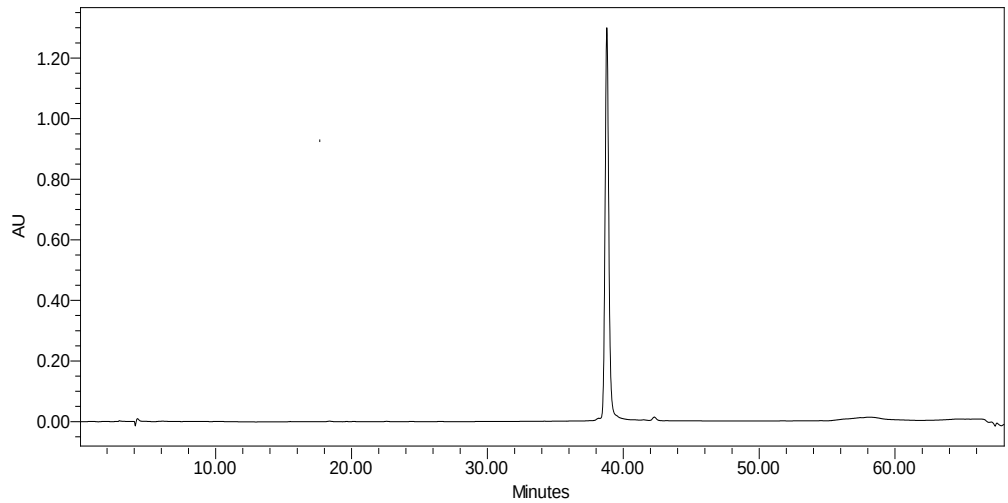

Fig. 3.7: HPLC Chromatogram of purified compound 1 (UV wavelength 340 nm, gradient method 2).

3.3. Structural determination of 1

1 was characterised using one and two-dimensional NMR spectroscopy and GC-MS. NMR spectral data determined for **1** was compared with the data determined from two reference compounds, 5-(2-nitrophenyl)-furfural (**3**) and 2-formyl-5-phenyl-pyrrole (**4**).

3.3.1. Characterisation of 1

3.3.1.1. ^{1}H NMR spectrum of 1

The ^{1}H NMR spectrum of **1**, in DMSO-d_6, is presented in **Fig. 3.8.** The ^{1}H NMR spectrum of **1** with presaturation of the DMSO and water (HOD) peaks and an expansion of the 6.7-7.9 ppm region are shown in **Fig. 3.9** and **Fig. 3.10** respectively. The chemical shifts and multiplicities of **1** are summarised in **Table 3.1**.

The chemical shift of the 3 proton singlet at 3.96 ppm is typical of a OCH_3 or $COOCH_3$ group, the 6 proton signals which occurred in the region 6-8 ppm are typical of aromatic or conjugated olefinic protons while the signal at 9.52 ppm is suggestive of a CHO group. The broad peak at 11.79 ppm can be attributed to an exchangeable proton (OH, COOH or NH) since this signal was absent (suppressed via exchange) in the water (HOD) presaturation experiment.

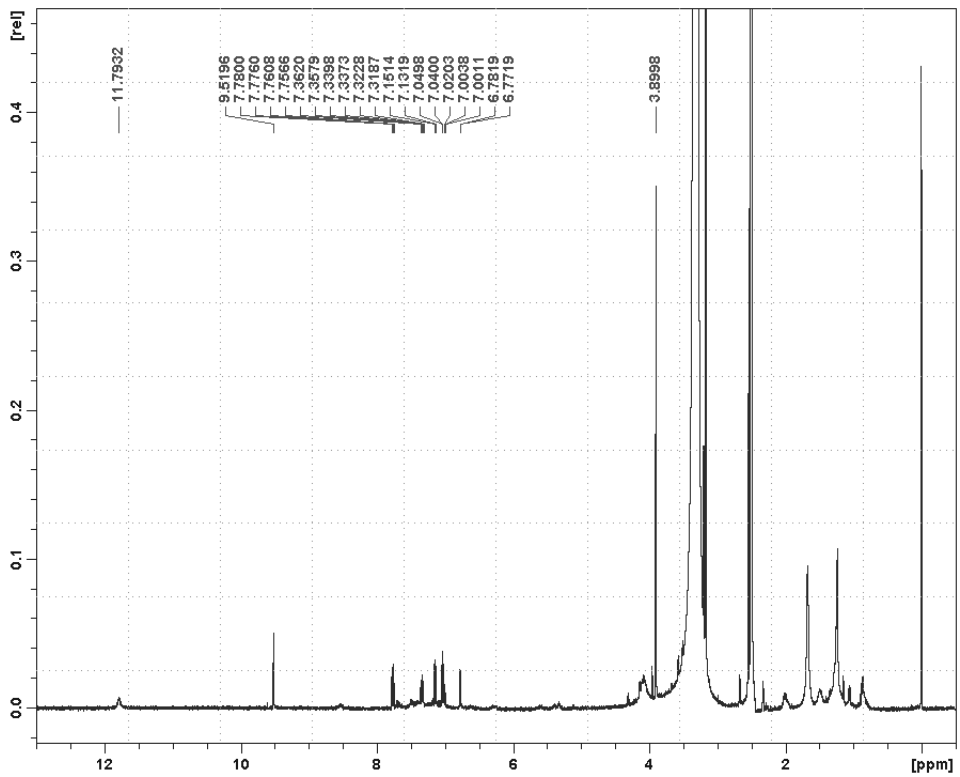

Fig. 3.8: ^{1}H NMR spectrum of 1 in DMSO-d_6.

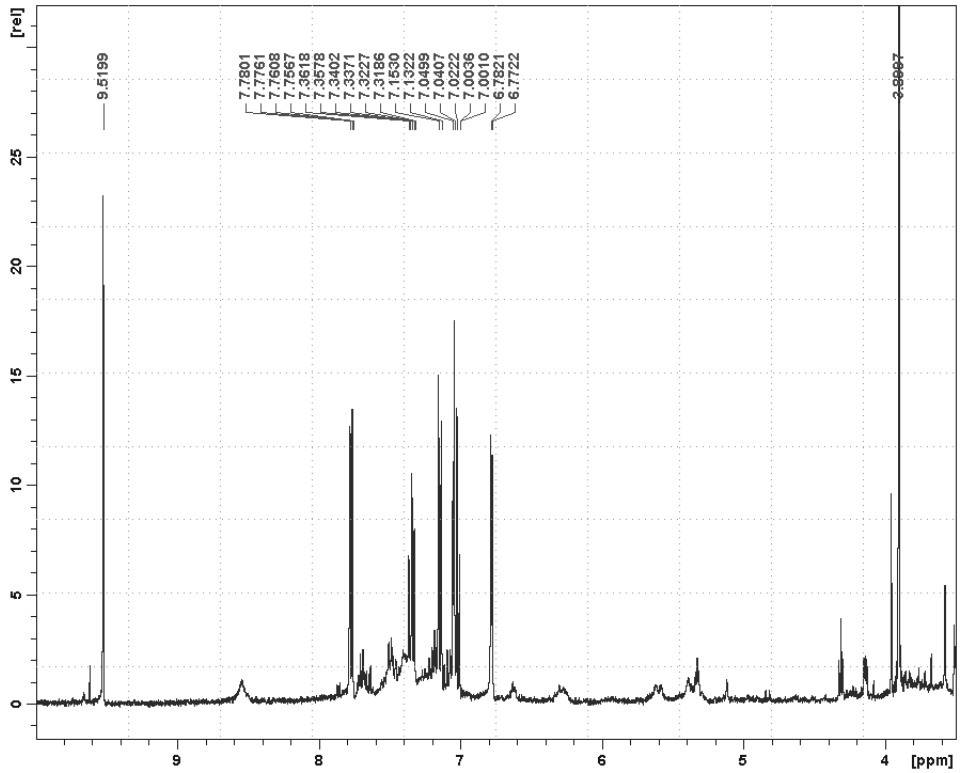

Fig. 3.9: ^{1}H NMR spectrum of 1 with water (HOD) and DMSO presaturation in DMSO-*d*$_6$.

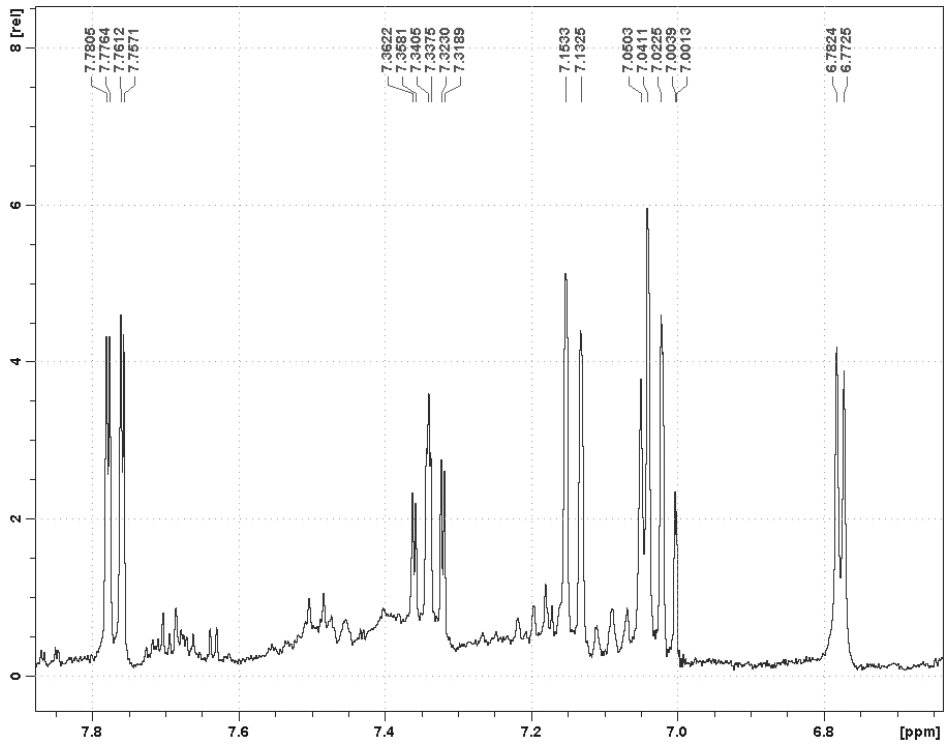

Fig. 3.10: Expansion of the 6.7-7.9 ppm region of the ^{1}H NMR spectrum of 1 in DMSO-*d*$_6$.

Table 3.1: ^{1}H NMR chemical shifts (δ in DMSO-d_6) and multiplicities of 1

Multiplicity	Chemical shift (ppm)
s	3.90
d (*J* = 3.9 Hz)	6.77
~td (*J* = 7.5, 1.2 Hz)	7.02
d (*J* = 3.9 Hz, partly concealed)	7.04
dd (*J* = 8.5, 1.2 Hz)	7.14
ddd (*J* = 8.5, 7.3, 1.7 Hz)	7.33
dd (*J* = 7.8, 1.7 Hz)	7.77
s	9.52
broad s	11.79

s: singlet; d: doublet; dd: doublet of doublets; ddd: doublet of doublets of doublets; td: triplet of doublets; *J*: coupling constant(s).

3.3.1.2. ^{1}H-^{1}H COSY spectrum of 1

The 6-8 ppm region of the homonuclear correlated spectroscopy (COSY) spectrum of **1** is shown in (**Fig. 3.11**). This spectrum was dominated by correlations arising from 3 bond couplings. Two independent spin systems, one comprised of 2 protons and the other 4 protons, were apparent in this region of the COSY spectrum. The 2 proton spin system was comprised of mutually coupled signals (*J* = 3.9 Hz) centred at 6.07 and 7.04 ppm. The coupling constant exhibited by these protons, while not typical of *cis* coupled aromatic protons, is typical of *cis*-coupled furan protons.

The 4 proton system was comprised of signals centered at 7.02, 7.14, 7.33 and 7.77 ppm. The signal at 7.77 ppm (dd, *J* = 7.8, 1.7 Hz) showed a correlation to the signal which occurred at 7.02 ppm (~td, *J* = 7.5, 1.2 Hz). This signal exhibited a correlation to the signal at 7.33 ppm (ddd, *J* = 8.5, 7.3, 1.7 Hz) which in turn showed a correlation to the signal at 7.14 ppm (dd *J* = 8.5, 1.2 Hz). The moderate ^3J (7-8 Hz) and smaller ^4J (1-2 Hz) couplings, combined with the COSY correlation pathway observed for these protons is typical of an *ortho*-substituted benzene (**Fig. 3.12**). If it was *para*-subsitituted only two ^{1}H peaks would be observed due to symmetry.

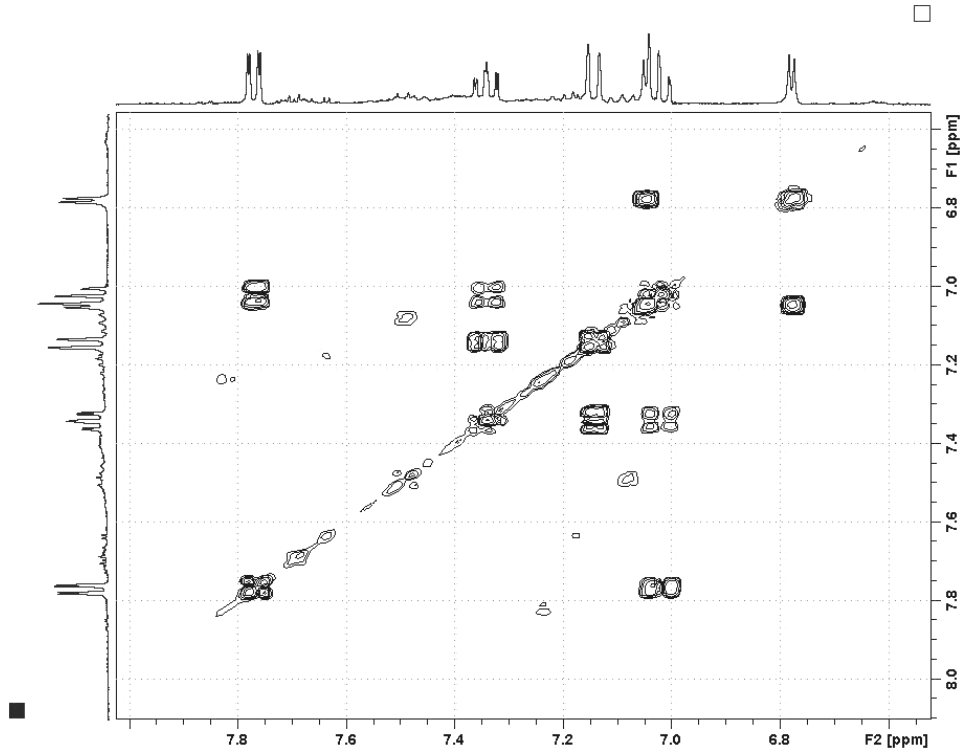

Fig. 3.11: ^{1}H-^{1}H COSY spectrum of the aromatic region of 1 in DMSO-*d*$_6$.

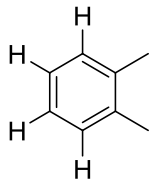

Fig. 3.12: An *ortho*-substituted benzene.

The conclusion that an *ortho*-substituted aromatic ring was present in **1** initially prompted the suggestion that it might be a disubstituted xanthone analogue (**Fig. 3.13**), one ring of which was 1,2- or 3,4-disubstituted and the other unsubstituted, rather than a flavonoid analogue. The UV maximum for most xanthones is >340 nm.

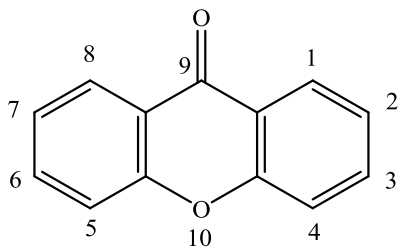

Fig. 3.13: General structure of a xanthone.[73]

However it was apparent that **1** cannot be a disubstituted xanthone. Firstly, the H-8 resonance of all xanthones with protons at 5, 6, 7 and 8 positions occur in the vicinity of 8.20 ppm[73] whereas the lowest field (highest ppm) proton resonance of **1** occurred at 7.77 ppm. Secondly the coupling constant (J = 3.9 Hz) of the signals which occurred at 6.07 and 7.04 ppm were not typical of those of mutually coupled aromatic protons (J = 7-9 Hz), no matter what other positions were substituted with OCH_3, OH or CHO groups (see **Section 3.2.1.1**).

3.3.1.3. ^{13}C NMR spectrum of 1

The ^{13}C NMR spectrum of compound **1**, in DMSO-d_6, is presented in **Fig. 3.14**. Tentative signal assignments are presented in **Table 3.2**. The signal to noise of the ^{13}C spectrum, after 72 hours was such that only protonated signals, namely OCH_3 (55.6 ppm), five or six aromatic or olefinic CH groups (114-129.5 ppm) (possibly including two signals at ca 120.7) and a conjugated aldehyde group (178.8 ppm). These groups were those indicated by ^{1}H NMR data (see **Section 3.2.1.1**). No quaternary carbon signals were observed after 72 hours of acquisition.

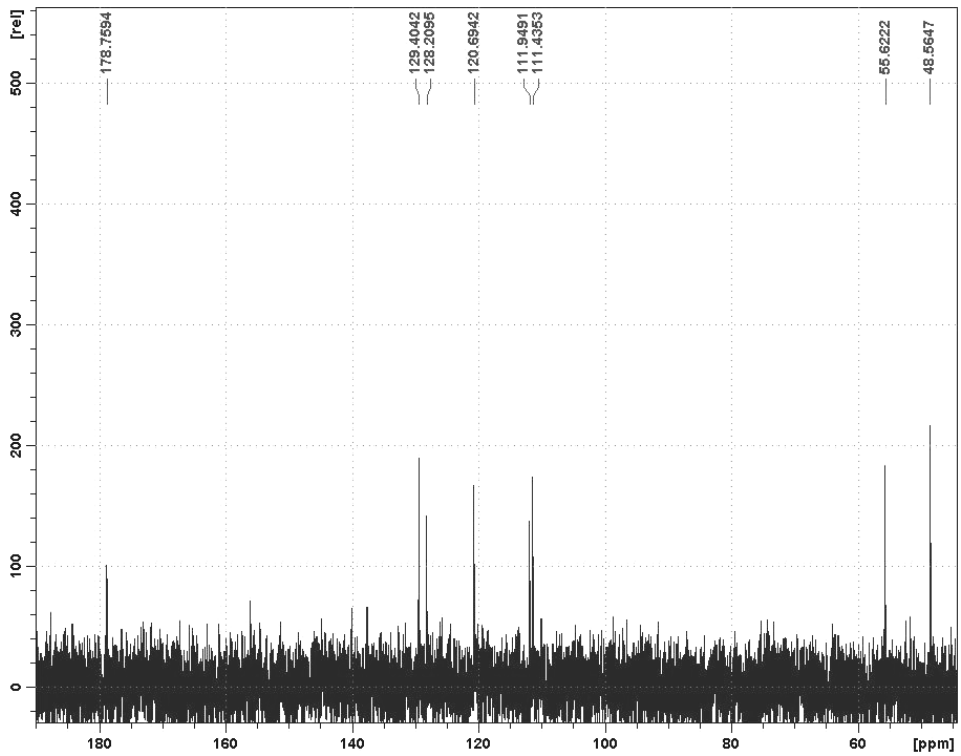

Fig. 3.14: ^{13}C NMR spectrum of 1 in DMSO-d_6.

Table 3.2: Tentative ^{13}C NMR signal assignments for 1 (δ ppm in DMSO-*d_6*)

Tentative assignment	Chemical shift (ppm)
CH_3OH (solvent)	48.6
OCH_3	55.6
Aromatic or conjugated olefinic CH's	111.4, 111.9, 120.7 (x2), 128.2, 129.5
conjugated CHO	178.8

3.3.1.4. HSQC spectrum of 1

The gradient edited ^{1}H detected Heteronuclear Single Quantum Coherence(HSQC) NMR spectrum (**Fig. 3.15**) showed correlations attributable to the ^{1}H and ^{13}C signals presented in **Tables 3.1** and **3.2** respectively. Correlations attributable to ^{1}J coupled ^{1}H and ^{13}C's are presented in **Table 3.3**. The HSQC spectrum verified that two carbons occurred at 120.7 ppm. These carbons showed correlations to protons which occurred at 7.02 and 7.04 ppm (see **Section 3.2.1.1**)

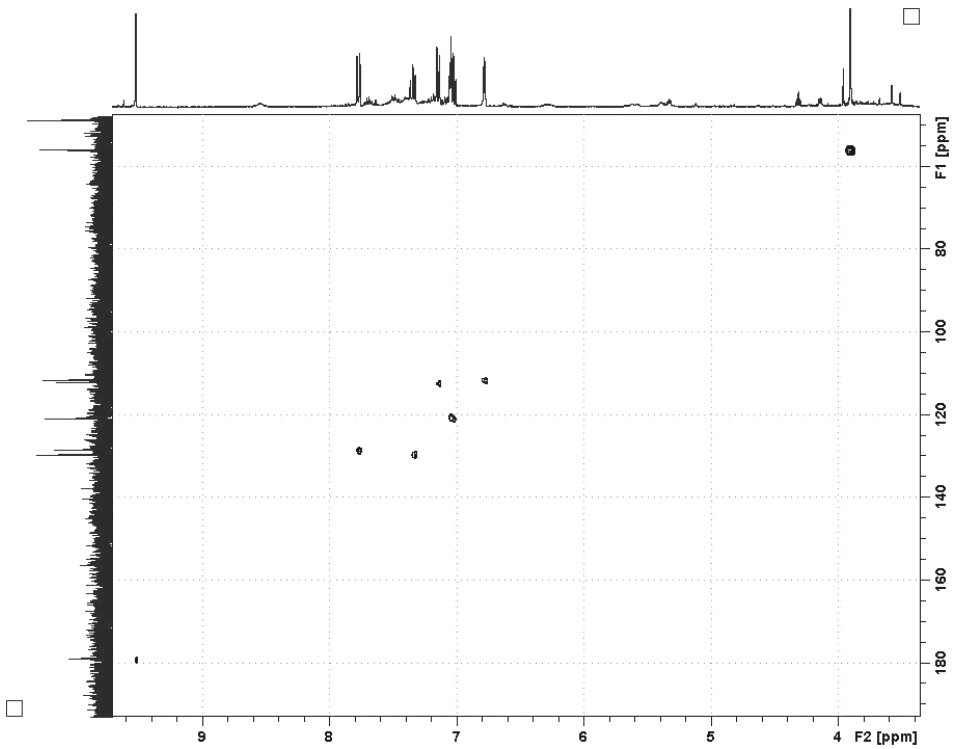

Fig. 3.15: HSQC spectrum of 1 in DMSO-*d_6*.

Table 3.3: HSQC correlations observed for 1 (δ ppm in DMSO-d_6)

Proton	3.90	6.77	7.02	7.04	7.14	7.33	7.77	9.52
Carbon	55.6	111.4	120.7	120.7	111.9	129.5	128.2	178.8

3.3.1.5. HMBC spectrum of 1

The Heteronuclear Multiple Bond Coherence (HMBC) spectrum of **1** determined with a mixing time of 65 msec showed correlations arising from ^2J, ^3J and possibly ^4J couplings (**Fig. 3.16**) which are summarised in **Table 3.4**. This revealed the presence of four quaternary carbons which were not visible in the ^{13}C or HSQC spectra.

The methoxyl (OCH_3) proton (3.96 ppm) showed a correlation to the quaternary carbon at 156.6 ppm. The aldehyde proton (9.52 ppm) showed a correlation to a quaternary carbon at 132.5 ppm. The large coupling constant (J = ~26 Hz at 2D resolution) is consistent with this proton exhibiting a ^2J, rather than a ^3J coupling to this carbon. The aromatic proton which occurred at 7.77 ppm showed a correlation to a quaternary carbon which occurred at 135.5 ppm, while the protons which occurred at 7.02 and 7.14 ppm showed correlations which occurred at 119.8 ppm. No long-range HMBC correlations were observed for the proton signals which occurred at 6.77 ppm and 7.04 ppm.

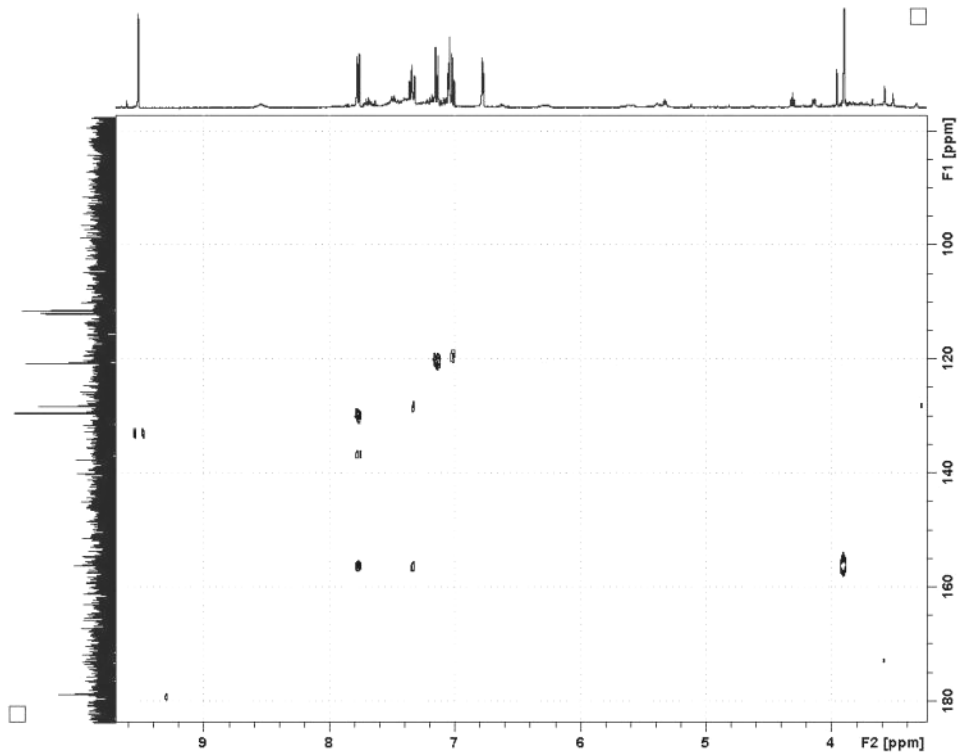

Fig. 3.16: HMBC spectrum of 1 in DMSO-d_6.

Table 3.4: ^{n}J HMBC correlations observed for 1 (δ ppm in DMSO-d_6)

Proton	3.90	7.02	7.14	7.33	7.77	9.52
Correlated Carbon(s)	156.6	119.8	119.8 120.7	128.2 156.6	129.5 135.5 156.6	132.5

3.3.1.6. SELNOESY spectra of 1

A 1D-selective NOESY (SELNOESY) experiment, in which the C<u>H</u>O signal (9.52 ppm) was irradiated, enhanced the signal which occurred at 7.04 ppm (d, J = 3.9 Hz) (see **Fig. 3.17 b**). This result demonstrated that the group was distant from the mutually coupled set of 4 aromatic protons (**Fig. 3.17 b**).

A SELNOESY experiment, in which the OC<u>H</u>$_3$ signal (3.96 ppm) was irradiated, enhanced the aromatic proton which occurred at 7.77 ppm (dd, J = 7.8, 1.7 Hz) (see **Fig. 3.17 c**). This observation showed that the OCH_3 group was attached to the benzene ring of **1**.

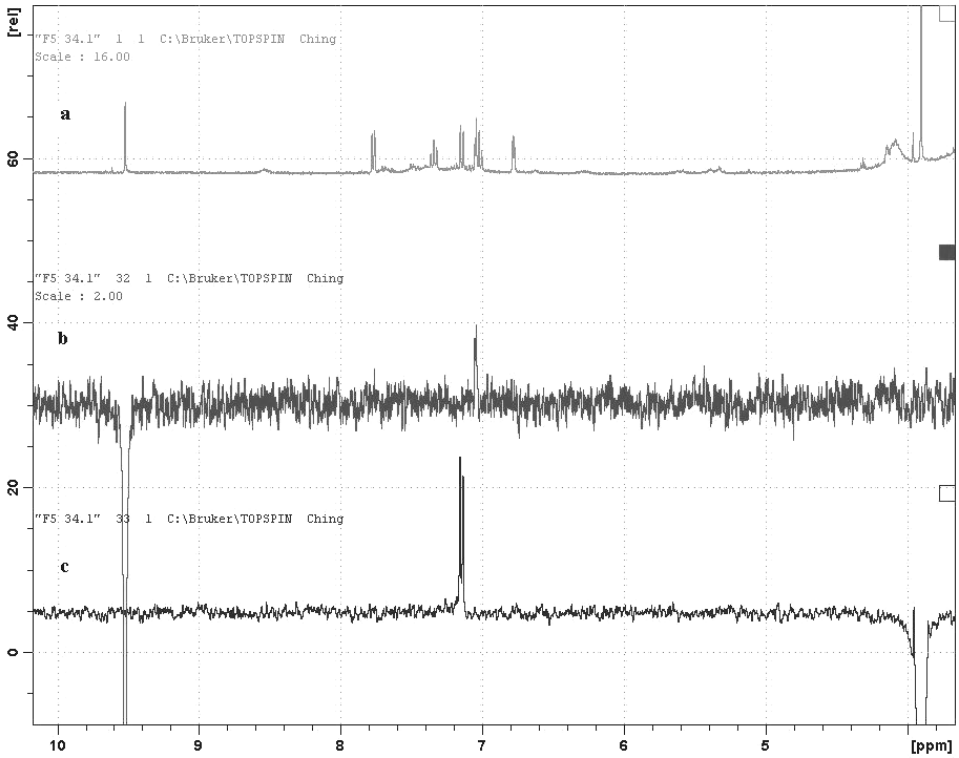

Fig. 3.17: SELNOESY spectra determined for 1 in DMSO-d_6 a: ^{1}H NMR. b: irradiation of the C<u>H</u>O signal (9.52 ppm). c: irradiation of the OC<u>H</u>$_3$ (3.96 ppm) signal.

The coupling constant of the olefinic proton (7.14 ppm, d, J = 3.9 Hz) which was enhanced when the aldehyde proton was irradiated, while not typical of a *cis*-coupled aryl proton or olefinic proton in a 7- or 8-membered ring, was typical of a *cis*-coupled proton in a 5-membered ring such as a furan ring (J = 3.9 Hz).[74]

Hence it was concluded that the structure of **1** was likely to be comprised of two parts: (i) an *ortho*-substituted benzene with an OCH_3 group (**Fig. 3.18)** and (ii) a 5-membered furan ring or one in which an X group (eg. an NH group) was present rather than an oxygen atom (**Fig. 3.19**)

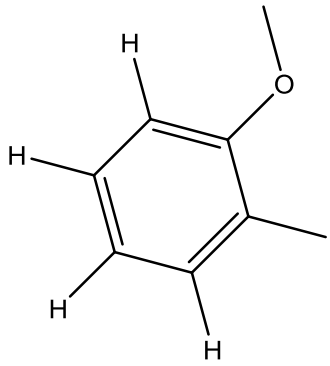

Fig. 3.18: An *ortho*-substituted benzene with a OCH_3 group.

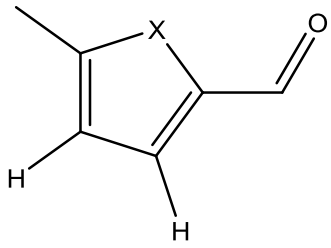

Fig. 3.19: *cis*-protons and a CHO group on a 5-membered ring where X can be O or N or S.

The nature of the X group, or that of the linkage between the two sub-units could not be deduced from the available NMR data because the quantity of the isolated material was too limited to yield sufficient spectral information.

The GC-MS characteristics of **1** were investigated in the belief that MS data might be able to establish the molecular weight of **1**, which, when combined with the available NMR information, should be able to identify the X-group and the nature of the linkage between the two sub units.

3.3.1.7. GC-MS analysis of 1

Gas Chromatography – Mass Spectrometry (GC-MS) analysis of **1** was performed using the conditions described in **Section 2.2.4.** This afforded a peak with a retention time of 10.05 minutes which showed a probable M^+ ion at *m/z* 201 and a series of fragment ions, including distinctive*m/z* 158 and 130 ions (**Fig. 3.20**).

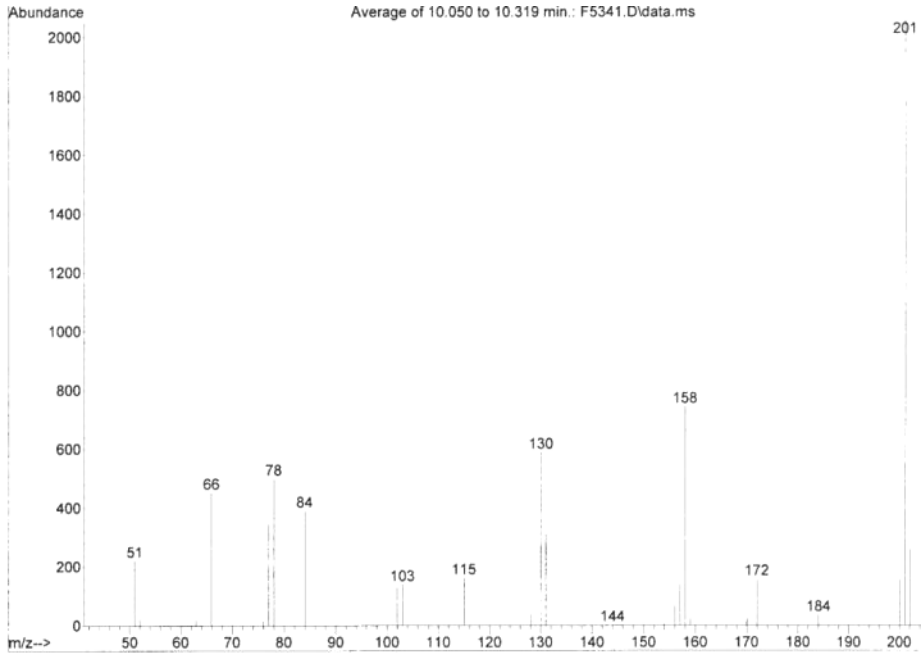

Fig. 3.20: Mass spectrum of 1.

Since compounds possessing an aldehyde group are frequently characterised by the loss of a hydrogen atom to afford a high intensity $(M-H)^+$ ion, the conclusion that the M^+ ion of **1** occurs at *m/z* 201 (the highest intensity ion observed in the mass spectrum) must be treated with caution since it can also indicate that the molecular ion of the compound which afforded the mass spectrum depicted in **Fig. 3.20** occurs at *m/z* 202 and that the base peak *m/z* 201 ion is a $(M-H)^+$ ion derived from it. It is however more likely that the *m/z* 202 ion is the ^{13}C isotope ion of the *m/z* 201 ion, and that only a weak $(M-H)^+$ ion occurs at *m/z* 200 (see **Fig. 3.20**).

No structural significance could be attached to the *m/z* 158, 130 and other fragment ions observed in the mass spectrum of **1**.

A search of the literature for compounds possessing molecular weights of 201 or 202 Daltons and subunits of the type presented in **Section 3.2.1.6** identified 5-(2-methoxyphenyl)-2-furaldehyde (**2**) as a compound which had a mass of 202 Daltons.

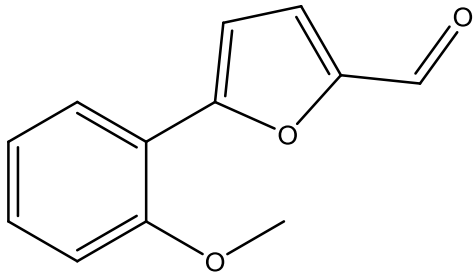

2

NMR data reported by Hosoya *el al.*[75] for 5-(2-methoxyphenyl)-2-furaldehyde (**2**) is: ^{1}H NMR (400MHz, $CDCl_3$) δ 3.97 (3H, s), 6.99–7.01 (1H, m), 7.07 (1H, dt, *J* = 7.6, 1.3 Hz), 7.14 (1H, d, *J* = 3.8 Hz), 7.34 (1H, d, *J* = 3.8 Hz), 7.35– 7.39 (1H, m), 8.05 (1H, dd, *J* = 7.6, 1.3 Hz), 9.65 (1H, s) and ^{13}C NMR (100MHz, $CDCl_3$) δ 55.4, 111.1, 112.5, 118.0, 120.9, 123.9, 127.4, 130.6, 150.9, 156.1, 156.8, 177.1.

Although the solvent used to determine NMR spectral data for **1** was DMSO-d_6 whereas for 5-(2-methoxyphenyl)-2-furaldehyde (**2**) it was chloroform-d_1, the absence of a proton signal at 11.79 ppm as recorded for **1** (see **Table 3.1**) indicated **1** could not be 5-(2-methoxyphenyl)-2-furaldehyde (**2**). The coupling constant observed for the two proposed furan protons (*J* = 3.8 Hz) was consistent with the suggestion that a 5 membered ring system, in which the O atom of **2** was replaced by an NH or S group, was present in **1**. Moreover replacement of the furan oxygen atom by an NH group would afford a substance with a molecular weight of 201 Daltons which appears to be the case for **1**.

3.3.2. 5-(2-nitrophenyl)-2-furaldehyde (3)

A specimen of 5-(2-methoxyphenyl)-2-furaldehyde (**2**) was not available in the Chemistry Department. However there was a specimen of 5-(2-nitrophenyl) -2-furaldehyde (**3)**. One and two dimensional NMR spectral data for this compound was acquired in DMSO-d_6 in the expectation that this data would serve as a useful model for substances possessing directly linked aromatic and furan or other aldehyde substituted 5-member ring heterocyclic compounds. It was of interest to establish if (for example) under the conditions used to determine the HMBC spectrum of **3** (and also **1**) H-6 would exhibit a ^{3}J correlation to C-5', or

H-4' exhibited a ^{3}J correlation to C-1, thereby demonstrating that the aromatic and furan rings were directly linked.

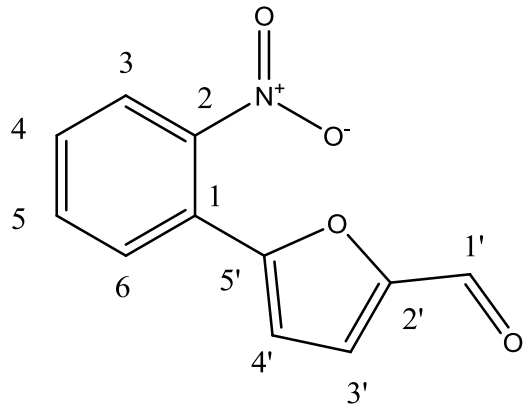

3

3.3.2.1. ^{1}H NMR spectrum of 3

The ^{1}H NMR spectrum of **3**, in DMSO-d_6, is presented in **Fig. 3.21**. Signal assignments are presented in **Table 3.5**.

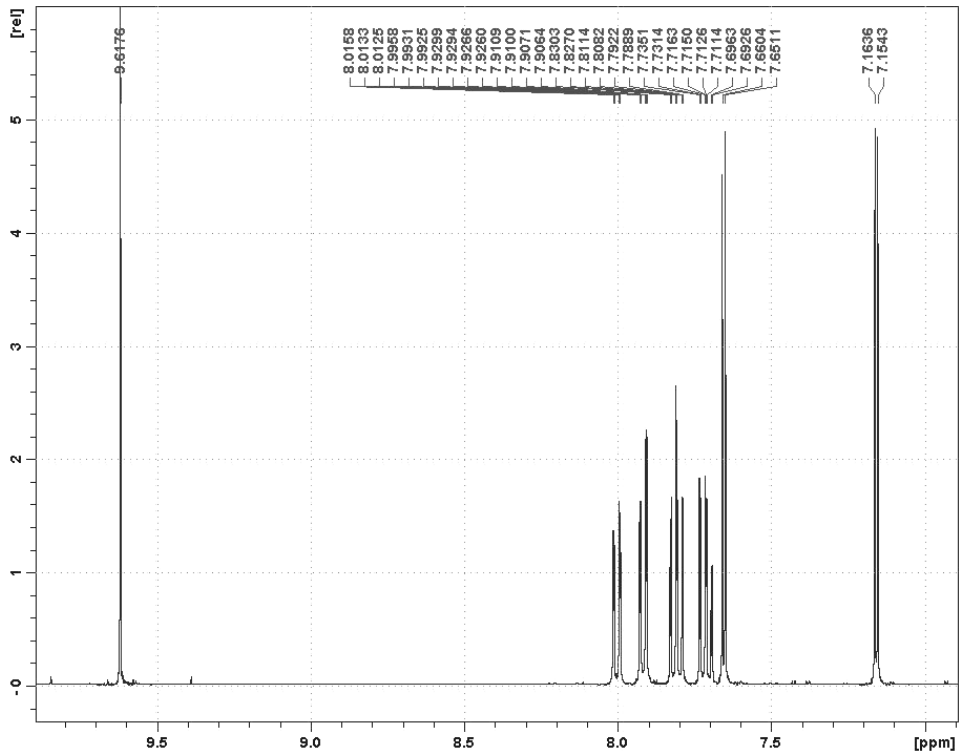

Fig. 3.21: ^{1}H NMR spectrum of 3 in DMSO-d_6.

Table 3.5: ^{1}H NMR assignments of 3 (δ ppm in DMSO-d_6)

Assignment	Multiplicity	Chemical shift
1'	s	9.62
3'	d (J = 3.7 Hz)	7.65
4'	d (J = 3.7 Hz)	7.15
3	dd (J = 8.0, 1.3 Hz)	8.01
4	ddd (J = 8.0, 7.5, 1.4 Hz)	7.71
5	td (J = 7.7, 1.3 Hz)	7.81
6	dd (J = 7.7, 1.4 Hz)	7.92

3.3.2.2. ^{13}C NMR spectrum of 3

The ^{13}C NMR spectrum of **3** in DMSO-d_6, is presented in **Fig. 3.22**. Signal assignments are given in **Table 3.6**.

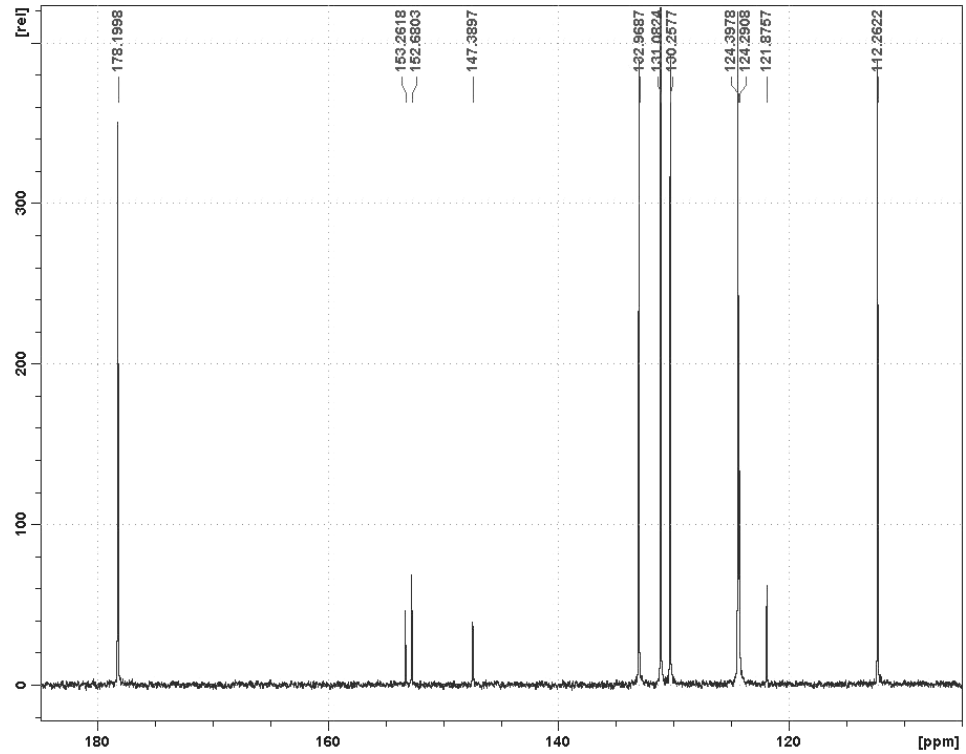

Fig. 3.22: ^{13}C NMR spectrum of 3 in DMSO-d_6.

Table 3.6: ^{13}C NMR assignments of 3 (δ in DMSO-d_6)

Assignment	Chemical shift (ppm)
1'	178.2
2'	152.7
3'	124.3
4'	112.3
5'	153.3
1	121.9
2	147.4
3	124.4
4	131.1
5	133.0
6	130.2

3.3.2.3. HMBC spectrum of 3

The gradient edited HMBC spectrum of **3**, in DMSO-d_6, is presented in **Fig. 3.23.** Correlations observed for **3** are listed in **Table 3.7** and depicted in **Fig 3.24.**

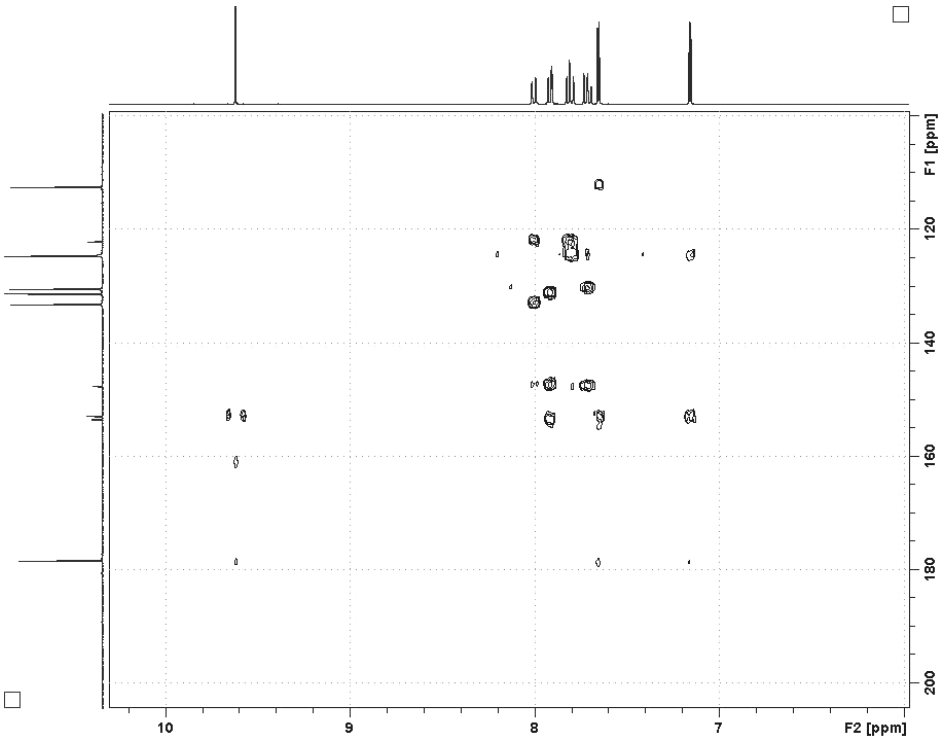

Fig. 3.23: HMBC spectrum of 3 in DMSO-d_6.

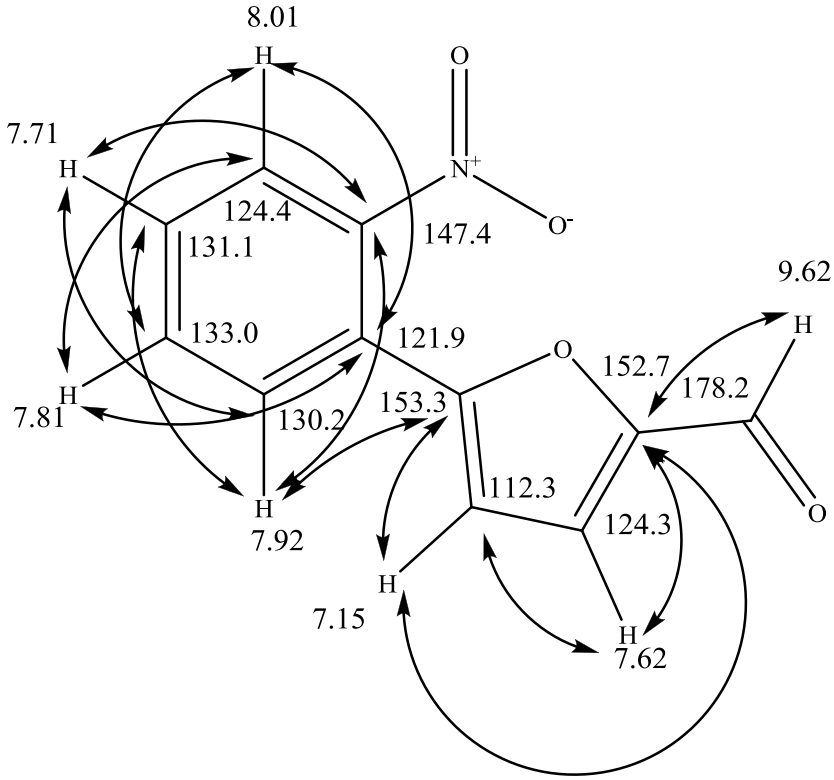

Fig. 3.24: HMBC correlations observed for 3 (δ ppm in DMSO- d_6).

Table 3.7: ^{n}J HMBC correlations observed for 3 (δ ppm in DMSO- d_6)

Proton	7.15 (H-4')	7.62 (H-3')	7.71 (H-4)	7.81 (H-5)	7.92 (H-6)	8.01 (H-3)	9.62 (H-1')
Correlated carbon (s)	124.3 (C-3') 152.7 (C-2')	112.3 (C-4') 152.7 (C-2')	130.2 (C-6) 147.4 (C-2)	121.9 (C-1) 124.4 (C-3)	131.1 (C-4) 147.4 (C-2) 153.3 (C-5')	121.9 (C-1) 133.0 (C-5)	152.7 (C-2')

Under standard HMBC conditions, using a 65 msec mixing time predominantly ^{3}J correlations were observed for **3**.

In particular it should be noted that the H-6 proton (7.92 ppm) showed a ^{3}J correlation to C-5'. This was the only proton, which under standard HMBC conditions, exhibited an inter-ring correlation. The correlations exhibited by H-6

of **3** can be viewed as being analogous to those which would be exhibited by the equivalent proton of **1**, namely the proton which occurs at 7.77 ppm.

In order to maximise the intensity for ^{n}J HMBC correlations observable for **3**, and by implication also for **1**, a series of eight HMBC experiments were run for **3** using mixing times (D6 values) of 35 msec (**Fig. 3.25**), 50 msec (**Fig. 3.26**), 65 msec (**Fig. 3.27**), 80 msec (**Fig. 3.28**), 100 msec (**Fig. 3.29**), 120 msec (**Fig. 3.30**), 160 msec (**Fig. 3.31**) and 200 msec (**Fig. 3.32**).

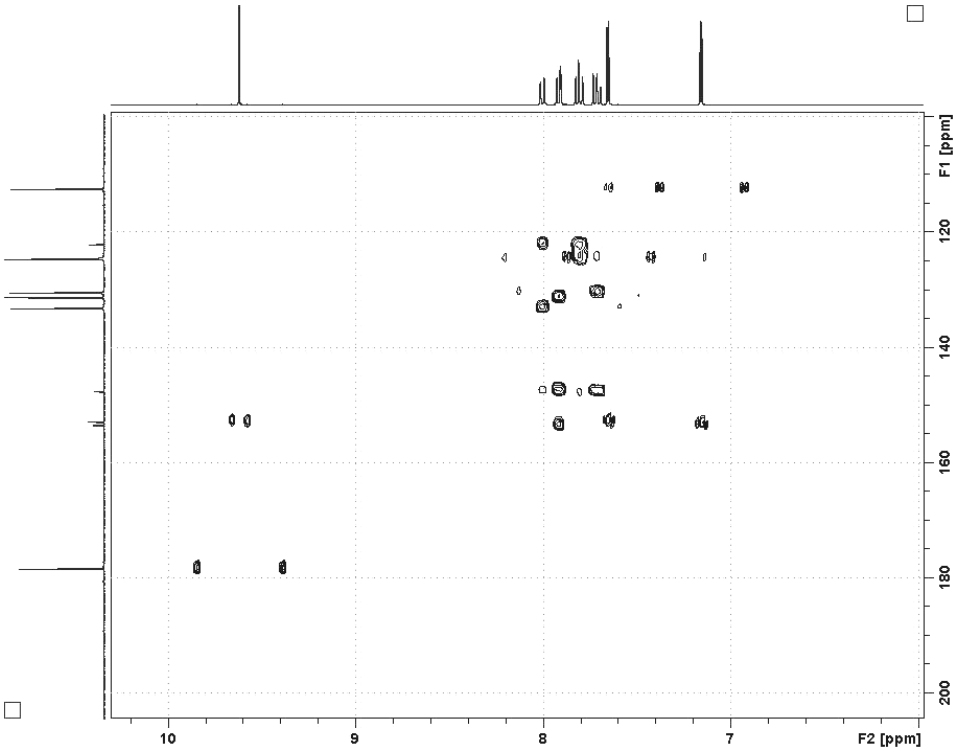

Fig. 3.25: HMBC spectrum of 3 in DMSO-d_6 with D6 = 35 msec.

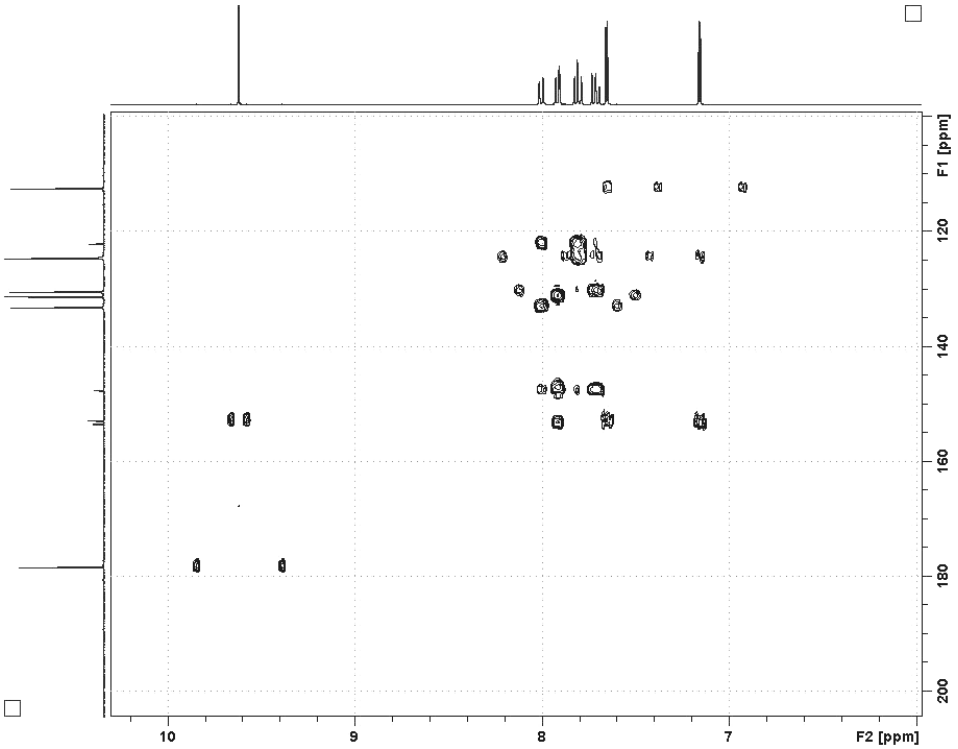

Fig. 3.26: HMBC spectrum of 3 in DMSO-d_6 with D6 = 50 msec.

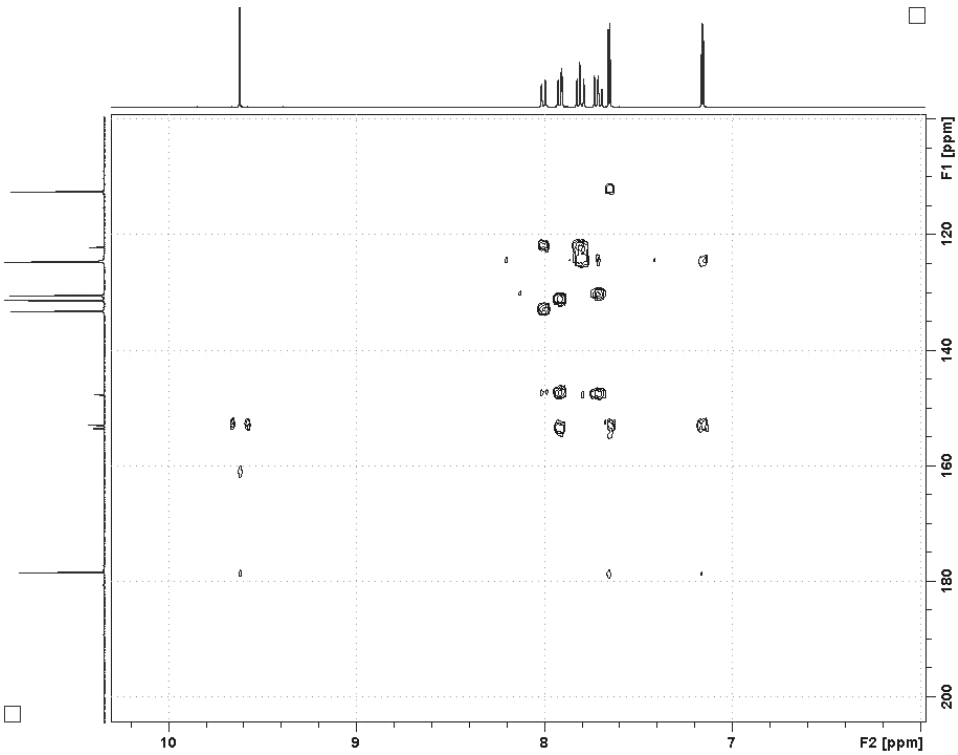

Fig. 3.27: HMBC spectrum of 3 in DMSO-d_6 with D6 = 65 msec.

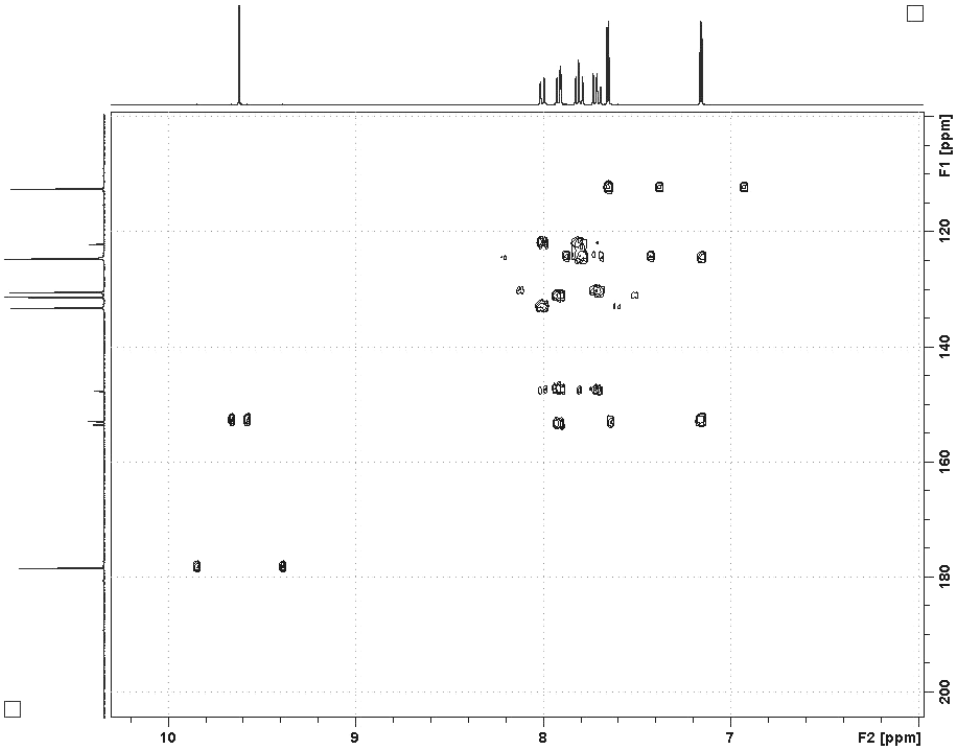

Fig. 3.28: HMBC spectrum of 3 in DMSO-d_6 with D6 = 80 msec.

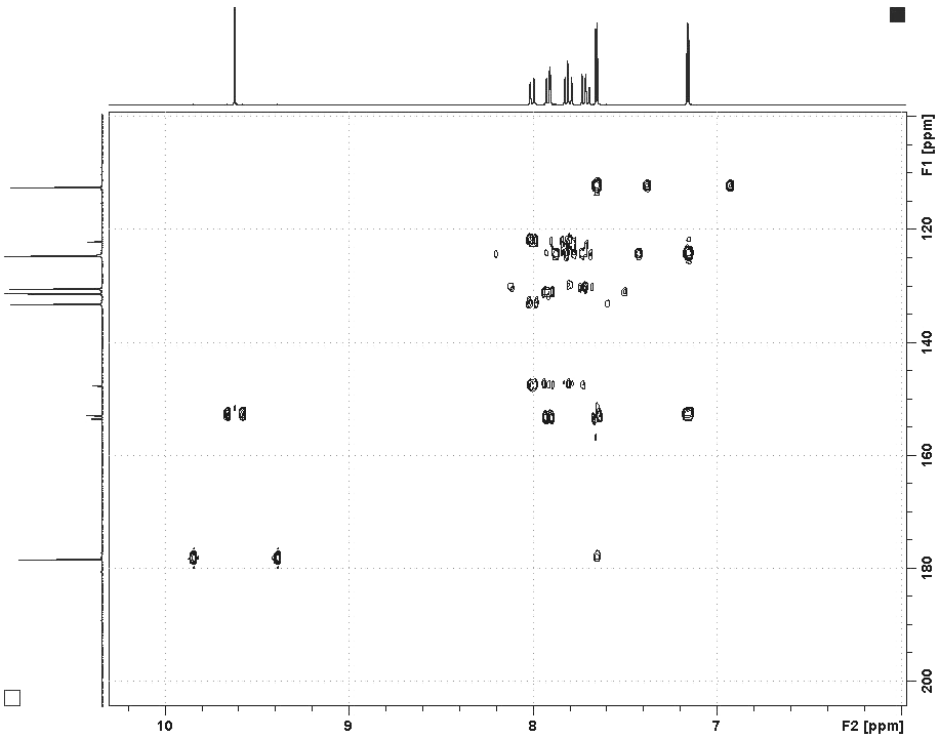

Fig. 3.29: HMBC spectrum of 3 in DMSO-d_6 with D6 = 100 msec.

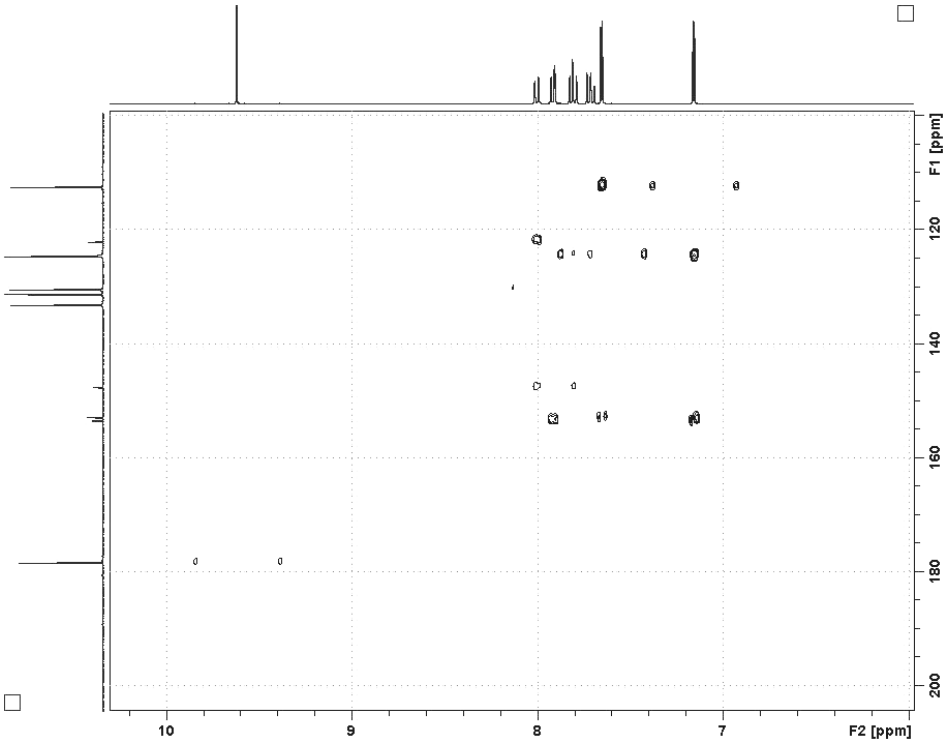

Fig. 3.30: HMBC spectrum of 3 in DMSO-d_6 with D6 = 120 msec.

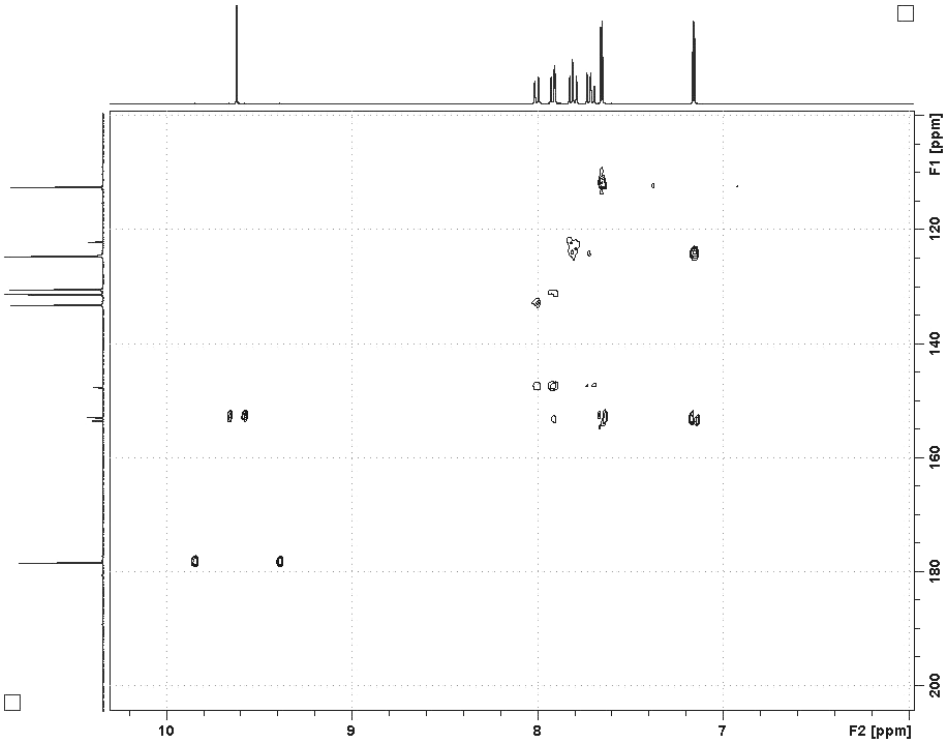

Fig. 3.31: HMBC spectrum of 3 in DMSO-d_6 with D6 = 160 msec.

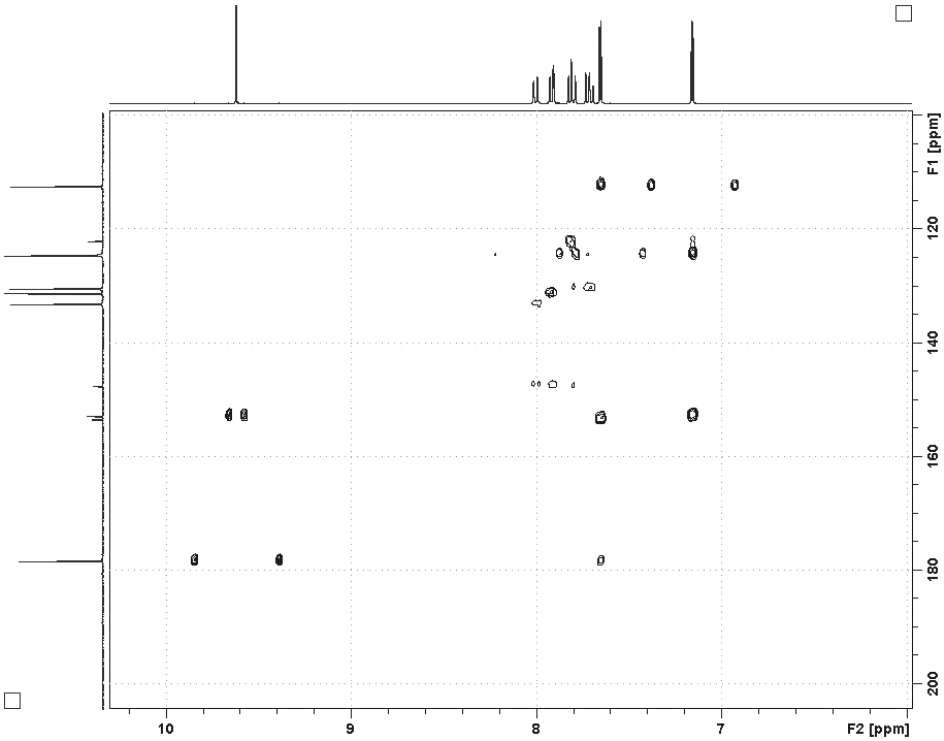

Fig. 3.32: HMBC spectrum of 3 in DMSO-d_6 with D6 = 200 msec.

The intensity of the carbon correlations exhibited by H-6 (7.92 ppm) of **3** as a function of the mixing time (D6 value) is depicted in **Fig 3.33**. The maximum intensity for the ^{3}J correlations exhibited by this proton to C-4 (131.1 ppm), C-2 (147.4 ppm) and C-5' (153.3 ppm) (the only observable inter-ring correlation) occurred with a mixing time of 50 msec. Weaker ^{2}J or ^{4}J correlations to C-1 (121.9 ppm) and C-3 (124.4 ppm) respectively were also observed in spectra determined with longer mixing times (see **Fig. 3.33**).

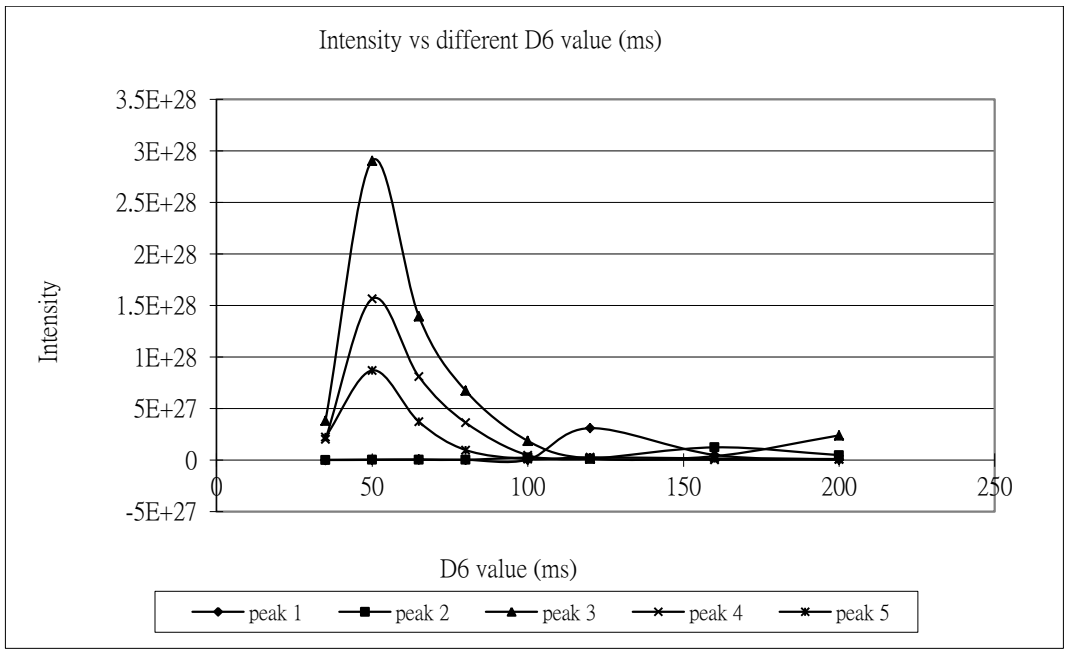

Fig. 3.33: Plot of the intensity of ^{n}J correlations exhibited by H-6 of 3 (7.92 ppm) *versus* mixing time (msec) (peak 1: C-1, 121.9 ppm (^{2}J); peak 2: C-3 124.4 ppm (^{4}J); peak 3: C-4- 131.1 ppm (^{3}J); peak 4: C-2, 147.4 ppm (^{3}J); peak 5: C-5', 153.3 ppm (^{3}J)).

3.3.2.4. HMBC spectrum of 1 with D6 = 50 msec

Since the maximum intensity of ^{3}J correlations exhibited by **3**, including the inter-ring H-6 to C-5' correlation occurred using a 50 msec mixing time, the HMBC spectrum of **1** was re-run with a mixing time of 50 msec. The HMBC spectrum of **1** determined using D6 = 50 msec is presented in **Fig. 3.34**. A greater number of scans per increment was also used when recording the 50 msec HMBC spectrum of **1** in the expectation that this would improve the signal to noise of the spectrum. There was an additional correlation from the 7.02 ppm proton signal to 111.4 ppm carbon signal which was not observed in the previous HMBC spectrum of **1** (see **Fig. 3.16**).

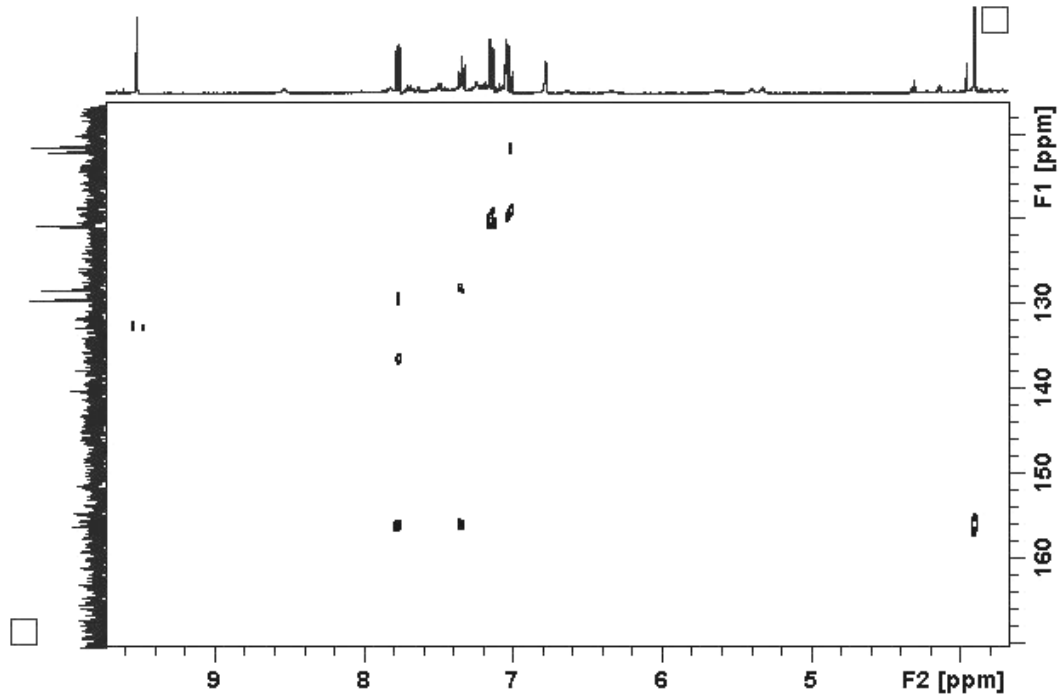

Fig. 3.34: HMBC spectrum of 1 with D6 = 50 msec in DMSO-d_6.

The three correlations observed in the 50 msec HMBC spectrum for the 7.77 ppm proton signal of **1** (see **Fig 3.34**) can be attributed to ^{3}J correlations rather than ^{2}J or ^{4}J correlations based on the model compound data presented in **Fig 3.32** for **3** since only high intensity correlations would be detectable in the HMBC spectrum, given the small quantity of **1** available for structural analysis.

Two of the observed correlations can be attributed to correlation between H-6 and C-2 (156.6 ppm) and C-4 (129.4 ppm) respectively. The third correlation, to the ^{13}C signal that occurred at 135.5 ppm can be attributed to an inter-ring correlation to C-5'. Whereas the C-5' of **3** occurs at 153.3 ppm, it can be anticipated, based on an analysis of chemical shift data for furans and pyrroles,[72] that the C-5' resonance of the pyrrole analogue of **3** (ie the structure proposed in **Section 3.2.1** for **1**) would occur at a lesser chemical shift, in the vicinity of 130-140 ppm. Moreover structure **1** is consistent with the detection in the ^{1}H NMR of **1** of a signal at 11.79 ppm, assignable to a pyrrole NH proton. Hence the structure proposed for **1** was 2-formyl-5-(2-methoxyphenyl)-pyrrole.

3.3.2.5. GC-MS analysis of 3

GC-MS analysis of **3,** under identical conditions used for **1,** afforded a peak which had a retention time 11.98 minutes and showed a weak M^+ ion at *m/z* 217 together with a base peak fragment ion at *m/z* 188 attributable to a $(M - CHO)^+$ ion (**Fig. 3.35**). The observation that the retention time of **3** was greater than that determined for **1** is consistent with the conclusion that **1**, showing that it was a less polar, lower molecular weight variant of **3**.

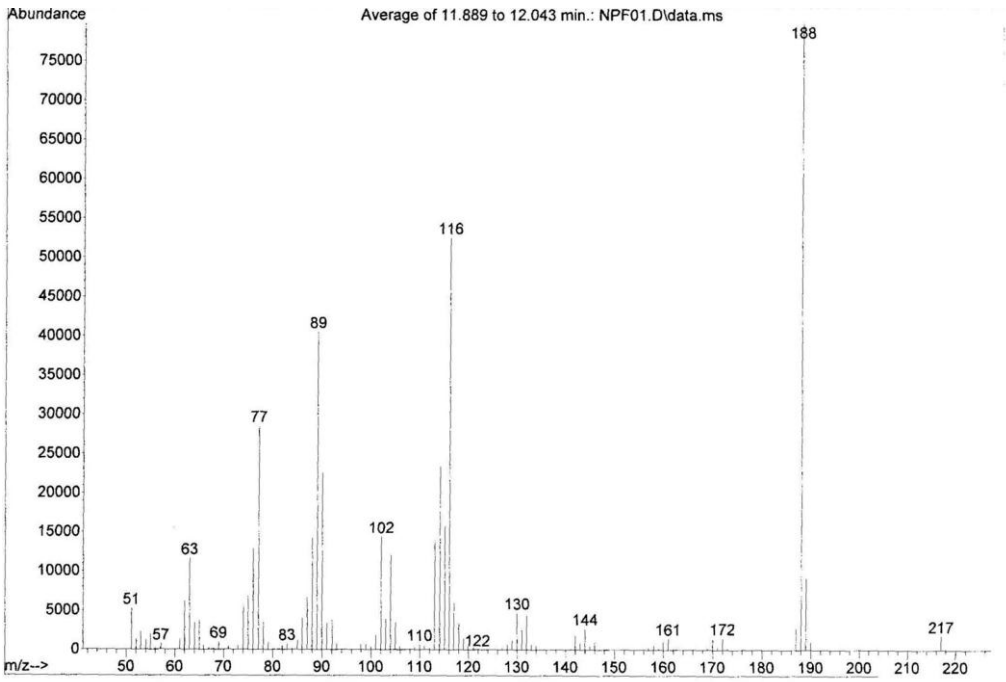

Fig. 3.35: Mass spectrum of the GC-MS peak which eluted at 11.98 minutes.

3.3.3. 2-formyl-5-phenyl-pyrrole (4)

The proposal that **1** might be a 2-formyl-5-(2-methoxyphenyl)-pyrrole prompted a search of the literature for reports of the occurrence or synthesis of this compound, or close analogues of it. Reeves *et al.*[72] has reported the synthesis of **4**. The structure of this compound only differs from that proposed for **1** in that it lacks the aryl ring methoxy group.

A specimen of **4**, generously donated by Dr J. T. Reeves, was used to determine the one and 2D-NMR spectral features of this compound in DMSO-d_6, in the expectation that this data would verify the presence of 2'-formyl substituted pyrrole ring system in **1**.

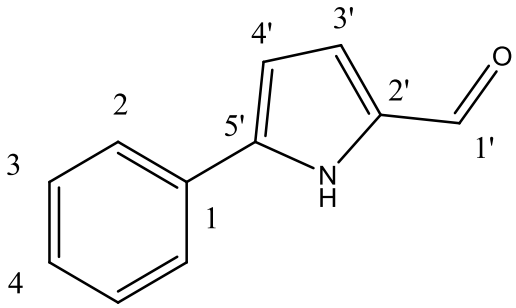

4

3.3.3.1. ^{1}H NMR spectrum of 4

The ^{1}H NMR spectrum of **4**, in DMSO-d_6, is presented in **Fig. 3.36.** Signal assignments are presented in **Table 3.8**. Notably the ^{1}H NMR spectrum of **4** included an aldehyde signal at 9.50 ppm and a broad singlet signal at 12.39 ppm, attributable to the NH proton of **4**. The chemical shift of this proton was reminiscent of that of the aldehyde signal at 9.52 ppm and broad singlet signal at 11.79 ppm observed in the ^{1}H NMR spectrum of **1** (see **Table 3.1**) .

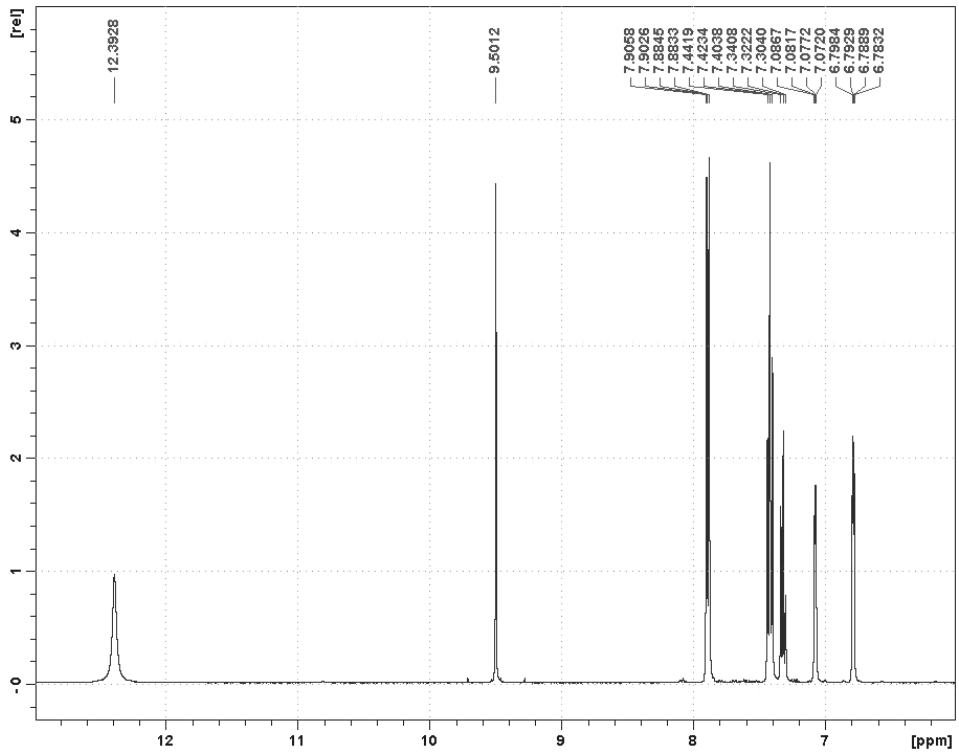

Fig. 3.36: ^{1}H NMR spectrum of 4 in DMSO-d_6.

Table 3.8: ^{1}H NMR assignments of 4 (δ in DMSO-d_6)

Assignment	Multiplicity	Chemical shift (ppm)
1'	s	9.50
3'	dd (*J* = 3.9, 2.3 Hz)	7.08
4'	dd (*J* = 3.9, 2.3 Hz)	6.79
2	d (*J* = 7.6 Hz)	7.89
3	t (*J* = 3.9, 2.0 Hz)	7.42
4	t (*J* = 3.9, 2.0 Hz)	7.32
NH	broad s	12.39

3.3.3.2. ^{13}C NMR spectrum of 4

The ^{13}C NMR spectrum of **4**, in DMSO-d_6, is presented in **Fig. 3.37.** Signal assignments are presented in **Table 3.9**.

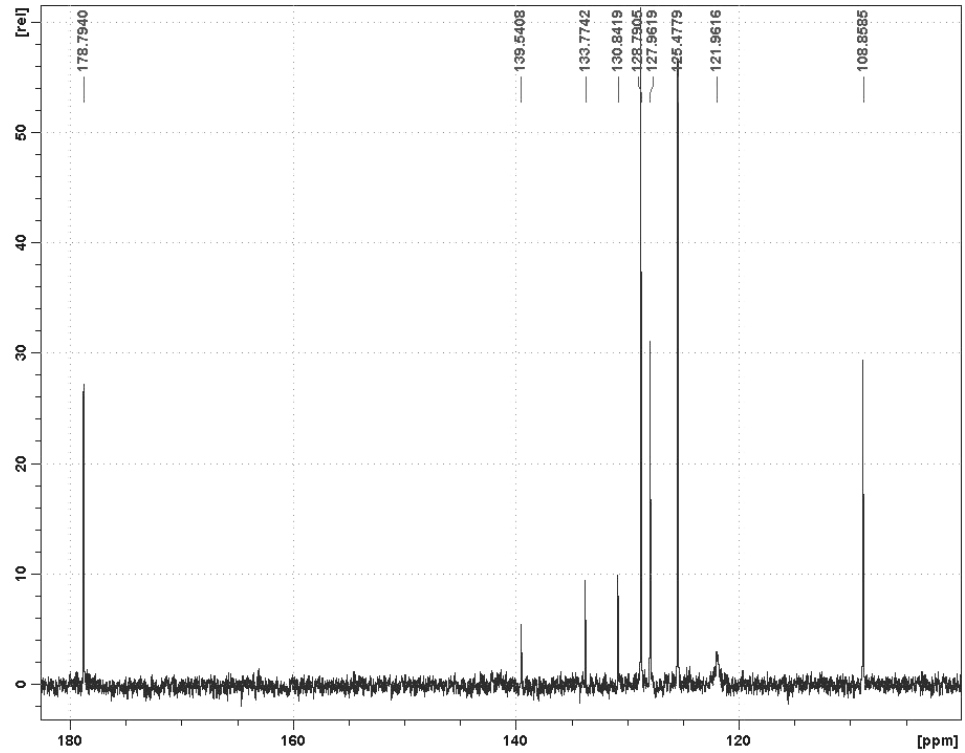

Fig. 3.37: ^{13}C NMR spectrum of 4 in DMSO-d_6.

.

Table 3.9: ^{13}C NMR signal assignments for 4 (δ ppm in DMSO-d_6)

Atom	Chemical shift
1'	178.8
2'	133.8
3'	121.9
4'	108.9
5'	139.5
1	130.8
2	125.5
3	128.8
4	128.0

3.3.3.3. HSQC spectrum of 4

The gradient edited HSQC spectrum of **4**, determined in DMSO-d_6, is presented in **Fig. 3.38**. ^1J correlations observed in the HSQC spectrum are given in **Table 3.10.**

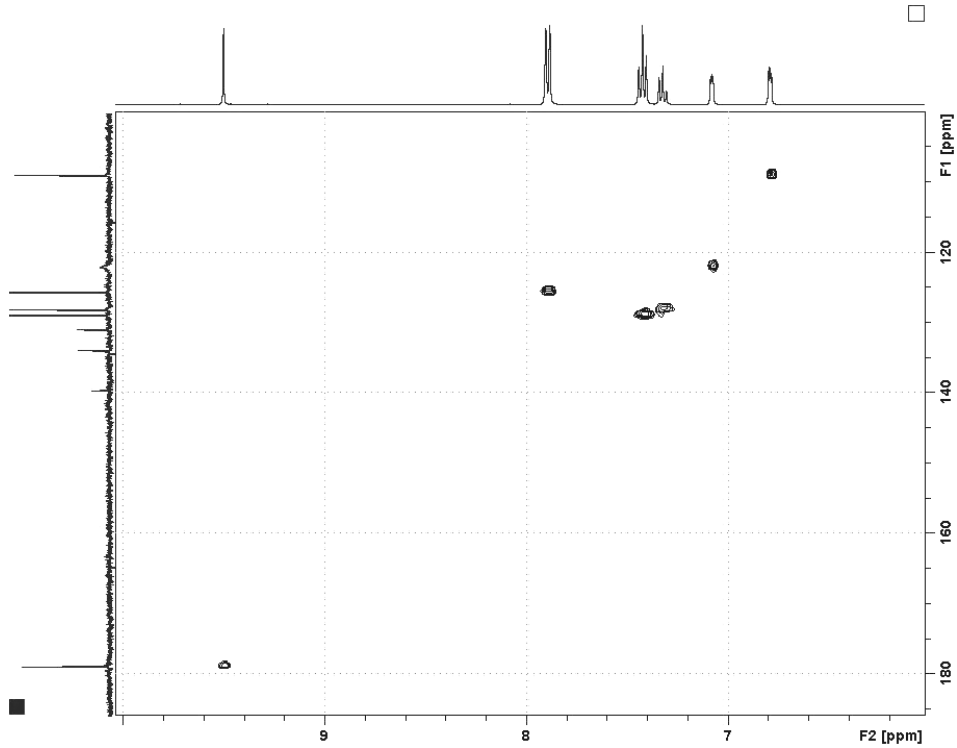

Fig. 3.38: HSQC spectrum of 4 in DMSO-d_6.

Table 3.10: HSQC correlations determined for 4 (δ ppm in DMSO-d_6)

Proton	6.79 (H-4')	7.08 (H-3')	7.32 (H-4)	7.42 (H-3)	7.89 (H-2)	9.50 (H-1')
Carbon	108.9	121.9	128.0	128.8	125.5	178.8

3.3.3.4. HMBC spectrum of 4

The gradient edited HMBC spectrum of **4**, determined in DMSO-d_6, is presented in **Fig. 3.39.** ^{n}J correlations observed in the HMBC spectrum of **4** are given in **Table 3.11** and depicted in **Fig. 3.40.** The signal to noise of this spectrum was much greater than that of the HMBC spectrum of **1**. Several of the carbon atoms of **4** also exhibited residual ^{1}J coupled correlations, the intensity of which was proportional to the difference between the ^{1}J coupling of the carbon in question (typically in the range 140-220 Hz) and value (160 Hz) used to define the D2 (= 1/2 *J*) delay time in the HMBC pulse sequence.

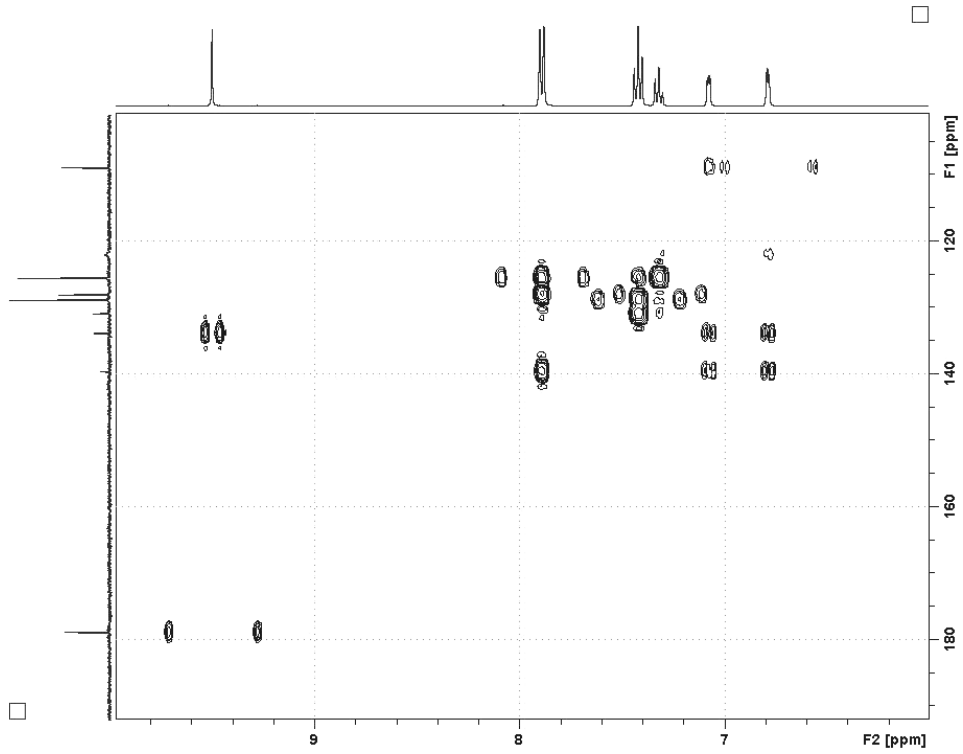

Fig. 3.39: HMBC spectrum of 4 in DMSO-d_6.

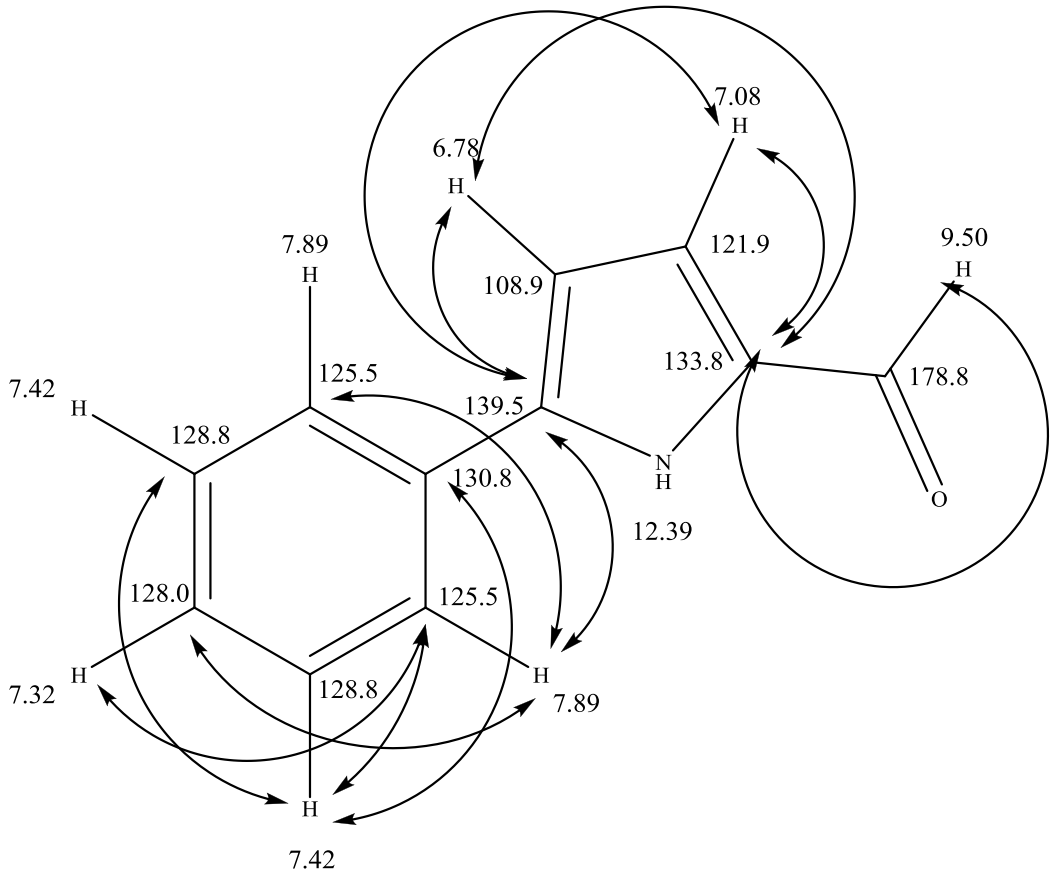

Fig. 3.40: HMBC correlations observed for 4 (δ ppm in DMSO-*d*$_6$).

Table 3.11: ^{n}J HMBC correlations observed for 4 (δ ppm in DMSO-*d*$_6$)

Proton	6.79 (H-4')	7.08 (H-3')	7.32 (H-4)	7.42 (H-3)	7.89 (H-2)	9.50 (H-1')
Correlated carbon(s)	133.8 (C-2') 139.5 (C-5')	133.8 (C-2') 139.8 (C-5')	125.5 (C-2)	125.5 (C-2) 128.8 (C-3) 130.8 (C-1)	125.5 (C-2) 128.0 (C-4) 139.5 (C-5')	133.0 (C-2')

The aldehyde proton which occurred at 9.50 ppm showed a ^{2}J correlation to the carbon at 133.8 ppm (C-2') while the aryl H-2 proton signal (7.89 ppm) showed an inter-ring ^{3}J correlation to C-5' (139.5 ppm). These correlations corresponded exactly to those observed in the HMBC spectrum of **1**.

The resolution of the HMBC spectra (which were in all cases determined without ^{1}H decoupling) was such that the magnitude of the ^{2}J H-1 - C-2' couplings could be determined with reasonable precision, and were found to be ca 26 Hz for **1** and **4**, compared to 32 Hz for **3** which possessed a furan ring.

3.3.3.5. GC-MS analysis of 4

GC-MS analyses of **4**, under identical conditions to those used to determine the GMS characteristics of **1** and **3,** afforded a peak which had a retention time of 8.23 minutes and showed a M^{+} ion at *m/z* 171, together with strong *m/z* 170 $(M-H)^{+}$, *m/z* 142 $[M - CHO]^{+}$ and *m/z* 115 $[M - C_2H_2ON]^{+}$ fragment ions (**Fig. 3.41**).

The observation that **4** eluted from the GC-MS column ca 2 minutes before compound **1** was eluted is consistent with the view that **1** is a higher molecular weight, methoxylated analogue of **4**.

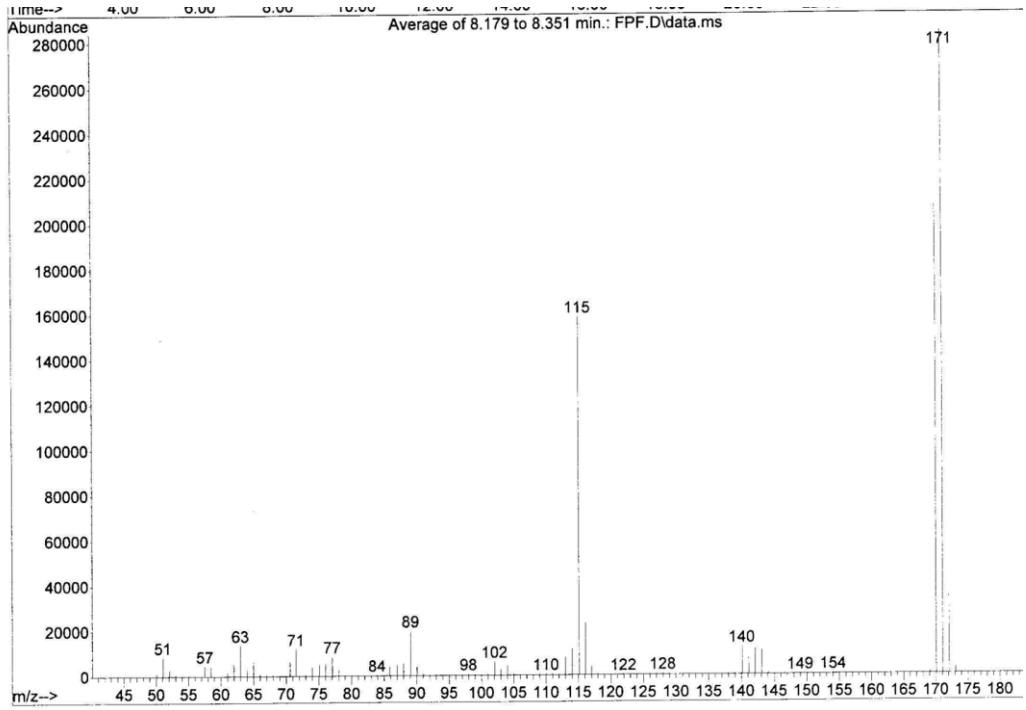

Fig. 3.41: Mass spectrum of the GC-MS peak which eluted at 8.20 minutes.

Based on the NMR and GC-MS data reported in **Sections 3.2.1**, and model compound data reported in **Sections 3.2.2** and **3.2.3**, it can be concluded

that **1** is a 2-formyl-5-(2-methoxyphenyl)-pyrrole. A complete assignment of the ^{1}H and ^{13}C signals of **1** in DMSO-d_6 is presented in **Table 3.12**. HMBC correlations observed for **1** are depicted in **Fig 3.42.**

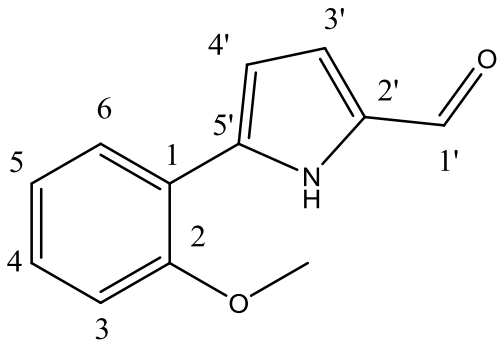

1

Table 3.12: NMR signal assignments for 1 (δ in ppm in DMSO-d_6)

Atom	^{13}C	^{1}H
1'	178.8	9.52 (s)
2'	132.5*	-
3'	120.7	7.04 (d, *J* =3.9 Hz, partly concealed)
4'	111.9	6.77 (d, *J* = 3.9 Hz)
5'	135.5*	-
1	119.8*	-
2	156.6*	-
3	111.4	7.14 (dd, *J* = 8.5, 1.2 Hz)
4	129.4	7.33 (ddd, *J* = 8.5, 7.3, 1.7 Hz)
5	120.7	7.02 (~td, *J* = 7.5, 1.2 Hz)
6	128.2	7.77 (dd, *J* = 7.8, 1.7 Hz)
OCH_3	55.6	3.90 (s)
NH	-	11.79 (broad s)

* ^{13}C chemical shifts determined at 2D-resolution.

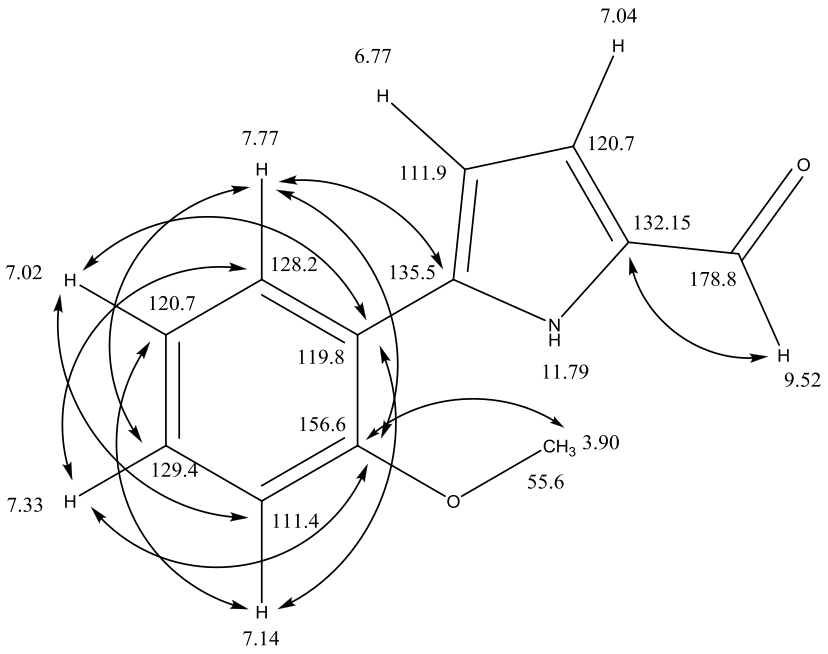

Fig. 3.42: HMBC correlations observed for 1 (δ in ppm in DMSO-d_6).

3.4. Synthesis of 1

A synthesis of **1** was attempted based on the synthetic route to **4** reported by Reeves *et al.*[72] (see **Section 2.2.8**). The proposed synthetic route to **1** is presented in **Fig. 3.43**.

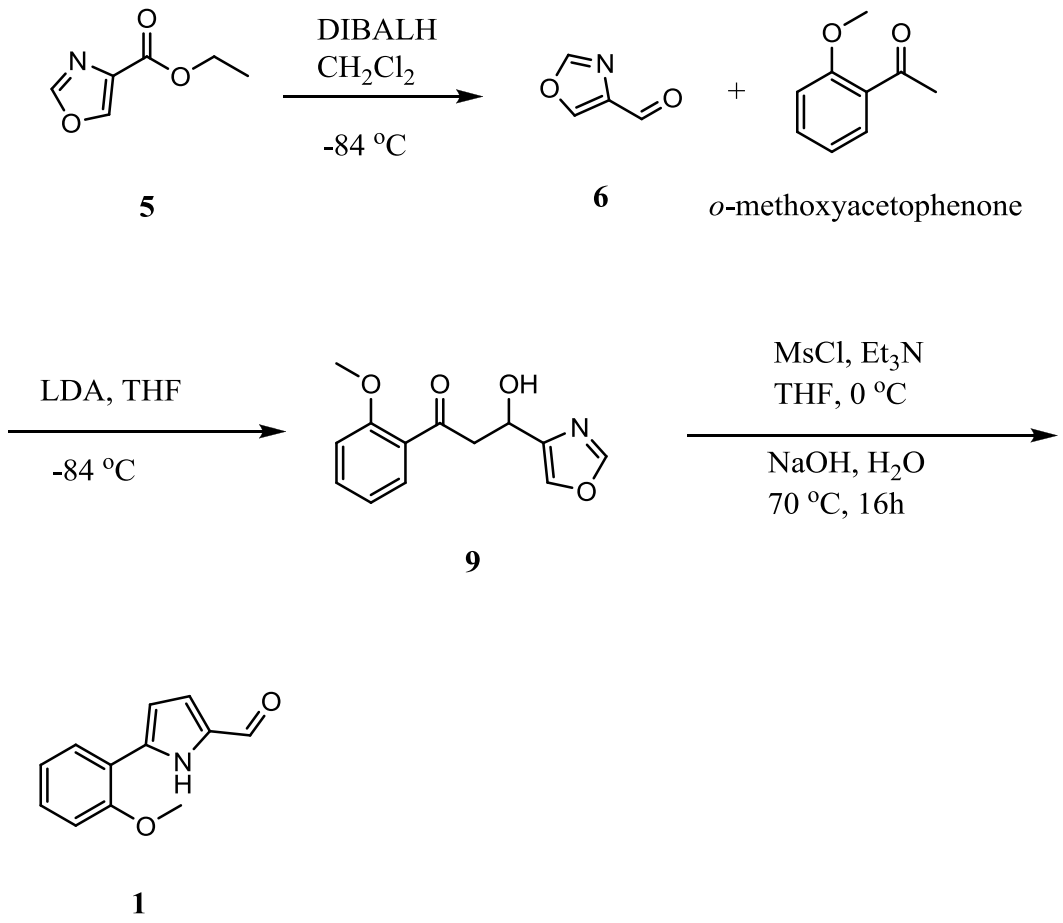

Fig. 3.43: The synthesis route of 1.

3.4.1. Synthesis of oxazole-4-carbaldehyde (6)

Synthesis of **6** (a white powder after crystallisation) from ethyl 4-oxazolecarboxylate (**5**) proceeded with a yield of 0.0109 g (1.42%, lit 64%). Mpt : found: 55-58°C; lit. 59-61°C.[72]

Hodges *et al.*[76] have stated that oxazole-2-carboxaldehyde (**7**) is prone to loss by vapourization during solvent evaporation. Benoit *et al.*[74] has reported that 2-methyloxazole-4-carboxaldehyde (**8**) is unstable to extremes of pH and is

rapidly decomposed by hydrolysis. It was therefore anticipated that **6** would share these characteristics with **7** and **8.**

The DIBALH is supplied commercially dissolved in hexane, the removal of which resulted in loss of product when the reaction mixture containing this reagent was concentrated on a rotary evaporator to give crude **6**. **6** may have been over-reduced as a 60 minute reaction time was utilised in the present investigation while the reaction mixture was held at lower temperature, whereas 30 minute reaction time was applied recorded in the literature,[72] After the removal of hexane, the reaction mixture was quenched with MeOH and 2 M HCl was added, possibly reducing the yield of **6** due to HCl promoted hydrolysis. Rather than spending time improving the methodology it was decided to purchase **6** for the attempted synthesis of **1**.

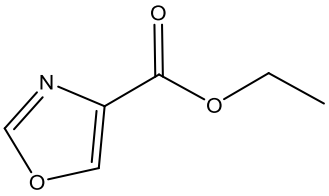

5

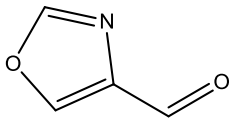

6

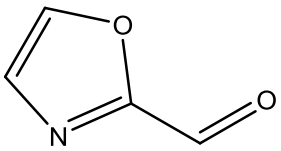

7

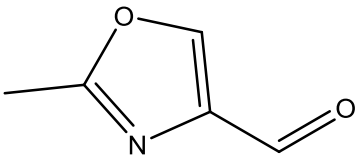

8

3.4.2. Synthesis of 3-hydroxy-1-(2-methoxyphenyl)-3-(oxazol-4-yl) propan-1-one (9)

Synthesis of **9** according to **Section 2.2.8.2**, afforded pale yellow crystals after crystallization, 0.751 g (67.5%). Mpt: 104 – 107^{o}C. ^{1}H and ^{13}C NMR data determined for this compound are reported in **Table 3.14** and **Table 3.15** respectively.

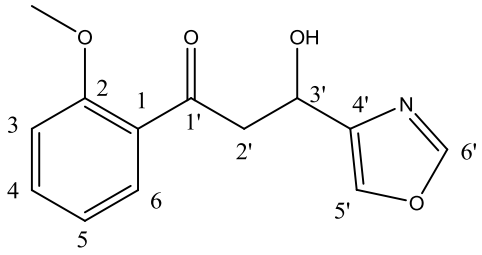

9

3.4.2.1. ^{1}H NMR spectrum of 9

The ^{1}H NMR spectrum of **9**, in DMSO-d_6, is presented in **Fig. 3.44.** Signal assignments are given in **Table 3.14**.

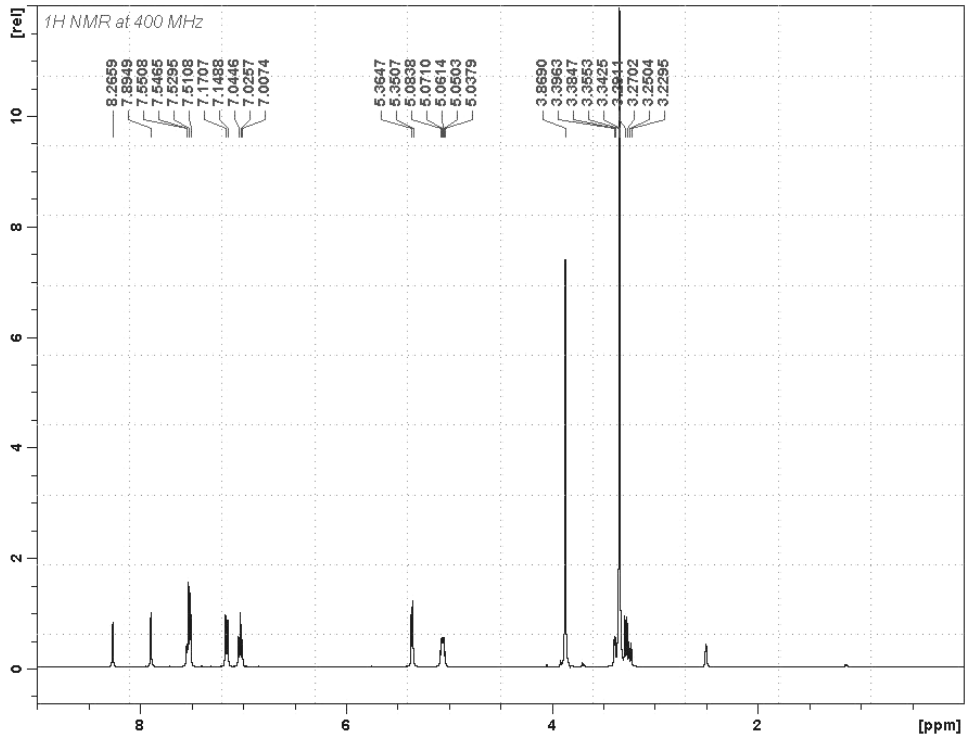

Fig. 3.44: ^{1}H NMR spectrum of 9 in DMSO-d_6.

Table 3.13 : ^{1}H NMR assignments of 9 (δ in DMSO-d_6)

Assignment	Multiplicity	Chemical shift (ppm)
OCH_3	s	3.87
OH	d (J = 5.4 Hz)	5.36
2'	dd (J = 8.2, 16.2 Hz) dd (J = 4.6, 16.2 Hz, partly concealed)	3.26, 3.37
3'	m ($W_{1/2}$ =18.0 Hz)	5.06
5'	s	7.89
6'	s	8.26
3	d (J = 8.6 Hz)	7.16
4	t (J = 7.5 Hz, partly concealed)	7.54
5	t (J = 7.5 Hz)	7.03
6	d (J = 8.6 Hz, partly concealed)	7.52

3.4.2.2. ^{13}C NMR spectrum of 9

The ^{13}C NMR spectrum of **9**, in DMSO-d_6, is presented in **Fig. 3.45**. Signal assignments are presented in **Table 3.19**.

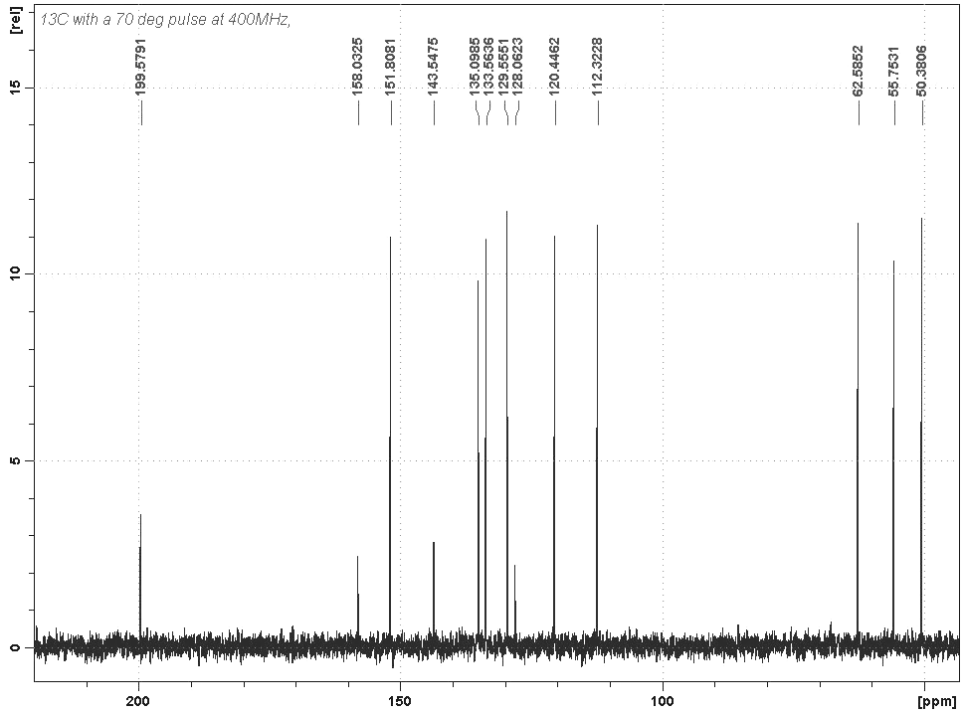

Fig. 3.45: ^{13}C NMR spectrum of 9 in DMSO-d_6.

Table 3.14: ^{13}C NMR assignments for 9 (δ in DMSO-d_6)

Assignment	Chemical shift (ppm)
1'	199.6
2'	50.4
3'	62.6
4'	143.3
5'	135.1
6'	151.5
1	128.1
2	158.0
3	112.3
4	133.6
5	120.9
6	129.4

3.4.2.3. HSQC spectrum of 9

The gradient edited HSQC spectrum of **9**, in DMSO-d_6, is presented in **Fig. 3.46.** Correlations observed for **9** are given in **Table 3.16.**

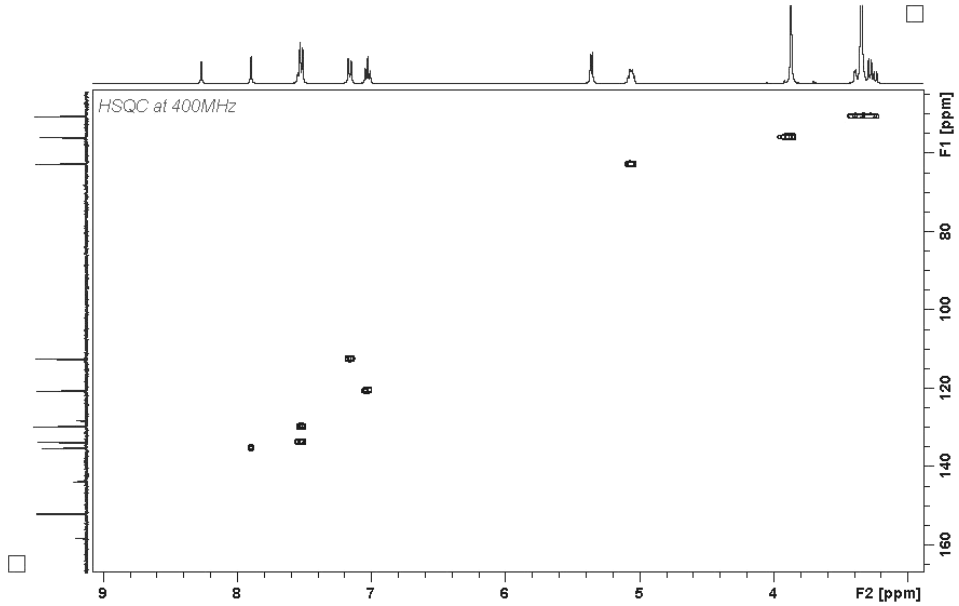

Fig. 3.46: HSQC spectrum of 9 in DMSO-d_6.

Table 3.15: HSQC correlations determined for 9 (δ ppm in DMSO-d_6)

Proton(s)	3.26, 3.37 (H-2')	3.87 ($OC\underline{H}_3$)	5.06 (H-3')	7.03 (H-5)	7.16 (H-3)	7.52 (H-6)	7.54 (H-4)	7.89 (H-5')
carbon	50.4	55.7	62.62	120.4	112.3	129.4	133.6	135.1

HSQC correlations were not observed for the ^{1}H signals that occurred at 5.36 and 8.26 ppm. The former signal arises from an O<u>H</u> proton so that an HSQC correlation will not be observed for this proton. It was considered that the lack of H-6' (8.26 ppm) correlation may be a consequence of the ^1J coupling of the proton being significantly different from the coupling constant (145 Hz) utilised to determine the HSQC spectrum. The ^1J coupling from H-6' (8.26 ppm) to C-6' (151.5 ppm) was confirmed by observation of the ^{13}C coupled signal in the HMBC. A re-run of the HSQC spectrum with ^1J coupling value set to 200 Hz identified a correlation between the proton signal at 8.26 ppm and the C-6' resonance which occurred at 151.5 ppm (**Fig 3.47**).

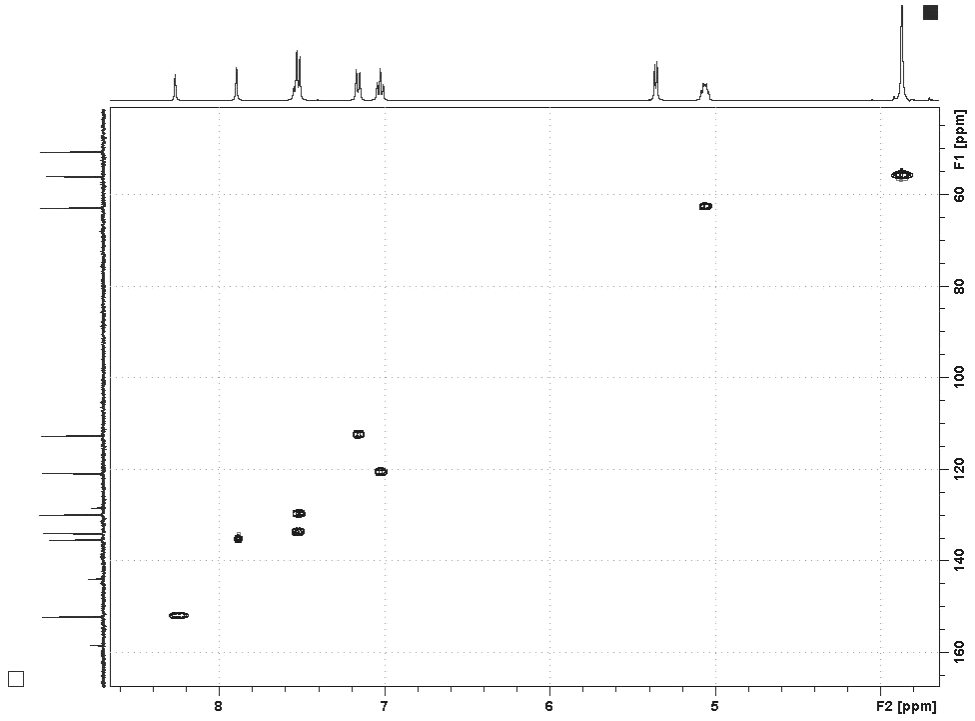

Fig. 3.47: HSQC spectrum of 9 in DMSO-d_6 with ^1J optimised for 200 Hz.

3.4.2.4. HMBC spectrum of 9

The gradient edited HMBC spectrum of **9** in DMSO-d_6 is presented in **Fig. 3.48**. Correlations observed in the HMBC spectrum are presented in **Table 3.17** and depicted **Fig. 3.49**.

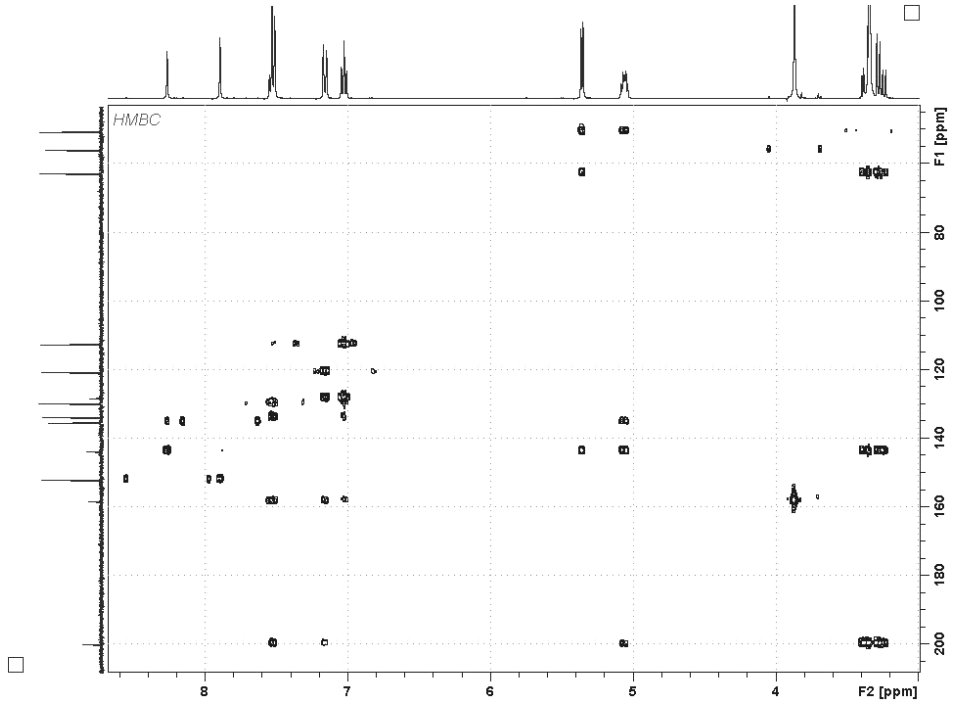

Fig. 3.48: HMBC spectrum of 9 in DMSO-d_6.

Table 3.16: ^{n}J HMBC correlations observed for 9 (δ ppm in DMSO-d_6)

Proton(s)	3.26, 3.37 (H-2')	3.87 ($OC\underline{H}_3$)	5.06 (H-3')	5.36 (OH)	7.03 (H-5)
Correlated carbons(s)	62.5 (C-3') 143.5 (C-5') 199.6 (C-1')	158.0 (C-2)	50.4 (C-2') 135.4 (C-5') 143.5 (C-4') 199.6 (C-1')	50.4 (C-2') 62.6 (C-3') 143.5 (C-4')	120.4 (C-5) 128.1 (C-1) 133.6 (C-4) 158.0 (C-2)
Proton	7.16 (H-3)	7.52 (H-6)	7.54 (H-4)	7.89 (H-5')	8.26 (H-6')
Correlated carbon(s)	120.4 (C-5) 128.1 (C-1) 158.0 (C-2) 199.6 (C-1')	128.1 (C-5) 133.6 (C-4) 158.0 (C-2) 199.6 (C-1')	158.0 (C-2)	151.5 (C-6')	135.1 (C-5') 143.5 (C-4')

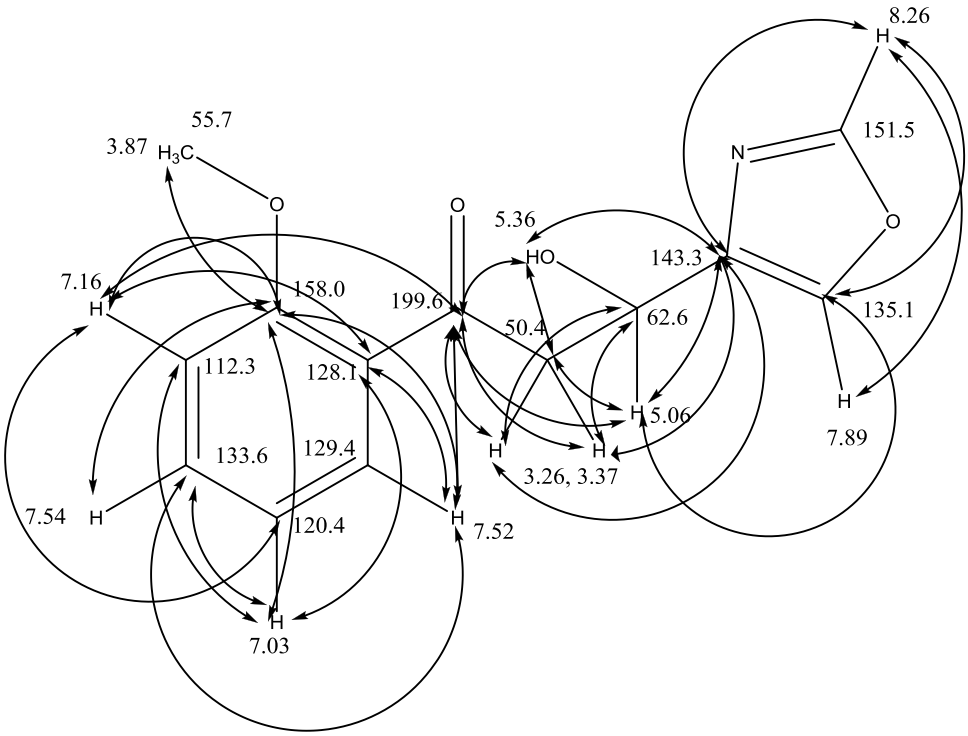

Fig. 3.49: HMBC correlations observed for 9 (δ ppm in DMSO-d_6).

3.4.2.5. HRMS of 9

High Resolution Mass Spectrometry (HRMS) of **9** gave: calculated for $C_{12}H_{12}NO_4Na$ $[M+Na]^+$: 270.0737 and found: 270.0735 (**Fig. 3.50**)

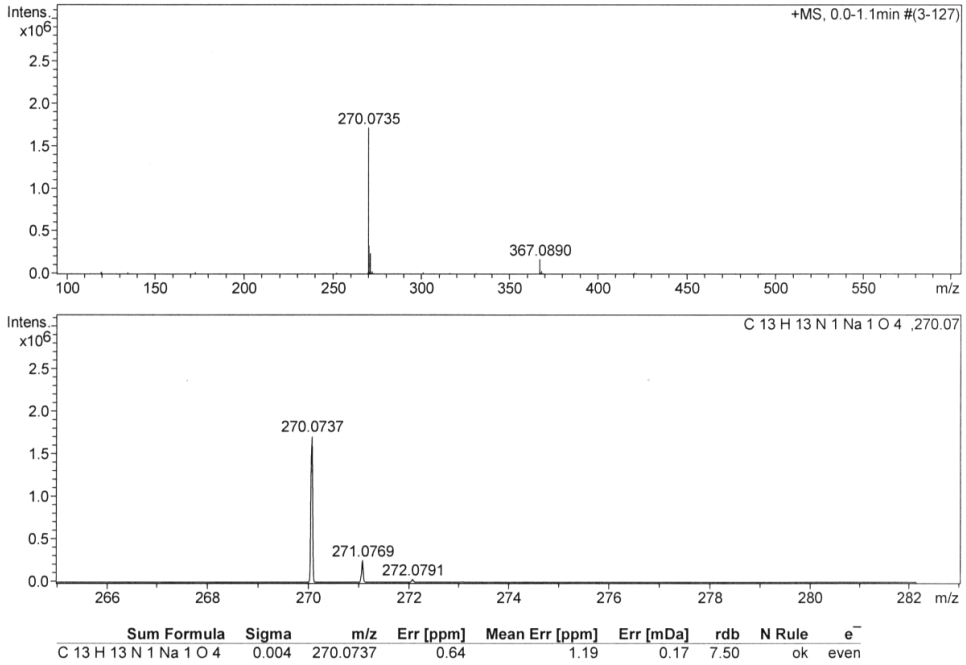

Sum Formula	Sigma	m/z	Err [ppm]	Mean Err [ppm]	Err [mDa]	rdb	N Rule	e⁻
C 13 H 13 N 1 Na 1 O 4	0.004	270.0737	0.64	1.19	0.17	7.50	ok	even

Fig. 3.50: HRMS of 9.

3.4.3. Synthesis of 1 from 9

GC-MS of the crude reaction product was obtained when **9** was reacted with MsCl and NaOH (see **Section 2.2.8.3**), which indicated the presence of only a small amount of **1** (ca 1 %). The retention time of the minor amount of compound in the reaction mixture (retention time of 9.85 minutes) (**Fig. 3.51**) was identical to that determined for the sample of **1** isolated from the mānuka flavonoid fraction **1 (**retention time of 9.85 minutes) (**Fig. 3.52**).

It was difficult to demonstrate the presence of a low level of **1** in the reaction mixture by inspection of the TIC profile of the mixture. Selected ion profiling (*m/z* 201, 158 and 130 ion profiles: see **Section 2.2.4**) verified the presence of a low level of **1**.

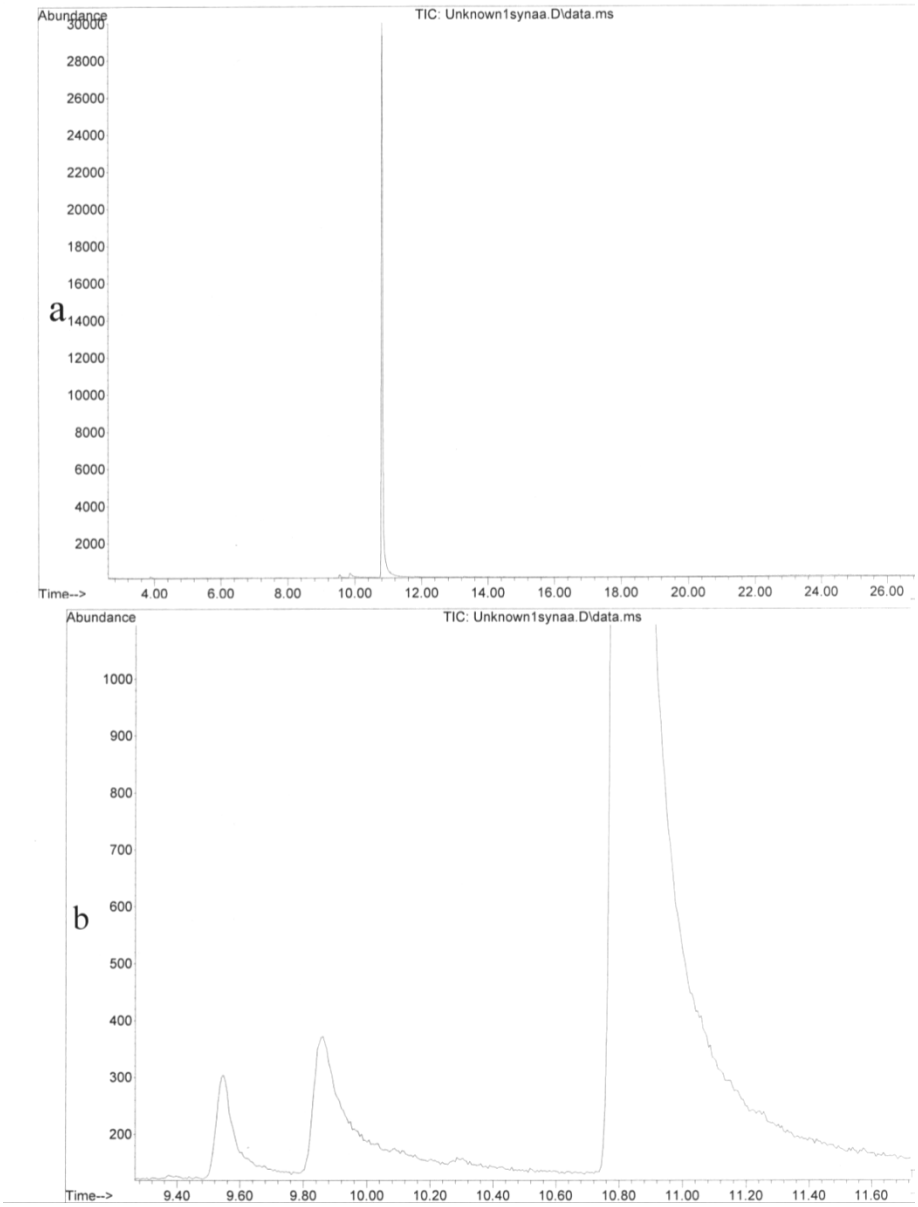

Fig. 3.51 a: Selected ion chromatogram of the crude product mixture (summed *m/z* 130, 158 and 201 ion currents); b: Expansion of the 9.20 to 11.80 minute region.

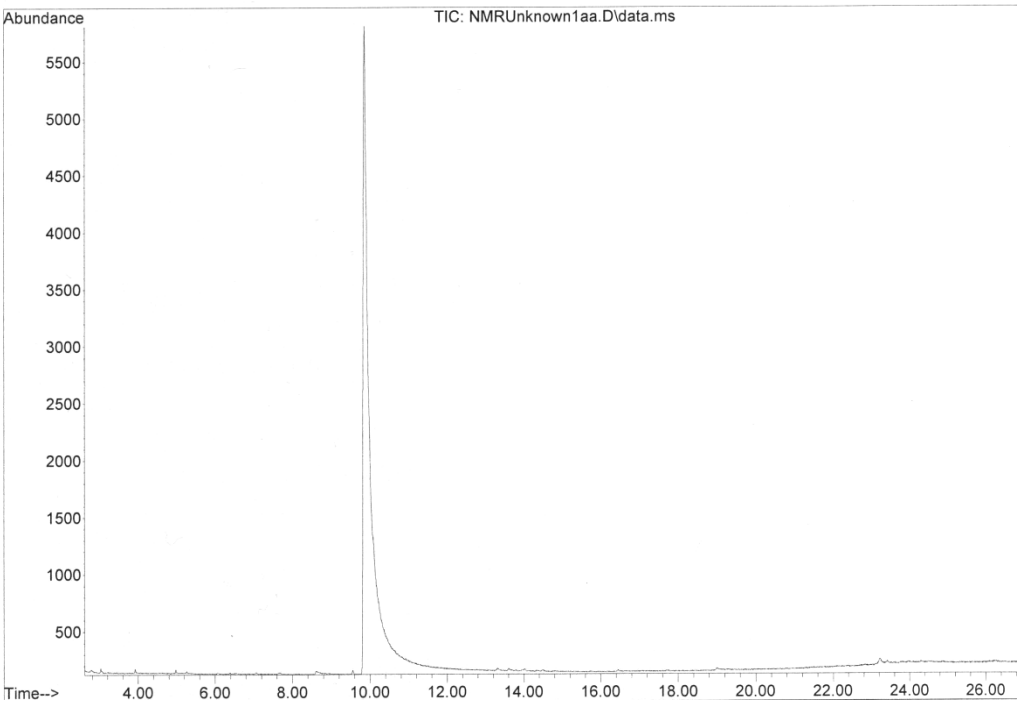

Fig. 3.52: Selected ion chromatogram of an isolated specimen of 1 (sum of *m/z* 130, 158 and 201 ions).

The relative ratio of the *m/z* 130, 158 and 201 ions observed for the reaction product mixture peak at retention time of 9.85 minutes was 1:1.35:3.32, whereas the relative ratio of that of previously isolated **1** at retention time of 9.85 minutes was 1:1.27:3.3. The close agreement between these ratios supports the conclusion that a low level of **1** was present in the mixture of reaction products.

The major component of the reaction was crystallized (yield of 0.222 g, 60.6%, Mpt: 75 - 80^{o}C.) and identified by detailed analyses of one and 2D-NMR data as (*E*)-1-(2-methoxyphenyl)-3-(oxazol-4-yl)prop-2-en-1-one (**10**). This compound is the dehydrated analogue of the starting material.

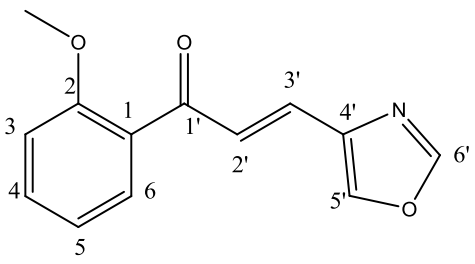

10

3.4.3.1. ^{1}H NMR spectrum of 10

The ^{1}H NMR spectrum of **10**, in DMSO-d_6, is presented in **Fig. 3.53**. Signal assignments are presented in **Table 3.17**.

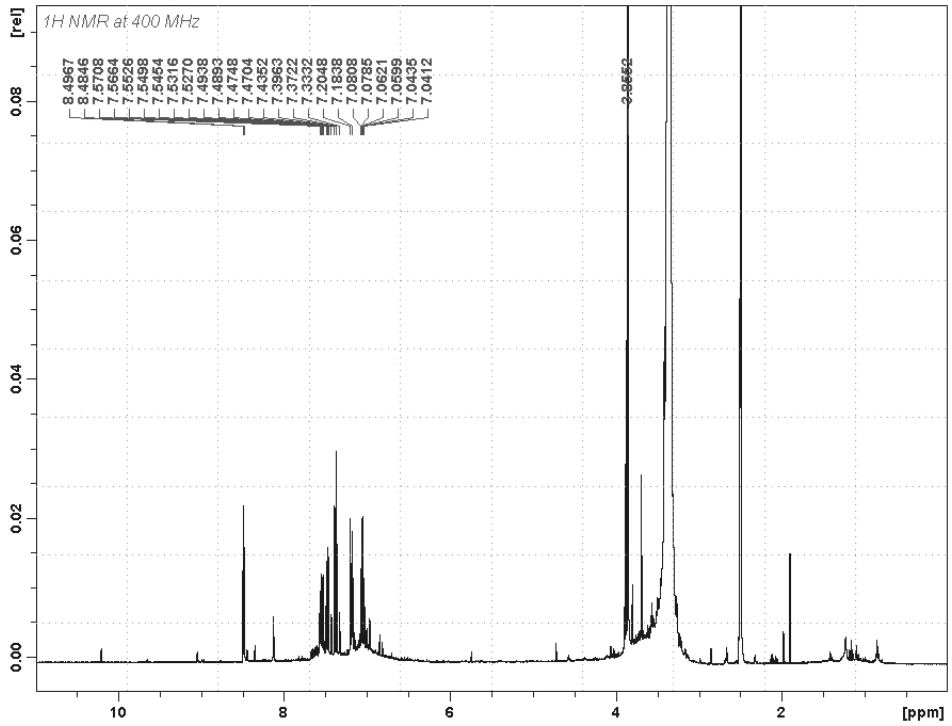

Fig. 3.53: ^{1}H NMR spectrum of 10 in DMSO-d_6.

Table 3.17 : ^{1}H NMR assignments for 10 (δ in DMSO-d_6)

Assignment	Multiplicity	Chemical shift (ppm)
OCH_3	s	3.86
2'	dd (J = 15.5, 0.8 Hz)	7.42
3'	d (J = 15.5 Hz)	7.35
5'	t (J = 0.8 Hz)	8.48
6'	s	8.50
3	dd (J = 8.3, 1.0 Hz)	7.19
4	td (J = 8.3, 1.8 Hz)	7.55
5	td (J = 7.5, 1.0 Hz)	7.06
6	dd (J = 7.5,1.8 Hz)	7.48

3.4.3.2. ^{13}C NMR spectrum of 10

The ^{13}C NMR spectrum of **10**, in DMSO-d_6, is presented in **Fig. 3.54**. Signal assignments are presented in **Table 3.18.**

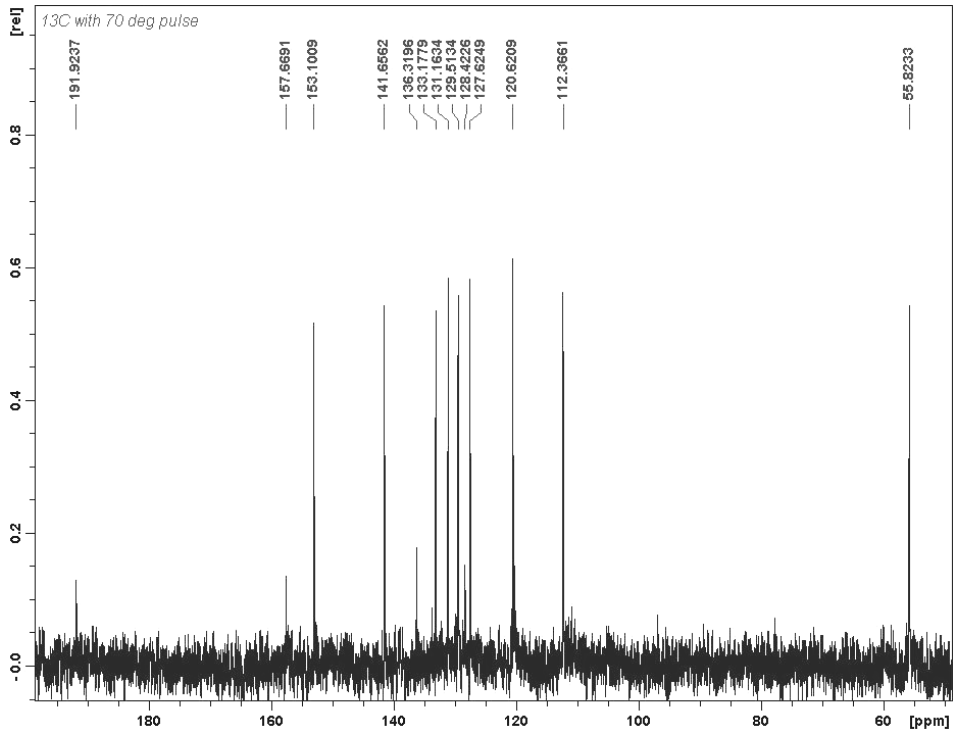

Fig. 3.54: ^{13}C NMR spectrum of 10 in DMSO-d_6.

Table 3.18: ^{13}C NMR signal assignments for 10 (δ in DMSO-d_6)

Assignment	Chemical shift (ppm)
1'	191.9
2'	131.1
3'	127.0
4'	136.3
5'	141.7
6'	153.1
1	128.4
2	157.7
3	112.3
4	133.1
5	120.6
6	129.5
OCH_3	55.8

3.4.3.3. HSQC spectrum of 10

The gradient edited HSQC spectrum of **10**, in DMSO-d_6, is presented in **Fig. 3.55.** Correlations observed in the HSQC spectrum are listed in **Table 3.19**.

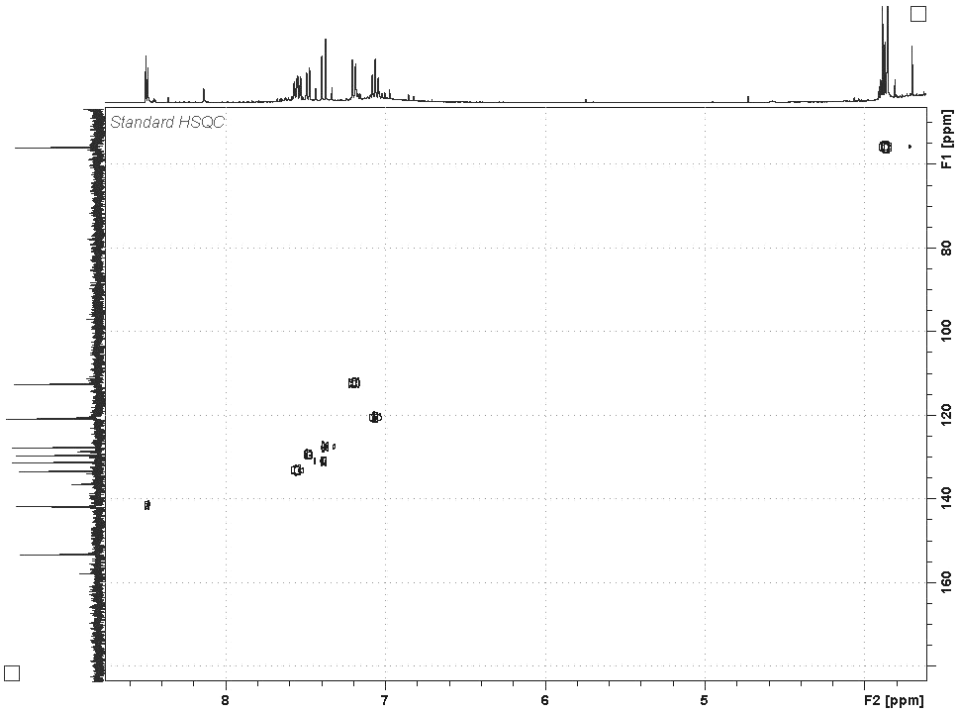

Fig. 3.55: HSQC spectrum of 10 in DMSO-d_6.

Table 3.19: HSQC correlations determined for 10 (δ in DMSO-d_6)

Proton (ppm)	3.87 ($OC\underline{H}_3$)	7.06 (H-5)	7.19 (H-3)	7.35 (H-3')	7.42 (H-2')	7.48 (H-6)	7.55 (H-4)	8.48 (H-5')
Carbon (ppm)	55.8	120.6	112.4	127.6	131.1	129.5	133.1	141.7

3.4.3.4. HMBC spectrum of 10

The gradient edited HMBC spectrum of **10**, in DMSO-d_6, is presented in **Fig. 3.56**. HMBC correlation observed for **10** are listed in **Table 3.20** and depicted in **Fig. 3.57**.

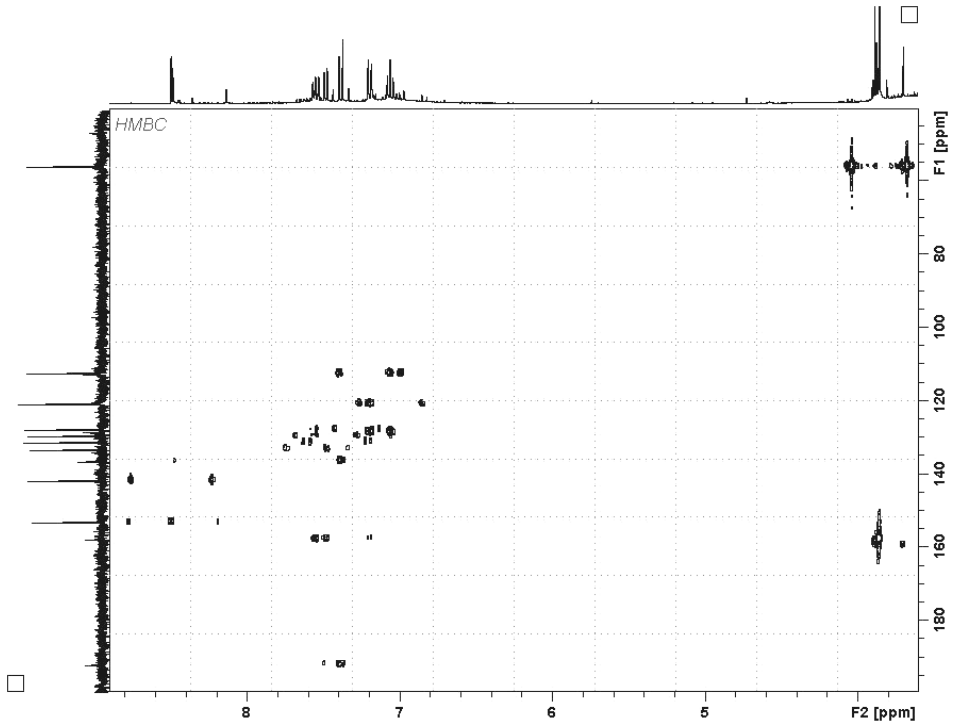

Fig. 3.56: HMBC spectrum of 10 in DMSO-d_6

Table 3.20: ^{n}J HMBC correlation observed for 10 (δ ppm in DMSO-d_6)

Proton	3.87 ($OC\underline{H}_3$)	7.06 (H-5)	7.19 (H-3)	7.35 (H-3')	7.42 (H-2')
Correlated carbon(s)	157.7 (C-2)	112.3 (C-3) 128.4 (C-1)	120.6 (C-5) 128.4 (C-1) 157.7 (C-2)	136.3 (C-4') 191.9 (C-1')	127.6 (C-3') 136.3 (C-4') 191.9 (C-1')
Proton	7.48 (H-6)	7.55 (H-4)	8.48 (H-5')	8.50 (H-6')	
Correlated carbon(s)	133.1 (C-4) 157.7 (C-2) 191.9 (C-1')	129.5 (C-6)	153.1 (C-6')	136.3 (C-4')	

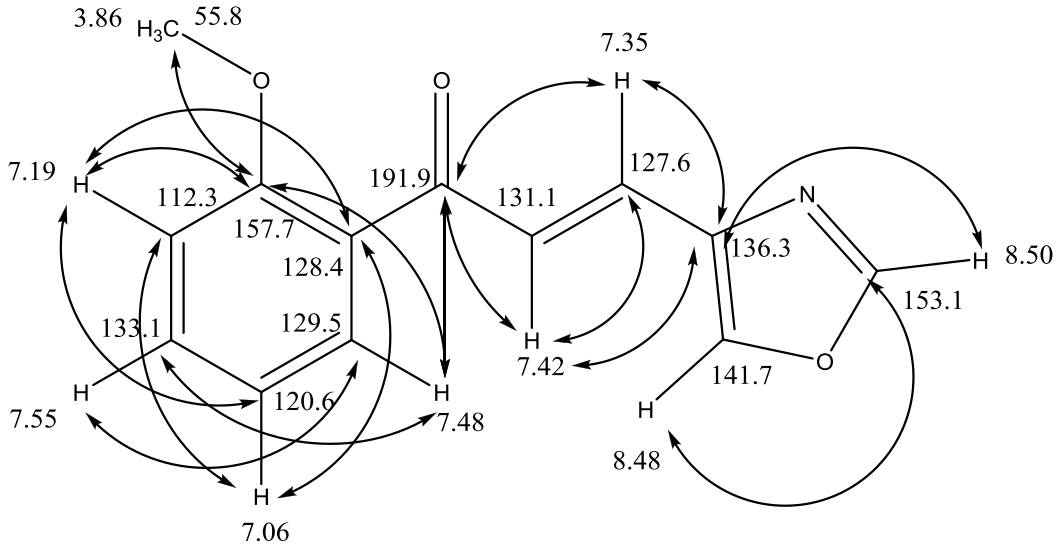

Fig. 3.57: HMBC correlations observed for 10 (δ ppm in DMSO-d_6).

3.4.3.5. HRMS of 10

High Resolution Mass Spectrometry (HRMS) gave: calculated for $C_{13}H_{11}NO_3Na$ $[M+Na]^+$: 252.0631; found: 252.0644 (**Fig. 3.58**).

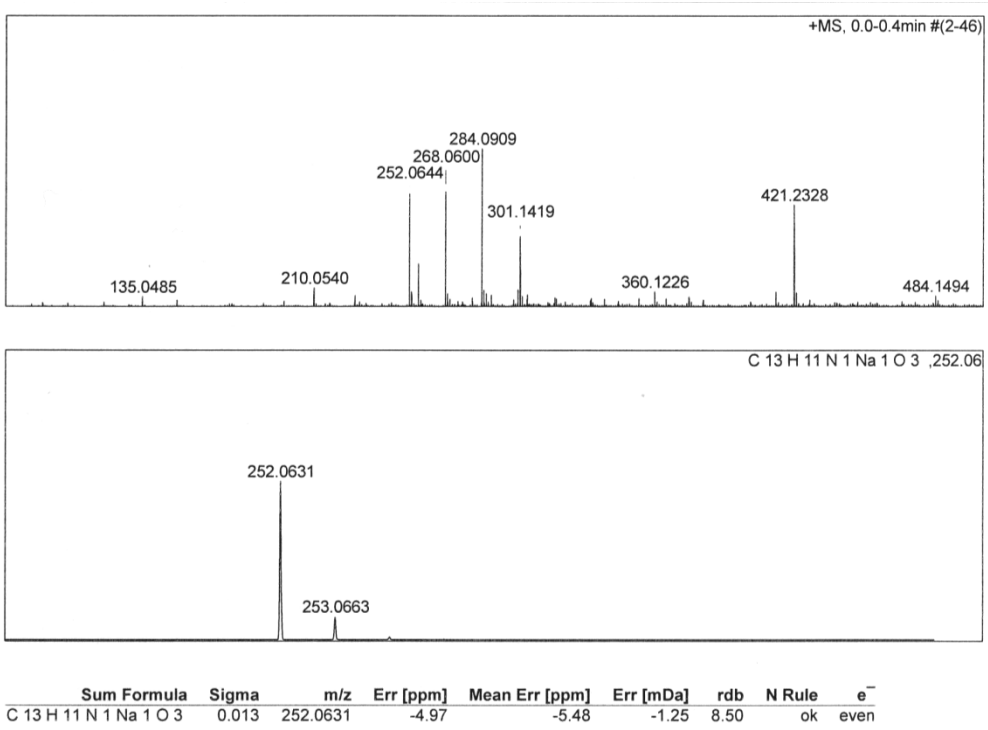

Sum Formula	Sigma	m/z	Err [ppm]	Mean Err [ppm]	Err [mDa]	rdb	N Rule	e⁻
C 13 H 11 N 1 Na 1 O 3	0.013	252.0631	-4.97	-5.48	-1.25	8.50	ok	even

Fig. 3.58: HRMS of 10.

On crystallization **10** yielded a pale orange solid covered by black oil. GC-MS showed that the black oil was *o*-methoxyacetophenone (**Fig. 3.59**). GC-MS analyses of *o*-methoxyacetophenone under the same condition as those utilised to determine the GC-MS characteristic of **1** afforded a peak which had a retention of time 3.89 minutes and showed an M^+ ion at *m/z* 150 and a $[M - CH_3]^{+\cdot}$ fragment ion at *m/z* 135. This compound can be viewed as a degradation product derived from **10.**

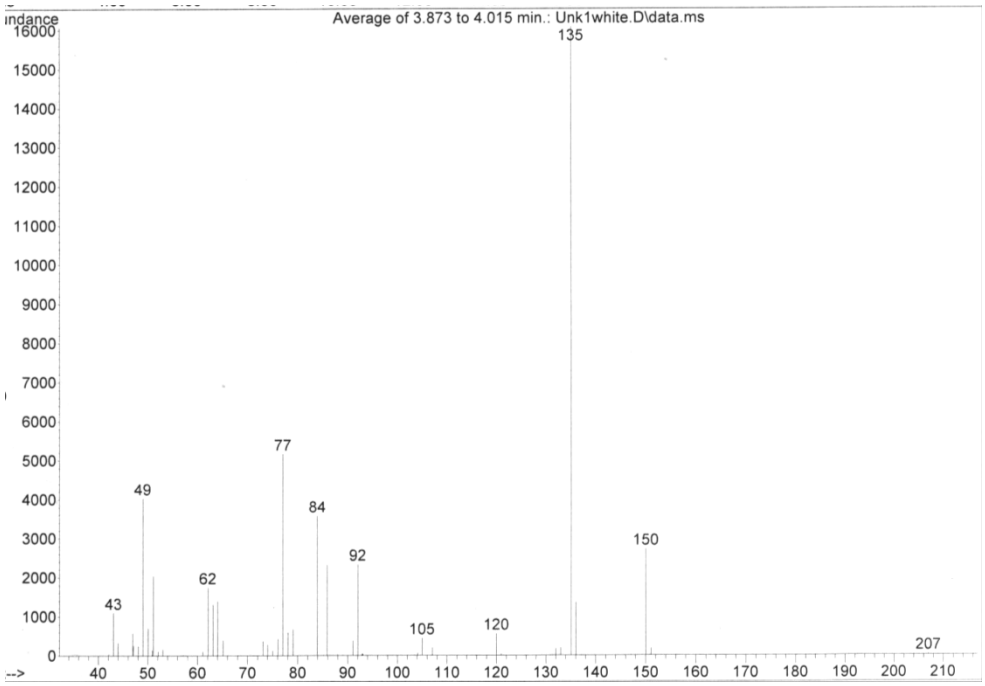

Fig. 3.59: Mass spectrum of *o*-methoxyacetophenone.

The solution after recrystallization of **10** was collected and examined by GC-MS under the same condition as those utilised to determine the GC-MS characteristic of **1**. This yielded three peaks (**Fig. 3.60**).

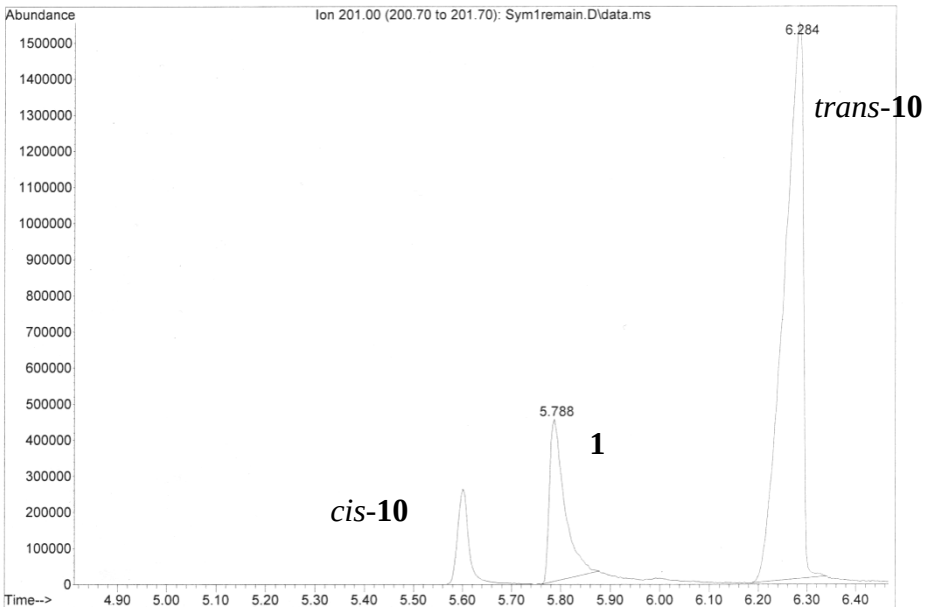

Fig. 3.60: Total ion chromatogram of the crude product mixture after recrystallization.

The mass spectra of the peaks at retention times of 5.60 minutes and 6.28 minutes were nearly identical (see **Figs. 3.61 and 3.62**). It is known that for cinnamic acid esters, *cis*-isomers will elute before *trans*-isomers in GC. For example, c*is*-cinnamic acid elutes before *trans*-cinnamic acid.[77] It can reasonably be concluded that the 5.60 minute peak was the *cis*-isomer of **10** and that the 6.28 minute peak was the *trans*-isomer of **10.**

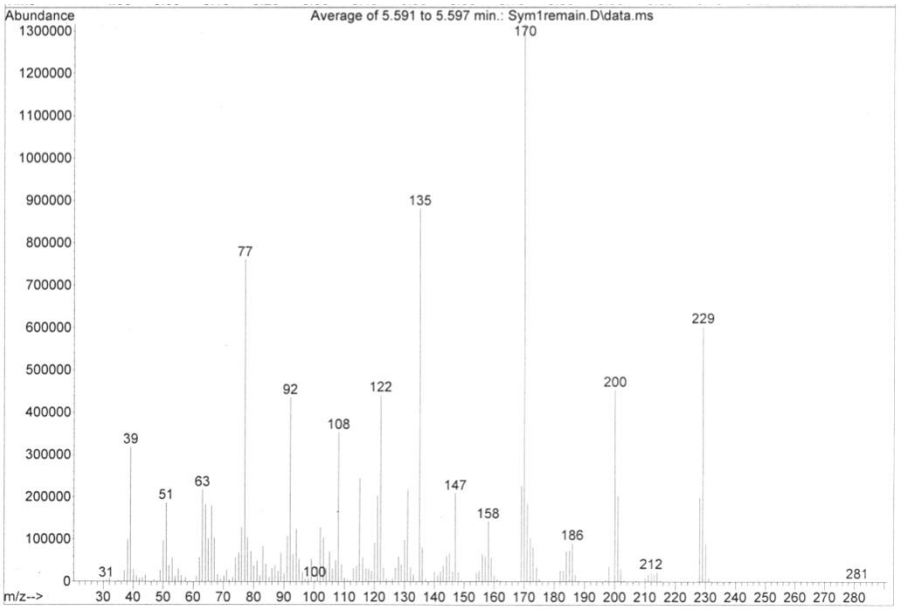

Fig. 3.61: Mass spectrum of the *cis*-isomer of 10.

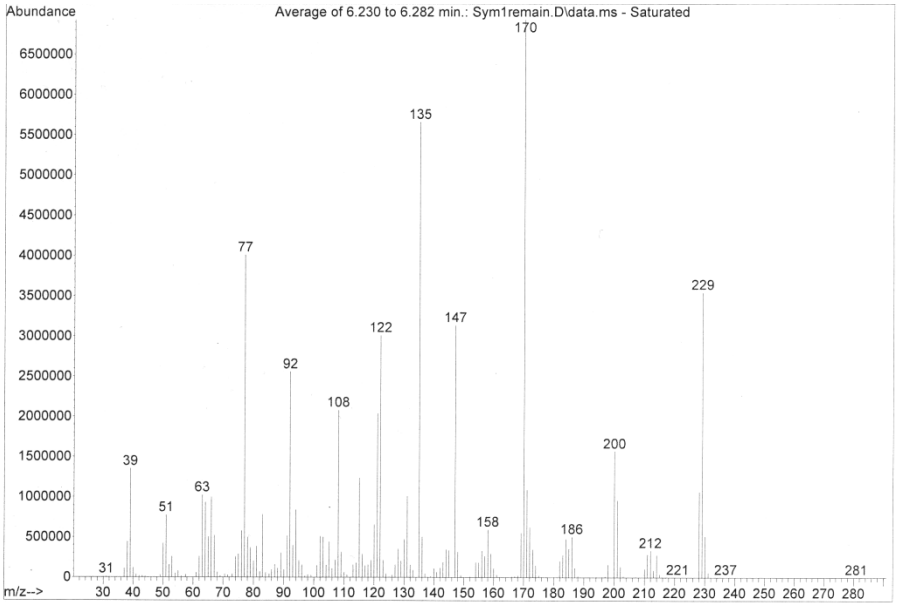

Fig. 3.62: Mass spectrum of the *trans*-isomer of 10.

The NMR data presented in **Table 3.17** is for *trans*-**10** since it includes a $J_{3',4'}$ coupling of 15.5 Hz. There was also evidence for the presence of a lower level of the cis-isomer in the NMR sample as evidenced by olefinic proton signals which showed couplings of 12.6 Hz (see **Fig. 3.63**). The coupling constants of c*is*- and *trans*-olefinic protons of cinnamic acid are 12.7 Hz and 16.1 Hz respectively.[78] This data verified the presence in the crude reaction mixture of the *cis*- and *trans*-isomers of **10** together with **1**.

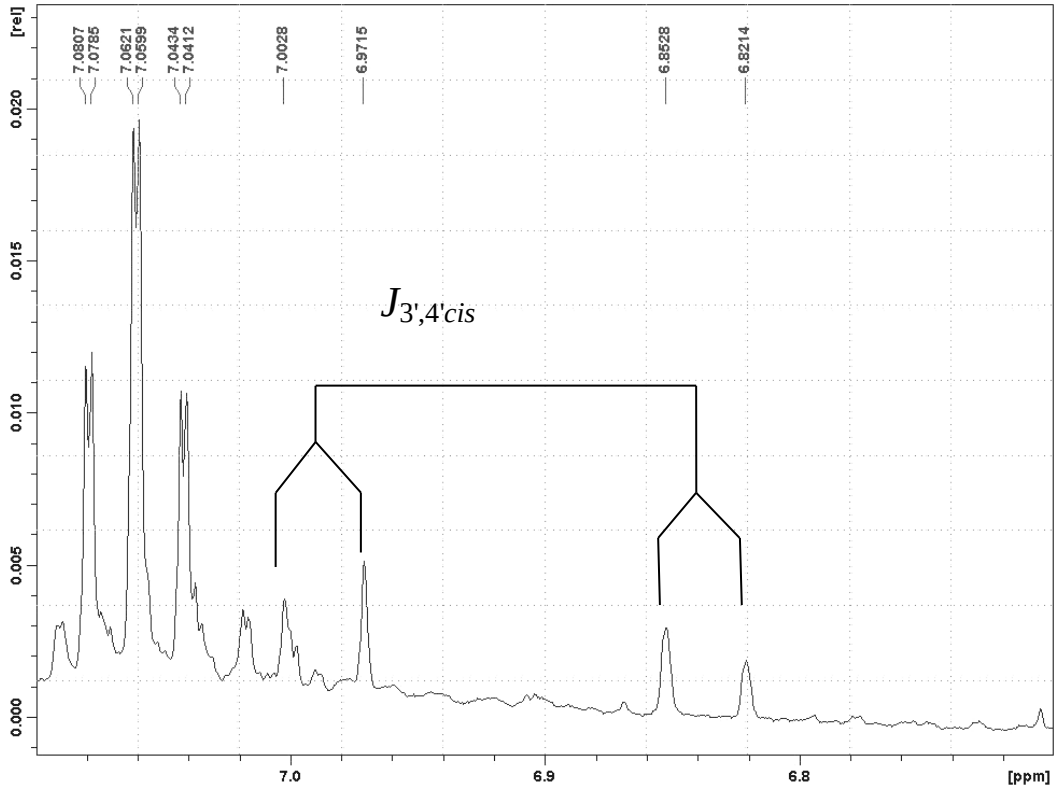

Fig. 3.63: Expansion of the 6.7-7.1 ppm region of the ^{1}H NMR spectrum of 10 in DMSO-d_6.

3.5. Repeat synthesis of 1 for bioassay

Ten fractions were eluted from a SiO_2 column and were examined by GC-MS under the same condition as those utilised to determine the GC-MS characteristic of **1**. The 5th fraction was found to be composed of a mixture of *cis*-**10** (at a retention time of 5.30 minutes)**, 1** (at a retention time of 5.51 minutes)**,** and *trans*-**10** (at a retention time of 5.86 minutes) (**Fig. 3.64**).

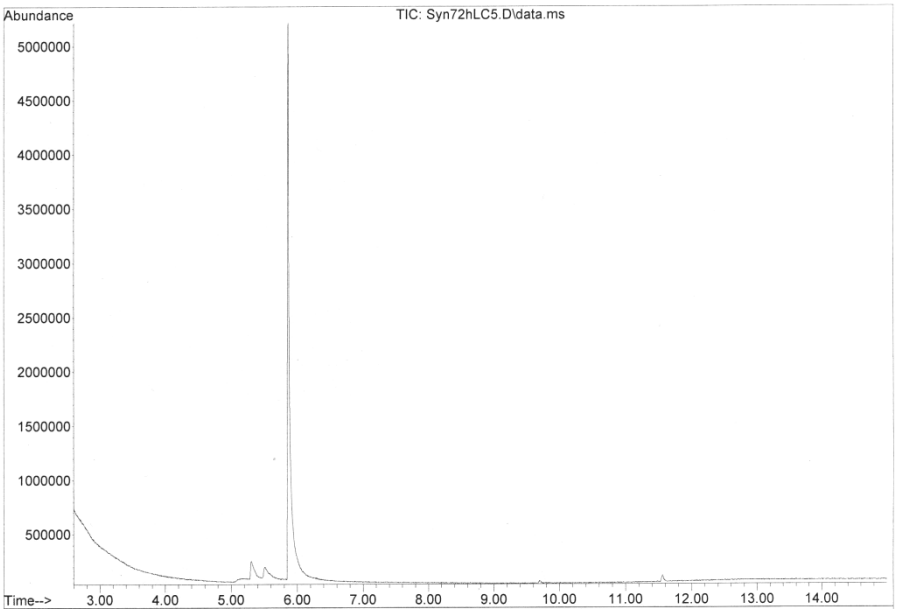

Fig. 3.64: Total ion chromatogram of 5th fraction from SiO_2 column.

The 5th fraction was purified by preparative layer chromatography. The initial bulk separation yielded eighteen fractions which were examined by GC-MS under the same condition as those utilised to determine the GC-MS characteristic of **1**. The 7th (**Fig. 3.65**), 8th (**Fig. 3.66**), 9th (**Fig. 3.67**) and 10th fractions (**Fig. 3.68)** were found to contain **1** (at a retention time of 5.51 minutes).

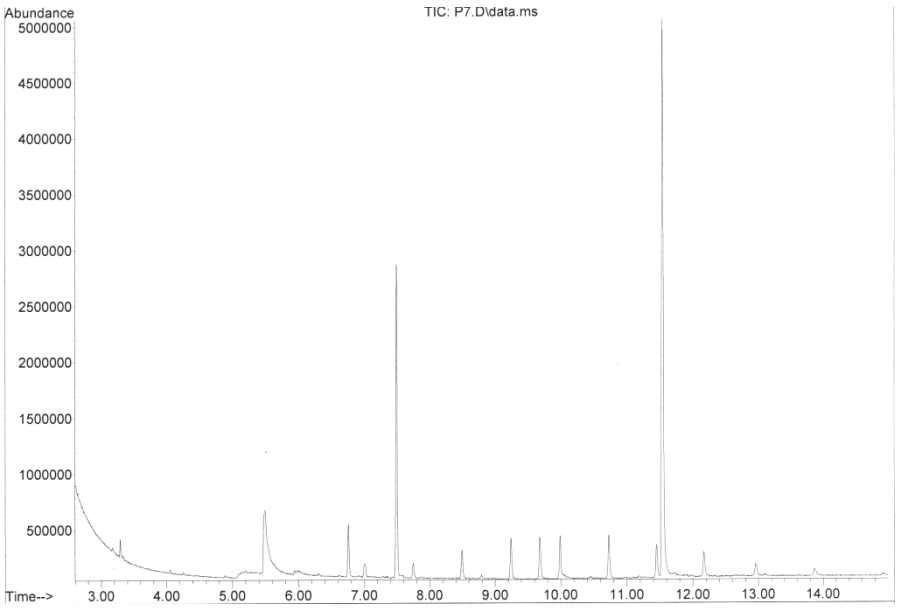

Fig. 3.65: Total ion chromatogram of 7th fraction eluted from preparative layer chromatography of the initial bulk separation.

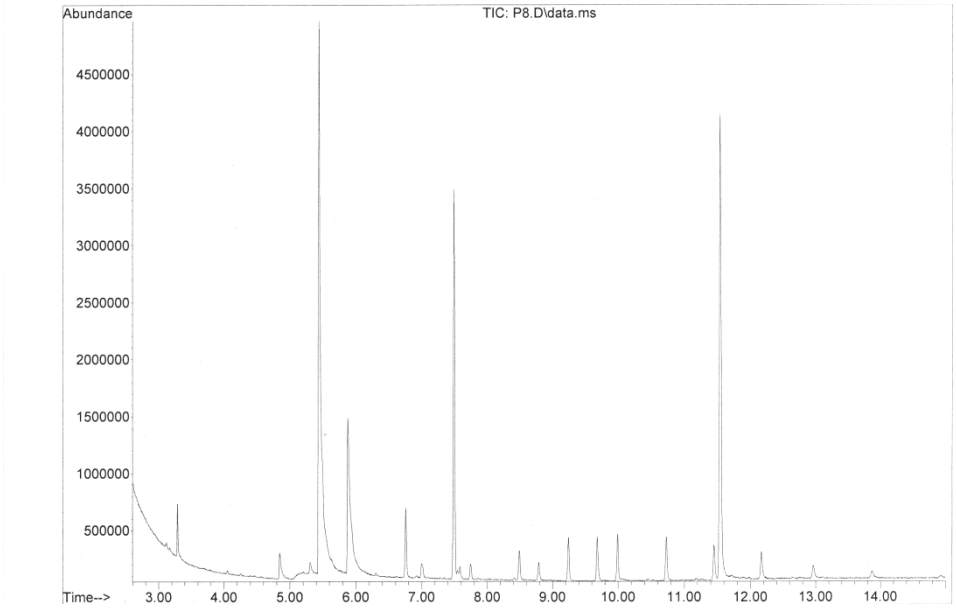

Fig. 3.66: Total ion chromatogram of 8th fraction eluted from preparative layer chromatography of the initial bulk separation.

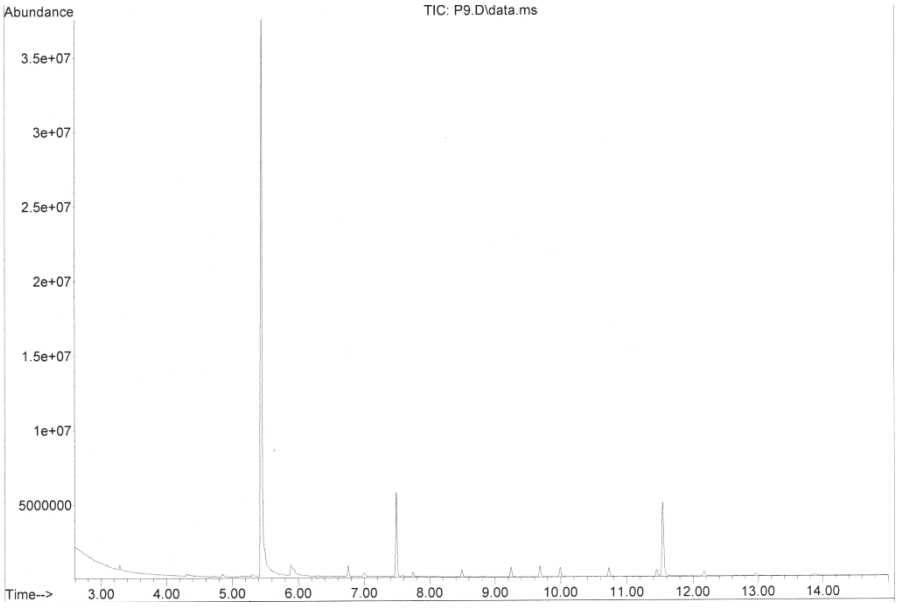

Fig. 3.67: Total ion chromatogram of 9th fraction eluted from preparative layer chromatography of the initial bulk separation.

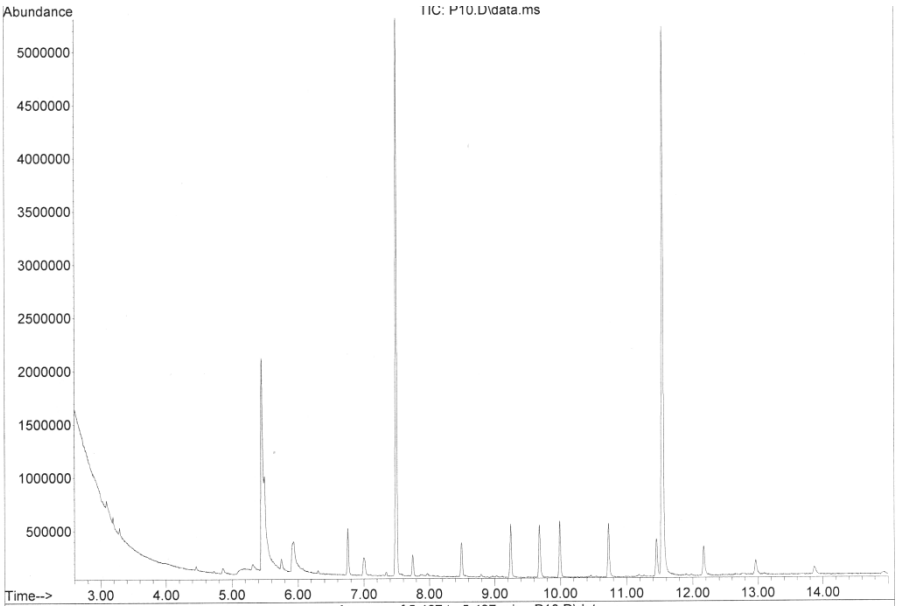

Fig. 3.68: Total ion chromatogram of 10th fraction eluted from preparative layer chromatography of the initial bulk separation.

The 9th fraction, which contained the largest amount of **1** based on the GC-MS ion intensities, was examined by NMR in $CDCl_3$ rather than DMSO-d_6 since the former solvent permitted recovery of the sample for bioassay.

3.5.1. ^{1}H NMR spectrum of 1

The ^{1}H NMR spectrum of **1**, in $CDCl_3$, is presented in **Fig. 3.69** and an expansion of the 6.5-7.9 ppm region is shown in **Fig. 3.70**. Signal assignments are given in **Table 3.21**.

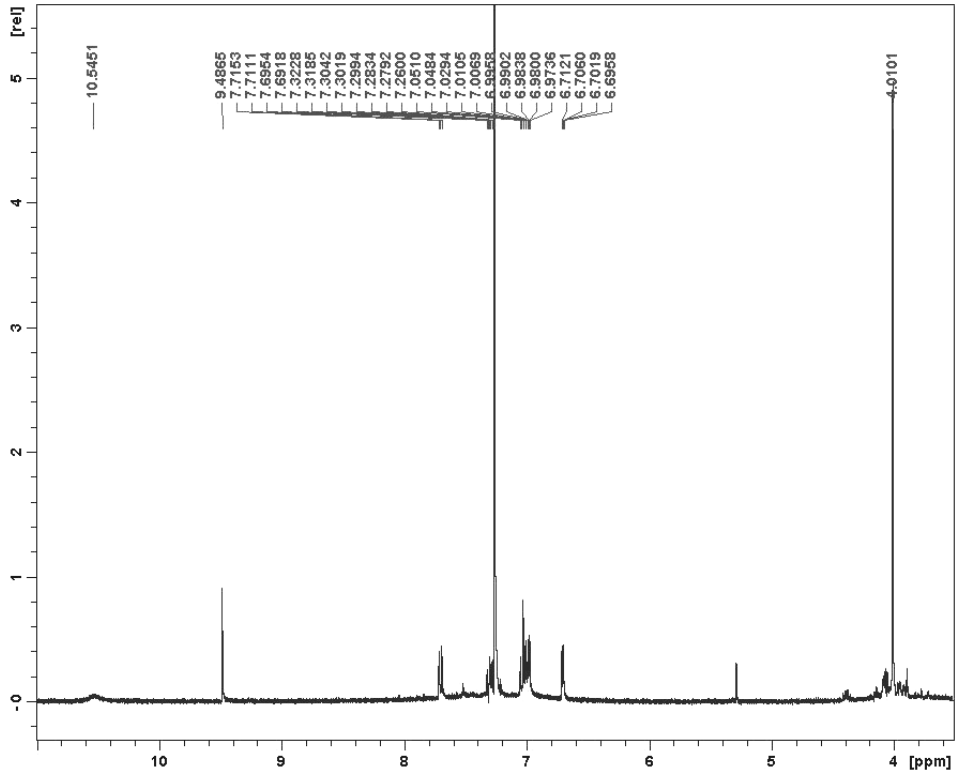

Fig. 3.69: ^{1}H NMR spectrum of 1 in $CDCl_3$.

Table 3.21: ^{1}H NMR assignments for 1 (δ ppm in $CDCl_3$)

Assignment	Multiplicity	Chemical shift (ppm)
1'	s	9.49
3'	dd (*J* = 3.9, 3.9 Hz)	6.98
4'	dd (*J* = 3.9, 3.9 Hz)	6.71
3	-	Not observed
4	d (*J* = 7.6 Hz)	7.89
5	t (*J* = 3.9, 2.0 Hz)	7.03
6	t (*J* = 3.9, 2.0 Hz)	7.32
OCH_3	s	4.01
NH	broad s	10.55

One signal (H-3) was not initially identified in the ^{1}H NMR spectrum. Subsequently this signal was found in the HSQC spectrum at 7.02 ppm (see **Section 3.5.3.2**).The two pyrrole protons (H-3' and H-4') which were detected as doublets only in DMSO-d_6 (see **Fig. 3.8**) were found to be doublets of doublets in

$CDCl_3$ (see **Fig. 3.70**). The homonuclear decoupling of the N-H proton signal reduced these to doublets with J = 3.9 Hz (see **Fig. 3.71**).

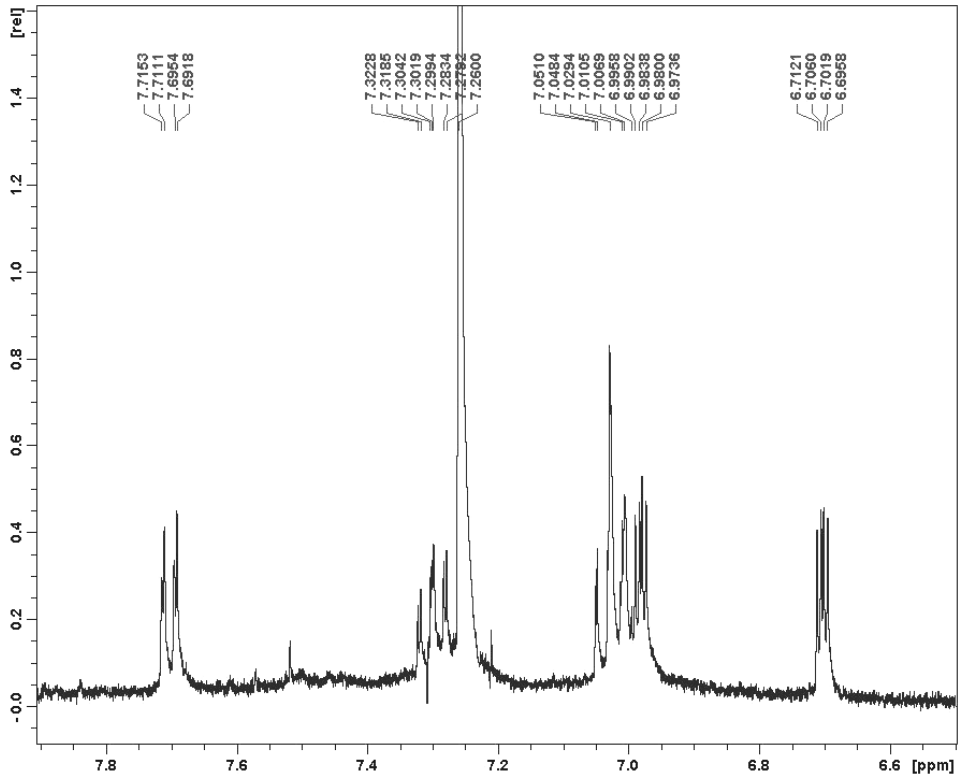

Fig. 3.70: Expansion of the 6.5-7.9 ppm region of the ^{1}H NMR spectrum of 1 in $CDCl_3$.

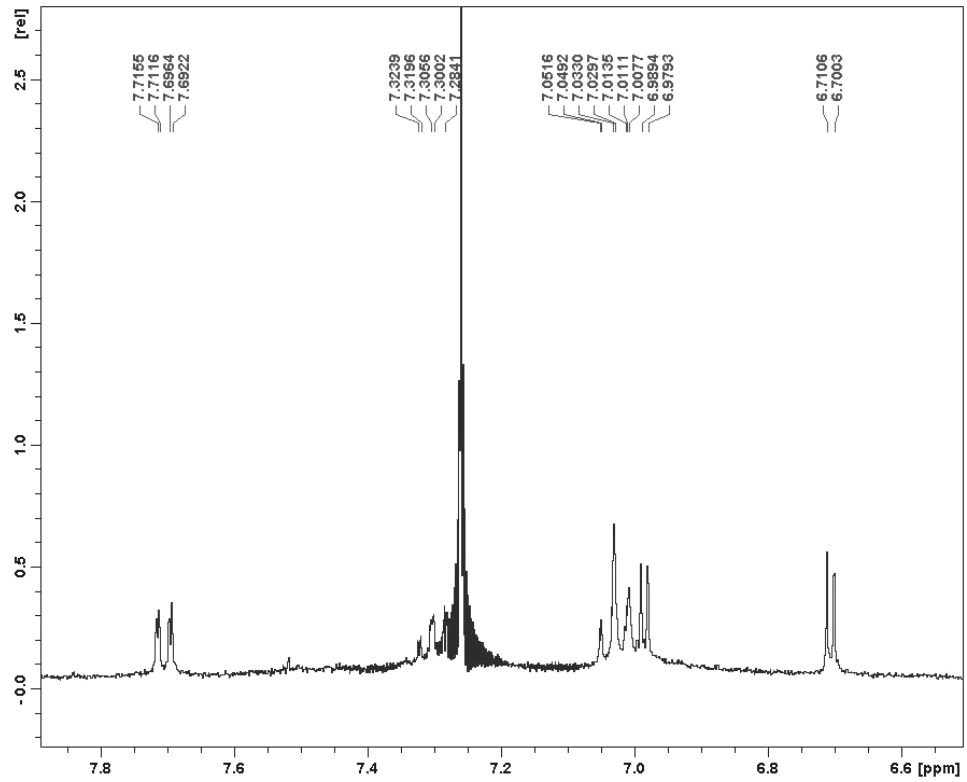

Fig. 3.71: Expansion of the 6.5-7.9 ppm region of the homonuclear decoupled spectrum of 1 irradiating the N-H proton signal in $CDCl_3$.

Similarly the H-3' and H-4' signals of compound **4** which appeared as a doublets of doublets in $CDCl_3$. They collapsed to doublets when N-H was irradiated (see **Fig. 3.73**).

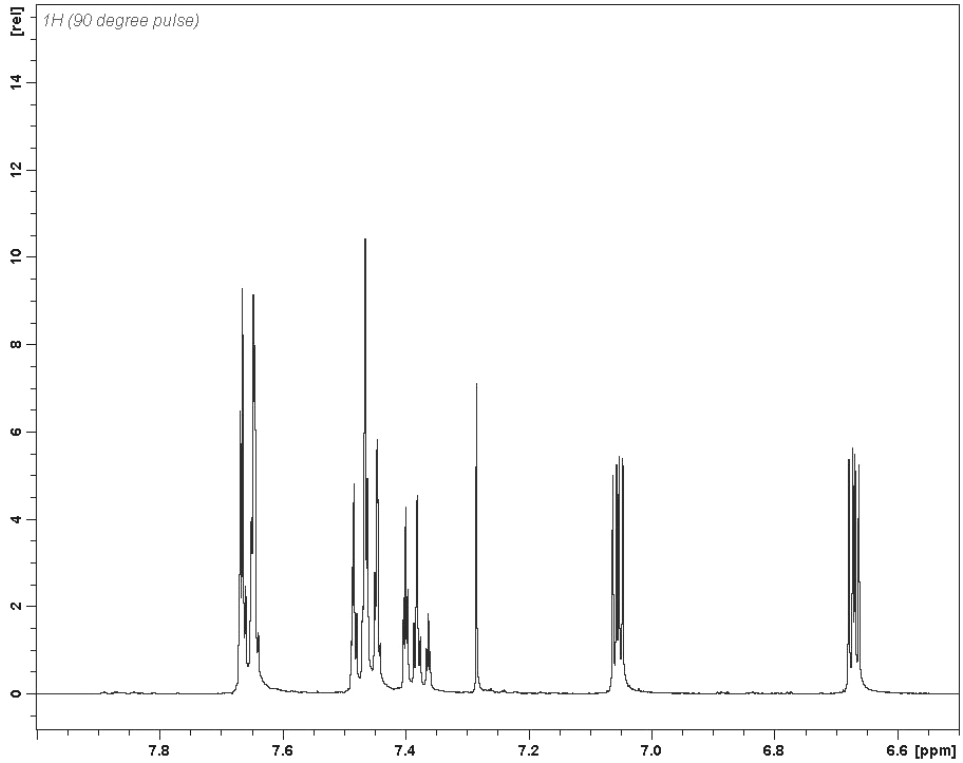

Fig. 3.72: Expansion of the 6.5-7.9 ppm region of ^{1}H NMR spectrum of 4 in $CDCl_3$.

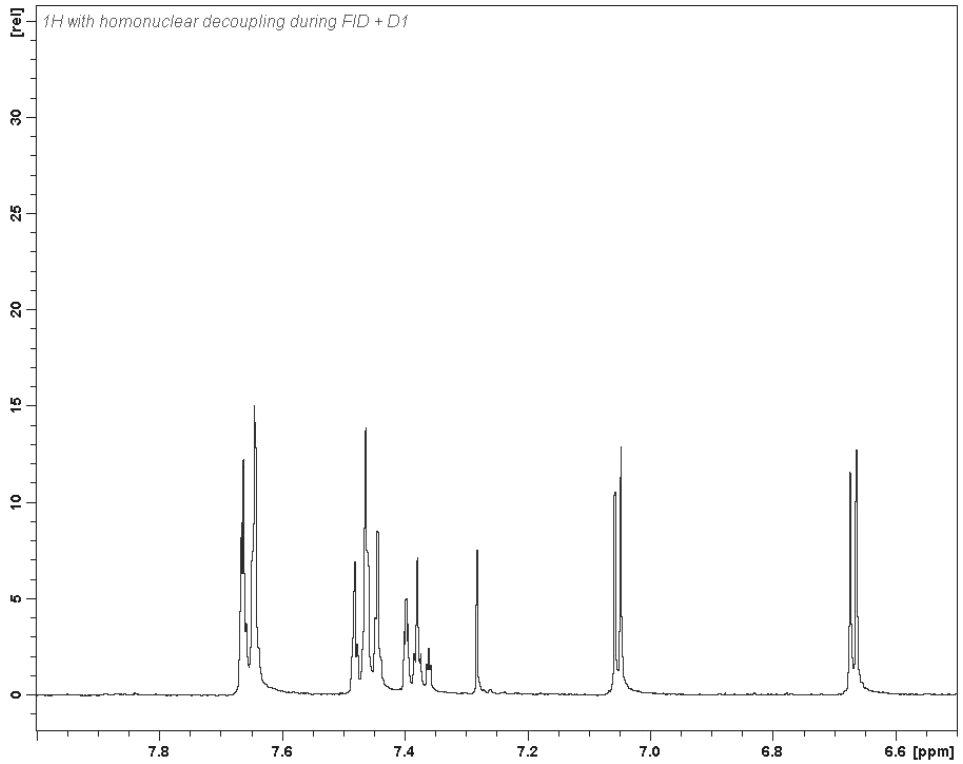

Fig. 3.73: Expansion of the 6.5-7.9 ppm region of the homonuclear decoupled spectrum of 4 irradiating the N-H proton signal in $CDCl_3$.

The effect of the N atom associated quadrupolar line broadening can also be seen in ^{13}C NMR spectrum of compound. The carbon signal at 121.9 ppm is broadened in DMSO-d_6 (**Fig, 3.74**) whereas the corresponding carbon signal at 122.6 ppm is a sharp peak in $CDCl_3$ (**Fig. 3.75**).

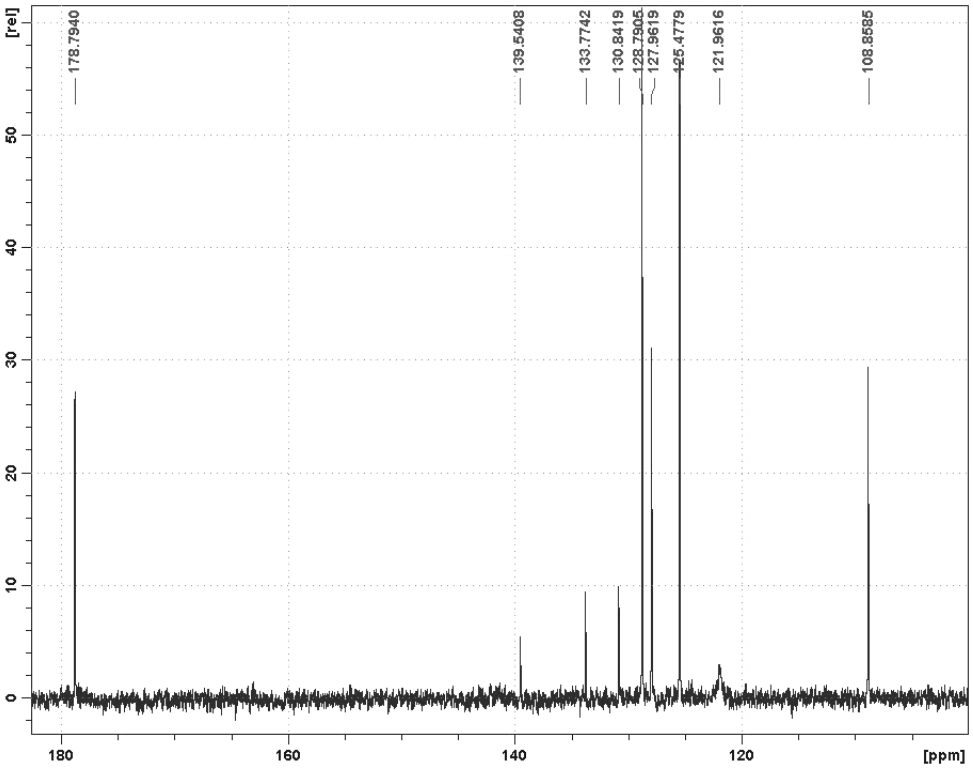

Fig. 3.74: ^{13}C NMR spectrum of 4 in DMSO-d_6.

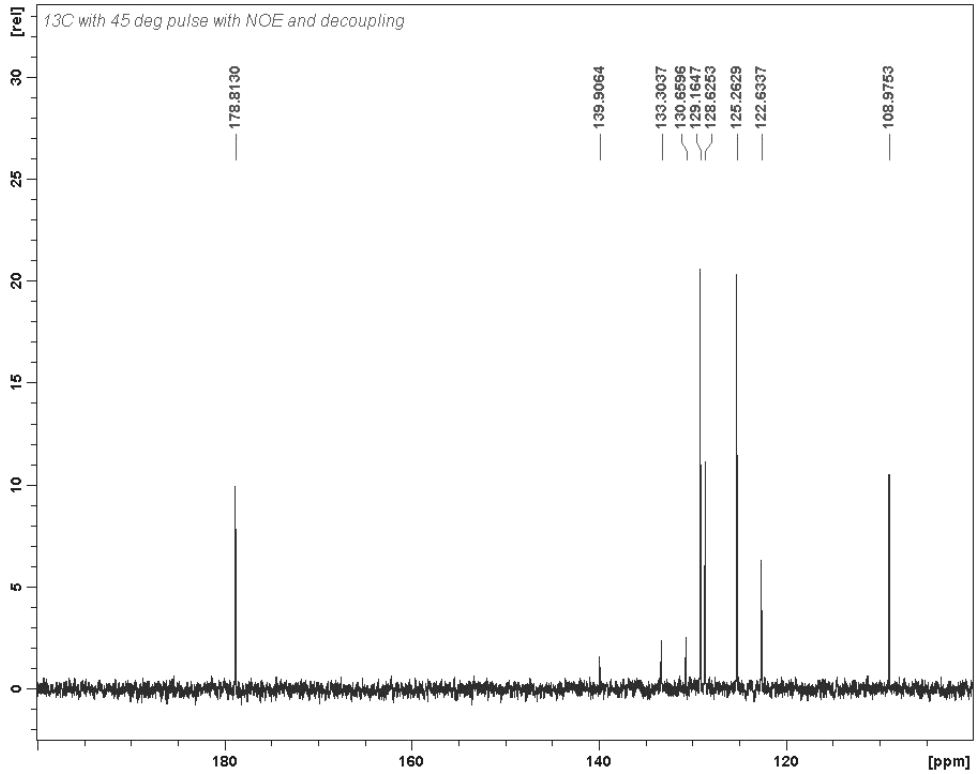

Fig. 3.75: ^{13}C NMR spectrum of 4 in $CDCl_3$.

3.5.2. HSQC spectrum of 1

The gradient edited HSQC spectrum of **1**, in $CDCl_3$, is presented in **Fig. 3.76.** Correlations observed in the HSQC spectrum are listed in **Table 3.21**.

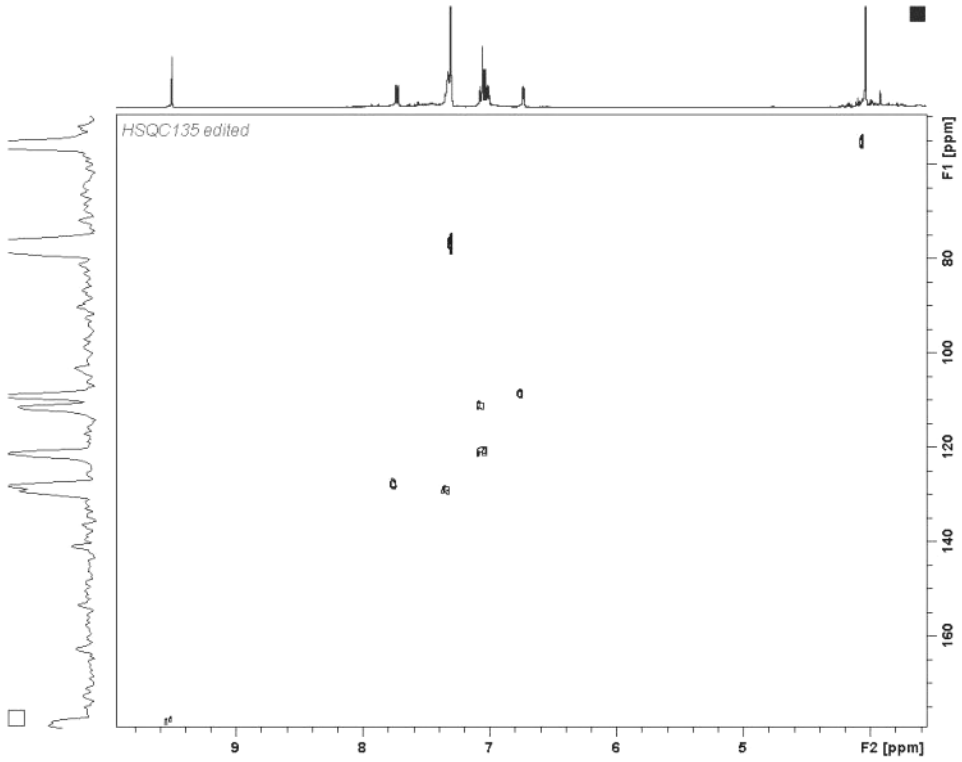

Fig. 3.76: HSCQ spectrum of 1 in $CDCl_3$.

Table 3.22: HSQC correlations determined for 1 (δ in $CDCl_3$)

Proton (ppm)	4.01 ($OC\underline{H}_3$)	6.71 (H-4')	6.98 (H-3')	7.02 (H-3)	7.03 (H-5)	7.30 (H-4)	7.70 (H-6)	9.49 (H-1')
Carbon (ppm)	55.6	108.9	121.0	111.6	121.5	129.3	128.2	178.4

3.5.3. HMBC spectrum of 1

The gradient edited HMBC spectrum of **1**, in $CDCl_3$, is presented in **Fig. 3.77**. HMBC correlation observed for **10** are listed in **Table 3.22** and depicted in **Fig. 3.78**.

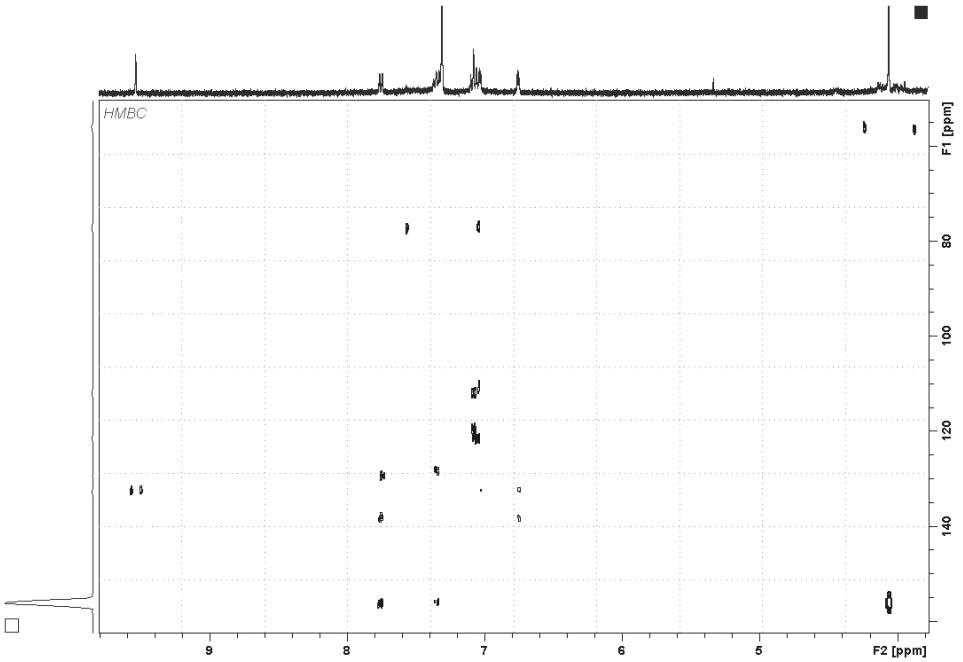

Fig. 3.77: HMBC spectrum of 1 in $CDCl_3$.

Table 3.23: ^{n}J HMBC correlation observed for 1 (δ ppm in $CDCl_3$)

Proton	4.01 ($OC\underline{H}_3$)	6.71 (H-2')	6.98 (H-3')	7.02 (H-3)
Correlated carbon(s)	155.8 (C-2)	131.7 (C-2') 138.0 (C-5')	131.7 (C-2')	121.5 (C-5)
Proton	7.03 (H-5)	7.30 (H-4)	7.70 (H-6)	9.49 (H-1')
Correlated carbon(s)	111.6 (C-3) 119.1 (C-1)	128.2 (C-6) 155.8 (C-2)	129.3 (C-4) 138.0 (C-5') 155.8 (C-2)	131.7 (C-2')

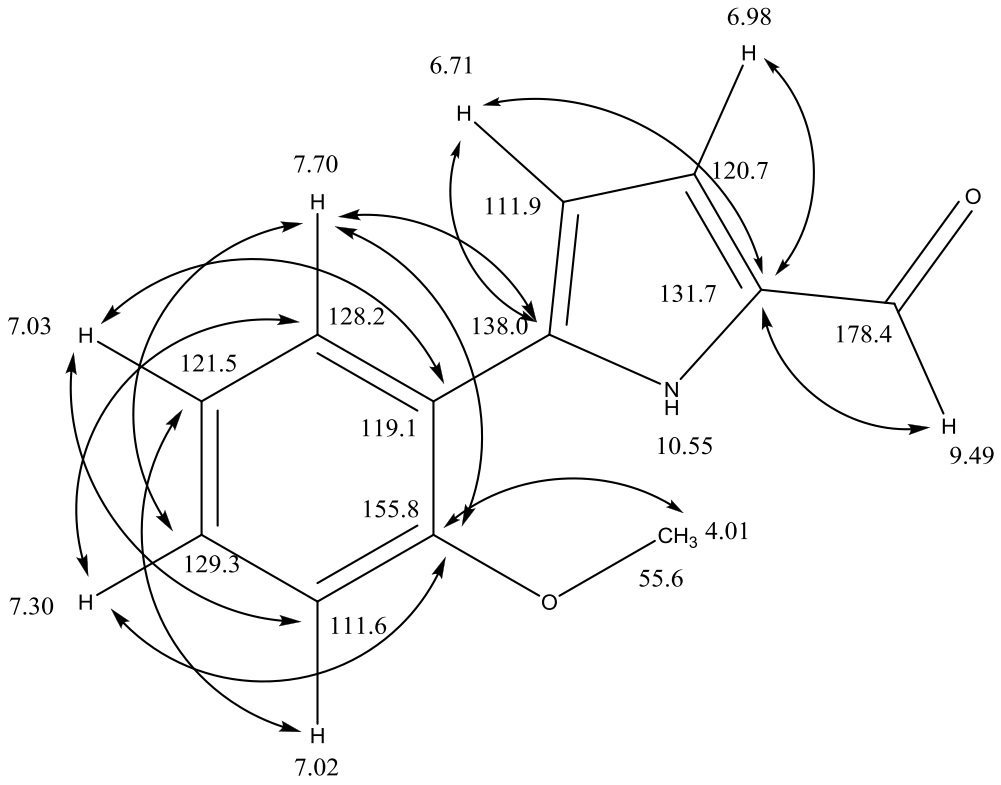

Fig. 3.78: HMBC correlations observed for 1 (δ in ppm in $CDCl_3$).

3.5.4. HRMS of 1

High Resolution Mass Spectrometry (HRMS) gave: calculated for $C_{12}H_{11}NO_2Na$ $[M+Na]^+$: 224.0682; found: 224.0653 (**Fig. 3.79**)

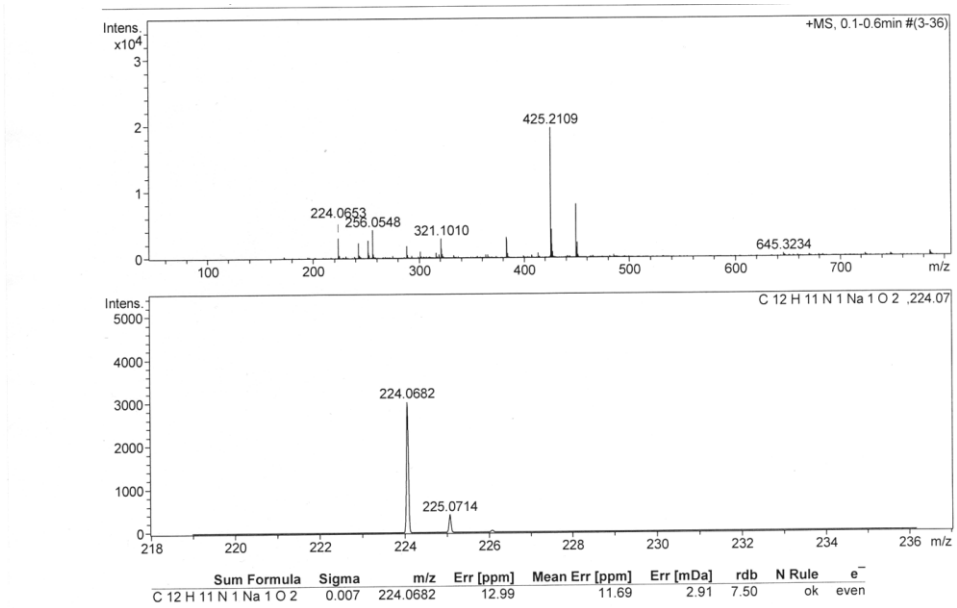

Fig. 3.79: HRMS of 1.

A complete assignment of the ^{1}H and ^{13}C signals of **1** in $CDCl_3$ is presented in **Table 3.23**. HMBC correlations observed for **1** are depicted in **Fig 3.80**.

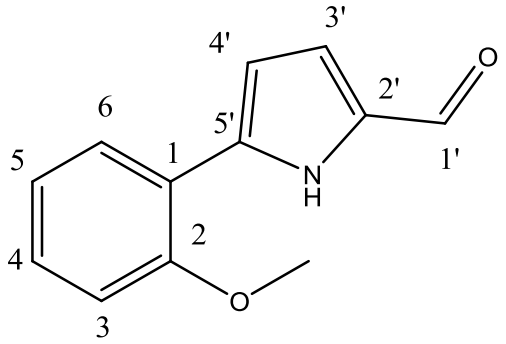

1

Table 3.24: NMR signal assignments for 1 (δ in ppm in $CDCl_3$)

Atom	^{13}C	^{1}H
1'	178.4*	9.49 (s)
2'	131.7*	-
3'	121.0*	6.98 (dd, *J* = 3.9, 3.9 Hz)
4'	108.9*	6.71 (dd, *J* = 3.9, 3.9 Hz)
5'	138.0*	-
1	119.1*	-
2	155.8*	-
3	111.6*	7.02* (m)
4	129.3*	7.30 (td, *J* = 7.5, 1.2 Hz)
5	121.5*	7.03 (td, *J* = 7.5, 1.2 Hz)
6	128.2*	7.70 (dd, *J* = 7.8, 1.7 Hz)
OCH_3	55.6*	4.01 (s)
NH	-	10.55 (broad s)

*Chemical shifts determined from 2D spectra.

3.5.5. Final purification of 1 for bioassay

The four fractions containing **1** collected from the initial bulk separation were combined and further purified by preparative layer chromatography which yielded twelve fractions. The fractions were examined by GC-MS under the same condition as those utilised to determine the GC-MS characteristic of **1. T**he 7th fraction was found to contain only **1** at a retention time of 5.41 minutes (see **Fig. 3.80**). The final yield of **1**, a yellow solid, was 0.36 mg (0.00179 mmol, 0.2%).

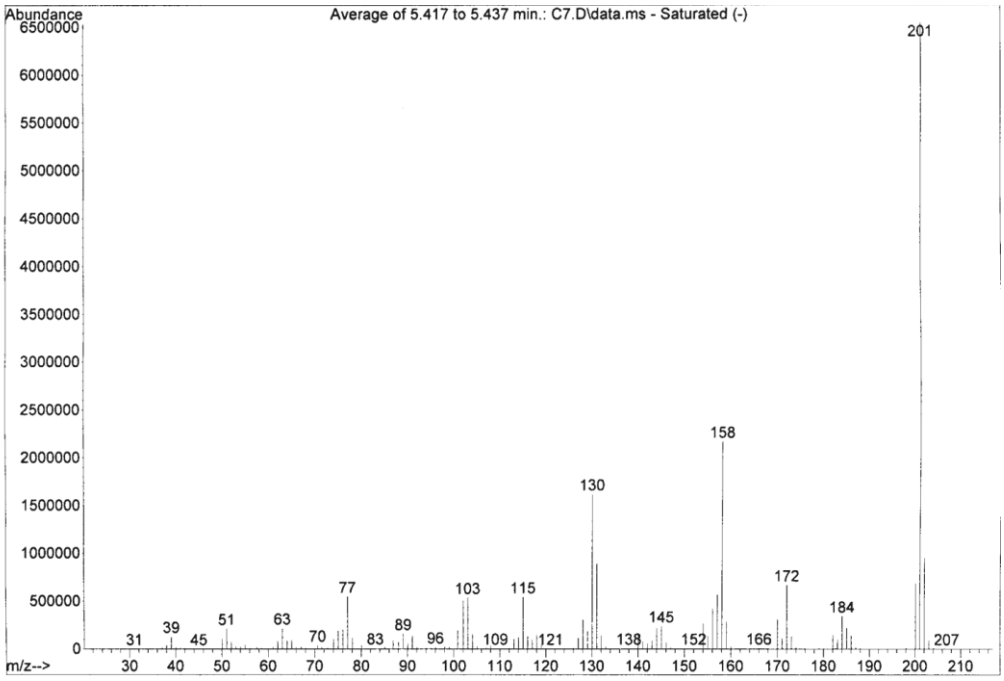

Fig. 3.80: Total ion chromatogram of the 7th preparative layer chromatography fraction.

3.5.6. Bioassay of 1

Due to the earthquake in Christchurch on February 22, 2011, which destroyed Canterbury Universitie's culture collection, the bioactivity of **1** against *Staphylococcus aureus* and other organisms could not be determined in New Zealand. Arrangements have now been made for bioassays to be performed by the Institute for the Biotechnology of Infectious Diseases (IBID) at University of Technology Sydney. However results will not be available until after July 2011. Unfortunately this date is beyond the submission date of this thesis.

3.6. Summary

1, which showed a weak positive correlation (R^2 = 0.36) with non-peroxide anti-bacterial activity,[45] was isolated from 15 kg of New Zealand mānuka honey. **1** showed a strong response in UV absorption at 340 nm. Since there was no standards for **1**, the concentration of **1** was estimated to be 0.064mg/100g of honey[45] based on the assumption that it showed a similar UV response to that determined for quercetin. However, the isolated sample of **1** was extremely small. This suggests that the actual concentration of **1** in honey could be much lower than that estimated above.

Analogues of **1,** such as benzyl 4-ethyl-2-formyl-5-(2-methoxyphenyl)-1*H*-pyrrole-3-carboxylate (**11**) and methyl 4-ethyl-2-formyl-5-(2-methoxyphenyl) -1*H*-pyrrole-3-carboxylate (**12**) are known to be a tyrosine kinase inhibitors[79] whereas 5-(3,5-dibromo-2-methoxyphenyl)-1*H*-pyrrole-2-carboxaldehyde (**13**) and 5-[3-bromo-5-(ethylsulfonyl)-2-methoxyphenyl]-1*H*-pyrrole-2-carboxaldehyde (**14**) are well established dopamine D3 receptor antagonist antipsychotic agents.[80]

It can therefore be speculated that **1** might exhibit other types of bioactivity, in addition to antibacterial activity.

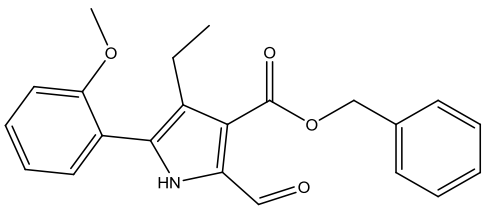

11

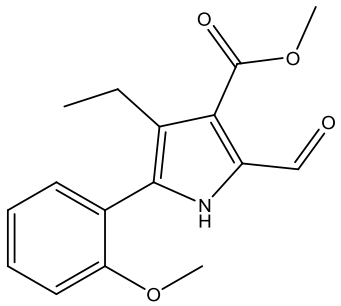

12

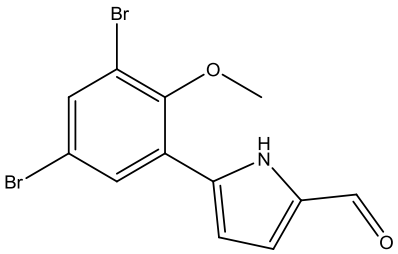

13

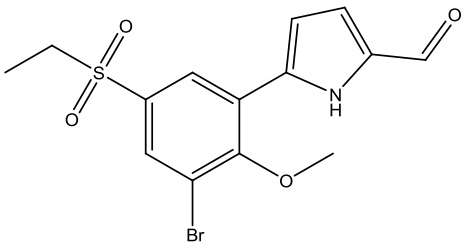

14

Conclusions

The flavonoid fraction of New Zealand mānuka honey (fraction 5) showed the presence of a complex series of peaks when examined by HPLC which showed the presence of several non-flavonoid compounds including **1** and the two predominant non-flavonoid components caffeic acid and *p*-coumaric acid. **1** showed a weak positive correlation (R^2 = 0.36) with non-peroxide anti-bacterial activity.[45]

1 was isolated from fifteen kg of New Zealand mānuka honey and showed a very strong response in UV absorption. Since a standard specimen of **1** was not available the concentration of **1** was estimated to be 0.064mg/100g of honey[45] based on the assumption that it showed a similar UV response to that determined for quercetin. However, the NMR sample of **1** shows only weak signals. This suggests that the actual concentration of **1** in honey was much lower than that estimated above.

Characterization of **1,** isolated from the flavanoid fraction of New Zealand mānuka honey**,** was achieved by ^{1}H and ^{13}C NMR spectroscopy and GC-MS with standards. This data identified **1** as 2-formyl-5-(2-methoxyphenyl)-pyrrole.

Synthesis of **6,** an intermediate in the synthesis of **1**, gave only an extremely low yield. Consequentially the decision was made to purchase **6**.

Synthesis of **9,** an intermediate in the route to **1**, gave a yield of 67.5% as pale yellow crystals after crystallization from CH_2Cl_2/hexane. **9** was characterised by ^{1}H and ^{13}C NMR spectroscopy and ESI-MS.

Synthesis of **1** from **9** only resulted in barely traceable amounts of **1**. The dominant product after recrystallization from CH_2Cl_2/hexane was **10**, as pale orange crystals. This compound was characterised by ^{1}H and ^{13}C NMR spectroscopy and ESI-MS.

The synthesis of **1** was repeated. The product mixture was fractionated on a silica gel column, followed by two cycles of preparative layer chromatography applied to the fractions which contained **1** and yield 0.36 mg of **1** (0.00179 mmol, 0.2%). The identify of **1** was established by ^{1}H NMR, and its molecular formula was confirmed by ESI-MS. The identical nature of the synthetic **1** with the specimen isolated from mānuka honey was confirmed by comparative GC-MS analysis.

Suggestions for further work

Arrangements are in place for the bioassay of **1** to be performed as soon as possible. If **1** is found to be significantly bioactive a new synthesis route for **1** is required in order to define the relationship with the non-peroxide antibacterial activity in mānuka honeys since the isolation of **1** from honey and its production via the current synthetic route is not feasible. A study to determine the biosynthetic origin of **1** is recommended.

The process of extracting and isolating flavonoids from 15 kg of mānuka honey has yielded several fractions which are rich in phenolic acid and flavonoids. In this study, two phenolic acids were isolated and identified. Future research should isolate and characterise the unknown phenolic acids and flavonoids from these fractions.

Appendix

6.1: ^{1}H NMR spectrum of the peak eluting between 22.5 – 24.0 minutes of flavonoid fraction of New Zealand mānuka honey (fraction 5)

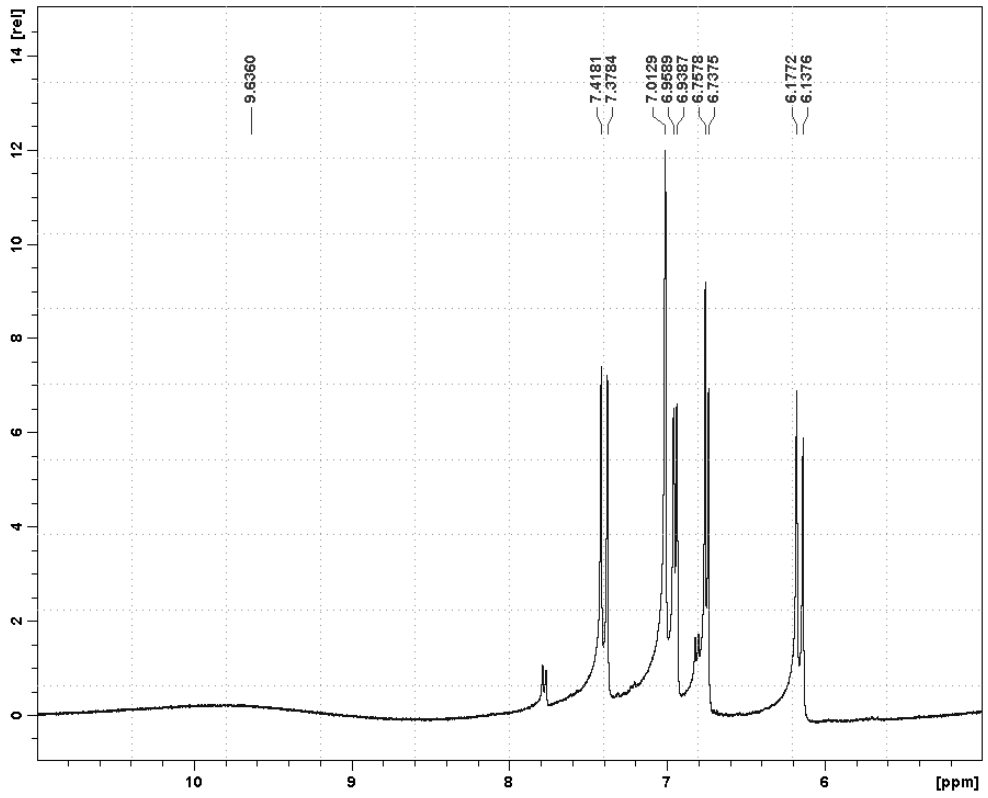

6.2: ^{1}H NMR spectrum of caffeic acid

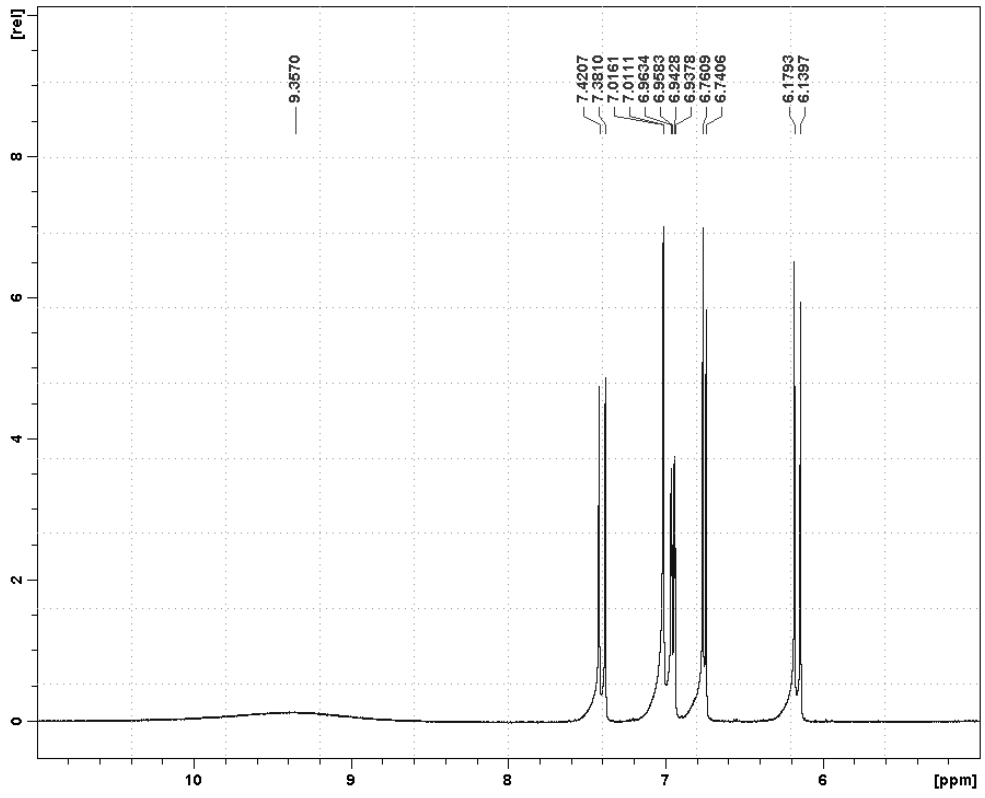

6.3: ^{1}H NMR spectrum of the peak eluting between 26.1 – 26.9 minutes of flavonoid fraction of New Zealand mānuka honey (fraction 5)

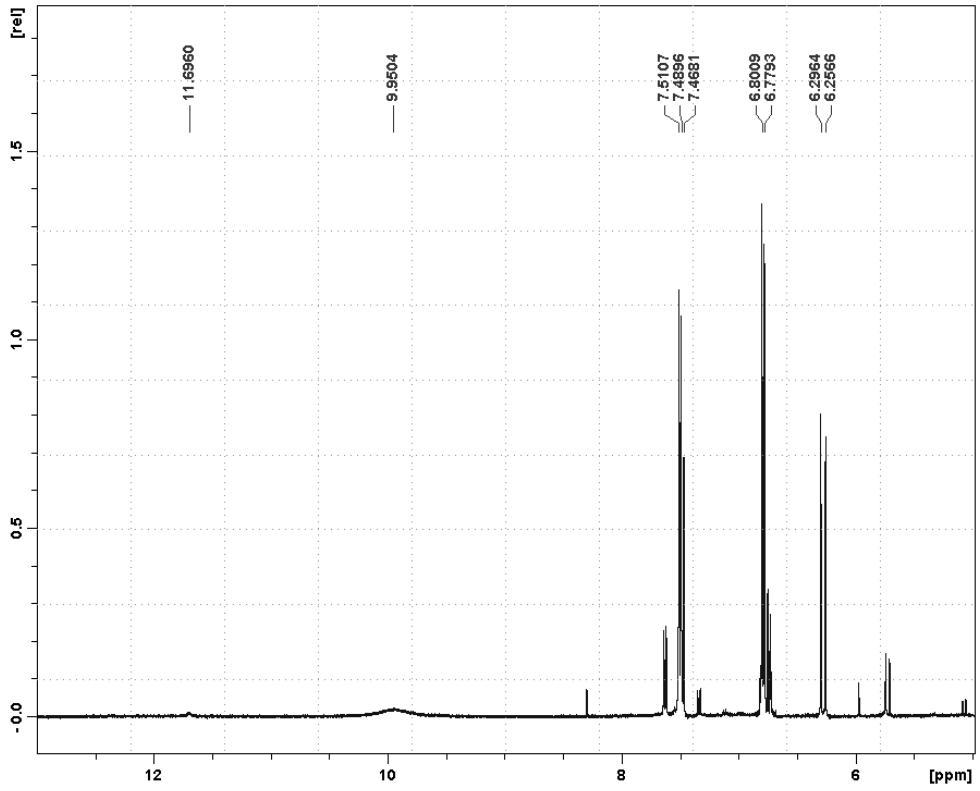

6.4: ^{1}H NMR spectrum of *p*-coumaric acid

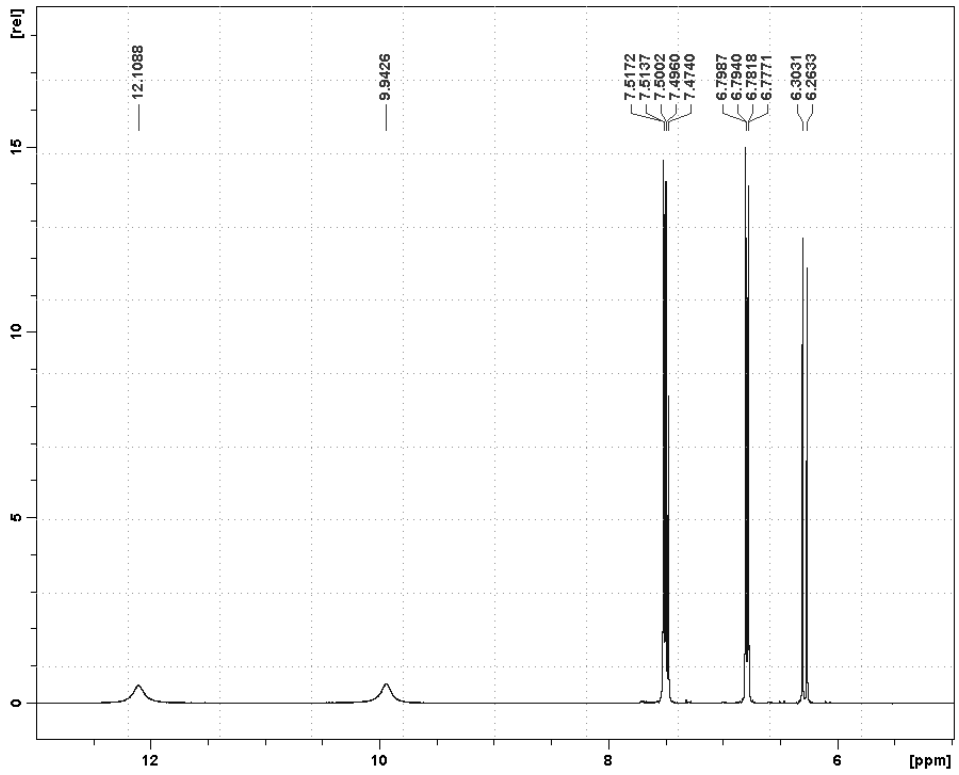

6.5: Raw data of the intensity of ^{n}J correlations exhibited by H-6 of 3 (7.92 ppm) *versus* mixing time (msec)

	35 (msec)	50 (msec)	65 (msec)	80 (msec)
peak 1	2.2350E+27	8.6989E+27	3.7116E+27	9.7122E+26
peak 2	2.0234E+27	1.5638E+28	8.0909E+27	3.6309E+27
peak 3	3.8246E+27	2.9056E+28	1.3937E+28	6.7328E+27
peak 4	8.6380E+24	3.5096E+25	2.6927E+25	2.1773E+25
peak 5	1.4947E+22	1.3342E+25	5.1310E+25	1.5754E+25
	100 (msec)	120 (msec)	160 (msec)	200 (msec)
peak 1	9.5517E+25	3.0926E+27	4.9671E+26	1.3428E+25
peak 2	4.5803E+26	1.1265E+26	1.2285E+27	4.7439E+26
peak 3	1.8516E+27	1.4630E+26	3.7228E+26	2.3900E+27
peak 4	2.3254E+26	9.6718E+25	2.5525E+25	4.7116E+25
peak 5	3.4497E+25	2.5862E+26	1.4772E+26	9.4933E+25

(peak 1: C-1, 121.9 ppm (^{2}J); peak 2: C-3 124.4 ppm (^{4}J); peak 3: C-4- 131.1 ppm (^{3}J); peak 4: C-2, 147.4 ppm (^{3}J); peak 5: C-5', 153.3 ppm (^{3}J).)

6.6: Raw data of the selected ion chromatogram of the crude product mixture

m/z	Abundance	Ratio
130.00	37	1.00
158.00	50	1.35
201.00	123	3.32

6.7: Raw data of the selected ion chromatogram of an isolated specimen of 1

m/z	Abundance	Ratio
130.00	569	1.00
158.00	723	1.27
201.00	1878	3.30

References

1. Doner, L. W., The sugars of honey - A review. *Journal of the Science of Food and Agriculture.* **1977,** *28*, 443-456.
2. Crane, E., *The archaeology of beekeeping.* Cornell University Press: Ithaca, N.Y., 1983.
3. Ward, C., Kānuka and Mānuka. *Forest and Bird* 2000, pp 24-27.
4. Morales, C. F., Margarodidae (Insecta:Hemiptera). *Fauna of New Zealand / Ko te Aitanga Pepeke o Aotearoa* **1991,** *21*, 16-17.
5. (a) Molan, P. C., The Antibacterial Activity of Honey .1. The Nature of the Antibacterial Activity. *Bee World* **1992,** *73* (1), 5-28; (b) Wahdan, H. A., Causes of the antimicrobial activity of honey. *Infection* **1998,** *26* (1), 26-31; (c) Efem, S. E. E.; Udoh, K. T.; Iwara, C. I., The antimicrobial spectrum of honey and its clinical significance. *Infection* **1992,** *20* (4), 227-229.
6. (a) Cooper, R. A.; Molan, P. C.; Krishnamoorthy, L.; Harding, K. G., Mānuka honey used to heal a recalcitrant surgical wound. *European Journal of Clinical Microbiology & Infectious Diseases* **2001,** *20* (10), 758-759; (b) Cooper, R. A.; Molan, P. C.; Harding, K. G., Antibacterial activity of honey against strains of *Staphylococcus aureus* from infected wounds. *Journal of the Royal Society of Medicine* **1999,** *92* (6), 283-5; (c) Cooper, R. A.; Halas, E.; Molan, P. C., The efficacy of honey in inhibiting strains of *Pseudomonas aeruginosa* from infected burns. *The Journal of burn care & rehabilitation* **2002,** *23* (6), 366-70; (d) Cooper, R. A.; Molan, P. C.; Harding, K. G., The sensitivity to honey of Gram-positive cocci of clinical significance isolated from wounds. *Journal of applied microbiology* **2002,** *93* (5), 857-63.
7. Bang, L. M.; Buntting, C.; Molan, P., The effect of dilution on the rate of hydrogen peroxide production in honey and its implications for wound healing. *Journal of Alternative & Complementary Medicine* **2003,** *9* (2), 267-273.
8. Dunford, C.; Molan, P. C., Using honey as a dressing for infected skin lesions. *Nursing Times* **2000,** *96*, 7-9.

9. Abuharfeil, N.; Al-Oran, R.; Abo-Shehada, M., The effect of bee honey on the proliferative activity of human B- and T-lymphocytes and the activity of phagocytes. *Food and Agricultural Immunology* **1999,** *11*, 169-177.
10. White, J. W., Jr.; Subers, M. H.; Schepartz, A. I., The identification of inhibine. *Am. Bee J.* **1962,** *102*, 430-1.
11. Ruegg, M.; Blanc, B., The water activity of honey and related sugar solutions. *Lebensmittel-Wissenschaft and Technologie* **1981,** *14*, 1-6.
12. (a) Truchado, P.; Ferreres, F.; Bortolotti, L.; Sabatini, A. G.; Tomás-Barberán, F. A., Nectar flavonol rhamnosides are floral markers of acacia (*Robinia pseudacacia*) honey. *Journal of Agricultural and Food Chemistry* **2008,** *56* (19), 8815-8824; (b) Molan, P., The antibacterial properties of honey. *Chemistry in New Zealand* **1995,** (July), 10-14.
13. White, J. W., Honey. In *The Hive and the Honey Bee*, Graham, J. M., Ed. Dadant & Sons: Hamilton, Illinois, 1992; pp 869-925.
14. White, J. W., Jr.; Subers, M. H.; Schepartz, A. I., The identification of inhibine, the antibacterial factor in honey, as hydrogen peroxide and its origin in a honey glucose-oxidase system. *Biochimica et Biophysica Acta, Specialized Section on Enzymological Subjects* **1963,** *73* (1), 57-70.
15. Cochrane, C. G., Cellular injury by oxidants. *American Journal of Medicine* **1991,** *91* (3C), 23S-30.
16. Molan, P. C.; Russell, K. M., Non-peroxide antibacterial activity in some New Zealand honeys. *Journal of Apicultural Research.* **1988,** *27* (1), 62-67.
17. Allen, K. L.; Molan, P. C.; Reid, G. M., A survey of the antibacterial activity of some New Zealand honeys. *Journal of Pharmacy and Pharmacology* **1991,** *43* (12), 817-22.
18. Stephens, J. M. C. The factors responsible for the varying levels of UMF in mānuka (*Leptospermum scoparium*) honey. The University of Waikato, 2006.
19. Willix, D. J.; Molan, P. C.; Harfoot, C. G., A comparison of the sensitivity of wound-infecting species of bacteria to the antibacterial activity of mānuka honey and other honeys. *Journal of Applied Bacteriology* **1992,** *73*, 388-394.

20. Adams, C. J.; Boult, C. H.; Deadman, B. J.; Farr, J. M.; Grainger, M. N. C.; Manley-Harris, M.; Snow, M. J., Isolation by HPLC and characterization of the bioactive fraction of New Zealand mānuka (*Leptospermum scoparium*) honey. *Carbohydr. Res.* **2008,** *343* (4), 651-659.

21. Mavric, E.; Wittmann, S.; Barth, G.; Henle, T., Identification and quantification of methylglyoxal as the dominant antibacterial constituent of mānuka (*Leptospermum scoparium*) honeys from New Zealand. *Mol. Nutr. Food Res.* **2008,** *52* (4), 483-489.

22. Donarski, J. A.; Roberts, D. P. T.; Charlton, A. J., Quantitative NMR spectroscopy for the rapid measurement of methylglyoxal in mānuka honey. *Analytical Methods* **2010,** *2* (10), 1479-1483.

23. Stephens, J. M.; Schlothauer, R. C.; Morris, B. D.; Yang, D.; Fearnley, L.; Greenwood, D. R.; Loomes, K. M., Phenolic compounds and methylglyoxal in some New Zealand mānuka and kānuka honeys. *Food Chemistry* **2010,** *120* (1), 78 - 86.

24. Hayashi, T.; Shibamoto, T., Analysis of methyl glyoxal in foods and beverages. *Journal of Agricultural and Food Chemistry* **1985,** *33*, 1090-1093.

25. Loeffler, K. W.; Koehler, C. A.; Paul, N. M.; De Hann, D. O., Oligomer formation in evaporating aqueous glyoxal and methyl glyoxal solutions. *Environmental Science & Technology* **2006,** *40* (20), 6318-6323.

26. Ghosh, M.; Talukdar, D.; Ghosh, S.; Bhattacharyya, N.; Ray, M.; Ray, S., In vivo assessment of toxicity and pharmacokinetics of methylglyoxal. Augmentation of the curative effect of methylglyoxal on cancer-bearing mice by ascorbic acid and creatine. *Toxicology and Applied Pharmacology* **2006,** *212*, 45-48.

27. Kalapos, M. P., Methylglyoxal in living organisms. Chemistry, biochemistry, toxicology and biological implications. *Toxicology Letters* **1999,** *110*, 145-175.

28. Tada, A.; Wakabayashi, K.; Totsuka, Y.; Sugimura, T.; Tsuji, K.; Nukaya, H., ^{32}P-Post labelling analysis of a DNA adduct, an N^2-acetyl derivative of guanine, formed in vitro by methylglyoxal and hydrogen peroxide in combination. *Mutation Research* **1996,** *351* (2), 173-180.

29. Dobler, D.; Ahmed, N.; Song, L.; Eboigbodin, K. E.; Thornalley, P. J., Increased dicarbonyl metabolism in endothelial cells in hyperglycemia induces anoikis and impairs anigiogenesis by RGD and GFOGER motif modification. *Diabetes* **2006,** *55*, 1961-1969.

30. Shamsi, F. A.; Partal, A.; Sady, C.; Glomb, M. A.; Nagaraj, R. H., Immunological evidence for methylglyoxal-derived modifications in vivo. *Journal of Biological Chemistry* **1998,** *273*, 6928-6936.

31. Peppa, M.; Brem, H.; Ehrlich, P.; Zhang, J.; Cai, W.; Li, Z.; Croitoru, A.; Thung, S.; Vlassara, H., Adverse effects of dietary glycotoxins on wound healing in genetically diabetic mice. *Diabetes* **2003,** *52*, 2805-2813.

32. Adams, C. J.; Manley-Harris, M.; Molan, P. C., The origin of methylglyoxal in New Zealand mānuka (*Leptospermum scoparium*) honey. *Carbohydrate Research* **2009,** *344* (8), 1050 - 1053.

33. Wang, Y.; Ho, C. T., Effects of *o*-phenylenediamine on methylglyoxal generation from monosaccharide: Comment on "correlation of methylglyoxal with acrylamide formation in fructose/asparagine Maillard reaction model system'. *Food Chemistry* **2008,** *109* (1), 1-3.

34. Havsteen, B. H., The biochemistry and medical significance of the flavonoids. *Pharmacology & Therapeutics.* **2002,** *96*, 67–202.

35. Britton, G., *The biochemistry of natural pigments.* Cambridge University Press: Cambridge, 1983.

36. Cushnie, T. P. T.; Lamb, A. J., Antimicrobial activity of flavonoids. *International Journal of Antimicrobial Agents* **2005,** *26* (5), 343-356.

37. Bohm, B. A., *Introduction to flavonoids.* Harwood Academic Publishers: Amsterdam, 1998.

38. (a) D'Arcy, B. R. *Antioxidants in Australian Floral Honeys - Identification of health-enhancing nutrient components*; Australian Government Rural Industries Research and Development Corporation: Barton, May 2005, 2005; (b) Havsteen, B. H., The biochemistry and medical significance of the flavonoids. *Pharmacology & Therapeutics* **2002,** *96* (2-3), 67-202.

39. Venkataraman, K., Methods for determining the structure of flavonoid compounds. In *The chemistry of flavonoid compounds.*, Geissman, T. A., Ed. The Macmillan Company: New York, 1962; pp 70-106.

40. (a) Markham, K. R.; Mabry, T. J., Ultraviolet-visible and proton magnetic resonance spectroscopy of flavonoids. In *The flavonoids.*, Harborne, J. B.; Mabry, H.; Mabry, T. J., Eds. Chapman and Hall: London, 1975; pp 46-56; (b) Jurd, L., Spectral properties of flavonoid compounds. In *The chemistry of flavonoid compounds.*, Geissman, T. A., Ed. The Macmillan Company: New York, 1962; pp 107-155; (c) Mabry, T. J.; Markham, K. R.; Thomas, M. B., *The Systematic Identification of Flavonoids*. Springer-Verlag: New York, 1970.

41. Harborne, J. B.; Mabry, T. J., *The Flavonoids: advances in research*. Chapman and Hall Ltd: Cambridge, 1982.

42. (a) Ferreres, F.; Tomás-Barberán, F. A.; Gil, M. I.; Tomás-Lorente, F., An HPLC technique for flavonoid analysis in honey. *Journal of the Science of Food and Agriculture* **1991,** *56* (1), 49-56; (b) Ferreres, F.; Tomás-Barberán, F. A.; Soler, C.; García-Viguera, C.; Ortiz, A.; Tomás-Lorente, F., A simple extractive technique for honey flavonoid HPLC analysis. *Apidologie* **1994,** *25* (1), 21-30.

43. (a) Weston, R. J.; Brocklebank, L. K.; Lu, Y., Identification and quantitative levels of antibacterial components of some New Zealand honeys. *Food Chemistry* **2000,** *70* (4), 427-435; (b) Weston, R. J.; Mitchell, K. R.; Allen, K. L., Antibacterial phenolic components of New Zealand mānuka honey. *Food Chemistry* **1999,** *64* (3), 295-301.

44. Yao, L.; Datta, N.; Tomás-Barberán, F. A.; Ferreres, F.; Martos, I.; Singanusong, R., Flavonoids, phenolic acids and abscisic acid in Australian and New Zealand *Leptospermum* honeys. *Food Chem.* **2003,** *81* (2), 159-168.

45. Deadman, B. J. The Flavonoid Profile of New Zealand Mānuka Honey. The University of Waikato, 2009.

46. Joule, J. A.; Mills, K., *Heterocyclic chemistry* 5th ed. ed.; Wiley: Chichester, U.K., 2010.

47. Walsh, C. T.; Garneau-Tsodikova, S.; Howard-Jones, A. R., Biological formation of pyrroles: Nature's logic and enzymatic machinery. *Natural Product Reports* **2006,** *23* (4), 517-531.

48. Banwell, M. G.; Goodwin, T. E.; Ng, S.; Smith, J. A.; Wong, D. J., Palladium-Catalysed Cross-Coupling and Related Reactions Involving Pyrroles. *European Journal of Organic Chemistry* **2006,** *2006* (14), 3043-3060.

49. (a) Williamson, N. R.; Fineran, P. C.; Gristwood, T.; Chawrai, S. R.; Leeper, F. J.; Salmond, G. P. C., Anticancer and immunosuppressive properties of bacterial prodiginines. *Future Microbiology* **2007,** *2* (6), 605-618; (b) Williamson, N. R.; Fineran, P. C.; Leeper, F. J.; Salmond, G. P. C., The biosynthesis and regulation of bacterial prodiginines. *Nat Rev Micro* **2006,** *4* (12), 887-899.

50. Fürstner, A., Chemistry and Biology of Roseophilin and the Prodigiosin Alkaloids: A Survey of the Last 2500 Years. *Angewandte Chemie International Edition* **2003,** *42* (31), 3582-3603.

51. Aldrich, L. N.; Stoops, S. L.; Crews, B. C.; Marnett, L. J.; Lindsley, C. W., Total synthesis and biological evaluation of tambjamine K and a library of unnatural analogs,. *Bioorganic & Medicinal Chemistry Letters* **2010,** *20* (17), 5207-5211.

52. Nettleton, D. E.; Doyle, T. W.; Krishnan, B.; Matsumoto, G. K.; Clardy, J., Isolation and structure of rebeccamycin - a new antitumor antibiotic from nocardia aerocoligenes. *Tetrahedron Letters* **1985,** *26* (34), 4011 - 4014.

53. Omura, S.; Iwai, Y.; Hirano, A.; Nakagawa, A.; Awaya, J.; Tsuchiva, H.; Takahashi, Y.; Masuma, R., A new alkaloid AM-2282 of Streptomyces origin: Taxonomy, fermentation and preliminary characterization. . *J. Antibiot.* **1977,** *30* (4), 275-285.

54. Rodrigues Pereira, E.; Belin, L.; Sancelme, M.; Prudhomme, M.; Ollier, M.; Rapp, M.; Severe, D.; Riou, J.-F.; Fabbro, D.; Meyer, T., Structure-activity relationships in a series of substituted indolocarbazoles: topoisomerase I and protein kinase C inhibition and antitumoral and antimicrobial properties. *Journal of Medicinal Chemistry* **1996,** *39* (22), 4471-4477.

55. Al-Obeidi, F.; Lam, K., Development of inhibitors for protein tyrosine kinases. *Oncogene* **2000,** *19* (49), 5690-5701.

56. Gossauer, A., Monopyrrolic natural compounds including tetramic acid derivatives. In *Progress in the Chemistry of Organic Natural Products*, Herz, W.; Falk, H.; Kirby, G. W., Eds. Springer-Verlag: Vienna: Austria, 2003; Vol. 86.

57. (a) Daly, J. W.; Witkop, B.; Bommer, P.; Biemann, K., Batrachotoxin. The active principle of the Colombian arrow poison frog, *Phyllobates bicolor*. *Journal of the American Chemical Society* **1965,** *87* (1), 124-126; (b) Tokuyama, T.; Daly, J., Structure of batrachotoxin, a steroidal alkaloid from the Colombian arrow poison frog, *Phyllobates aurotaenia*, and partial synthesis of batrachotoxin and its analogs and homologs. *Journal of the American Chemical Society* **1969,** *91* (14), 3931-3938.

58. Heide, L., Chapter 18 Aminocoumarins: Mutasynthesis, Chemoenzymatic Synthesis, and Metabolic Engineering. In *Methods in Enzymology*, Hopwood, D. A., Ed. Academic Press: 2009; Vol. 459, pp 437-455.

59. Jerković, I.; Mastelić, J.; Marijanović, Z.; Klein, Z.; Jelić, M., Comparison of hydrodistillation and ultrasonic solvent extraction for the isolation of volatile compounds from two unifloral honeys of *Robinia pseudoacacia L.* and *Castanea sativa L. Ultrasonics Sonochemistry* **2007,** *14* (6), 750 - 756.

60. Jerković, I.; Mastelić, J.; Marijanović, Z., A variety of volatile compounds as markers in unifloral honey from Dalmatian Sage (*Salvia officinalis L.*). *Chemistry & Biodiversity* **2006,** *3* (12), 1307-1316.

61. Jerković, I.; Tuberoso, C. I. G.; Marijanović, Z.; Jelić, M.; Kasum, A., Headspace, volatile and semi-volatile patterns of *Paliurus spina-christi* unifloral honey as markers of botanical origin. *Food Chemistry* **2009,** *112* (1), 239 - 245.

62. Jerković, I.; Kasum, A.; Marijanović, Z.; Tuberoso, C. I. G., Contribution to the characterisation of honey-based Sardinian product abbamele: Volatile aroma composition, honey marker compounds and antioxidant activity. *Food Chemistry* **2011,** *124* (1), 401 - 410.

63. Eraslan, G.; Kanbur, M.; Silici, S.; Mürsel Karabacak, Beneficial effect of pine honey on trichlorfon induced some biochemical alterations in mice. *Ecotoxicology and Environmental Safety* **2010,** *73* (5), 1084-1091.

64. Andersen, R. J.; Faulkner, D. J.; He, C. H.; Van Duyne, G. D.; Clardy, J., Metabolites of the marine prosobranch mollusk *Lamellaria sp. Journal of the American Chemical Society* **1985,** *107* (19), 5492-5495.

65. Fan, H.; Peng, J.; Hamann, M. T.; Hu, J.-F., Lamellarins and related pyrrole-derived alkaloids from marine organisms. *Chemical Reviews* **2007,** *108* (1), 264-287.

66. van Pée, K.-H.; Ligon, J. M., Biosynthesis of pyrrolnitrin and other phenylpyrrole derivatives by bacteria. *Natural Product Reports* **2000,** *17* (2), 157-164.

67. Morrison, M. D.; Hanthorn, J. J.; Pratt, D. A., Synthesis of pyrrolnitrin and related halogenated phenylpyrroles. *Organic Letters* **2009,** *11* (5), 1051-1054.

68. Martin, R.; Jäger, A.; Böhl, M.; Richter, S.; Fedorov, R.; Manstein, D. J.; Gutzeit, H. O.; Knölker, H.-J., Total synthesis of pentabromo- and pentachloropseudilin, and synthetic analogues—Allosteric inhibitors of myosin ATPase. *Angewandte Chemie International Edition* **2009,** *48* (43), 8042-8046.

69. Reeves, J. T.; Fandrick, D. R.; Tan, Z.; Song, J. J.; Lee, H.; Yee, N. K.; Senanayake, C. H., Copper-catalyzed annulation of 2-formylazoles with *o*-aminoiodoarenes. *Journal of Organic Chemistry* **2010,** *75* (3), 992-994.

70. Campiani, G.; Aiello, F.; Fabbrini, M.; Morelli, E.; Ramunno, A.; Armaroli, S.; Nacci, V.; Garofalo, A.; Greco, G.; Novellino, E.; Maga, G.; Spadari, S.; Bergamini, A.; Ventura, L.; Bongiovanni, B.; Capozzi, M.; Bolacchi, F.; Marini, S.; Coletta, M.; Guiso, G.; Caccia, S., Quinoxalinylethylpyridylthioureas (QXPTs) as potent non-nucleoside HIV-1 reverse transcriptase (RT) inhibitors. Further SAR studies and identification of a novel orally bioavailable hydrazine-based antiviral agent. *Journal of Medicinal Chemistry* **2001,** *44* (3), 305-315.

71. (a) Biftu, T.; Feng, D.; Ponpipom, M.; Girotra, N.; Liang, G.-B.; Qian, X.; Bugianesi, R.; Simeone, J.; Chang, L.; Gurnett, A.; Liberator, P.; Dulski, P.; Leavitt, P. S.; Crumley, T.; Misura, A.; Murphy, T.; Rattray, S.; Samaras, S.; Tamas, T.; Mathew, J.; Brown, C.; Thompson, D.; Schmatz, D.; Fisher, M.; Wyvratt, M., Synthesis and SAR of 2,3-diarylpyrrole

inhibitors of parasite cGMP-dependent protein kinase as novel anticoccidial agents. *Bioorganic & Medicinal Chemistry Letters* **2005,** *15* (13), 3296-3301; (b) Qian, X.; Liang, G.-B.; Feng, D.; Fisher, M.; Crumley, T.; Rattray, S.; Dulski, P. M.; Gurnett, A.; Leavitt, P. S.; Liberator, P. A.; Misura, A. S.; Samaras, S.; Tamas, T.; Schmatz, D. M.; Wyvratt, M.; Biftu, T., Synthesis and SAR studies of diarylpyrrole anticoccidial agents. *Bioorganic & Medicinal Chemistry Letters* **2006,** *16* (10), 2817-2821.

72. Reeves, J. T.; Song, J. J.; Tan, Z.; Lee, H.; Yee, N. K.; Senanayake, C. H., A general synthesis of substituted formylpyrroles from ketones and 4-formyloxazole. *Organic Letters* **2007,** *9* (10), 1875-1878.

73. Fernandes, E. G. R.; Silva, A. M. S.; Cavaleiro, J. A. S.; Silva, F. M.; Fernanda, M.; Borges, M.; Pinto, M. M. M., ^{1}H and ^{13}C NMR Spectroscopy of mono-, di-, tri- and tetrasubstituted xanthones. *Magn. Reson. Chem.* **1998,** *36* (4), 305-309.

74. Benoit, G.-E.; Carey, J. S.; Chapman, A. M.; Chima, R.; Hussain, N.; Popkin, M. E.; Roux, G.; Tavassoli, B.; Vaxelaire, C.; Webb, M. R.; Whatrup, D., Large-scale preparation of 2-methyloxazole-4-carboxaldehyde. *Org. Process Res. Dev.* **2007,** *12* (1), 88-95.

75. Hosoya, T.; Aoyama, H.; Ikemoto, T.; Kihara, Y.; Hiramatsu, T.; Endo, M.; Suzuk, M., Dantrolene analogues revisited: General synthesis and specific functions capable of discriminating two kinds of Ca^{2+} release from sarcoplasmic reticulum of mouse skeletal muscle. *Bioorganic & Medicinal Chemistry* **2003,** *11* (5), 663-673.

76. Hodges, J. C.; Patt, W. C.; Connolly, C. J., Reactions of lithiooxazole. *Journal of Organic Chemistry* **1991,** *56* (1), 449-452.

77. Wong, W. S.; Guo, D.; Wang, X. L.; Yin, Z. Q.; Xia, B.; Li, N., Study of *cis*-cinnamic acid in *Arabidopsis thaliana. Plant Physiology and Biochemistry* **2005,** *43* (10-11), 929-937.

78. Hanai, K.; Kuwae, A.; Takai, T.; Senda, H.; Kunimoto, K.-K., A comparative vibrational and NMR study of *cis*-cinnamic acid polymorphs and *trans*-cinnamic acid. *Spectrochimica Acta Part A: Molecular and Biomolecular Spectroscopy* **2001,** *57* (3), 513-519.

79. Kim, A. S.; Zhang, X. Preparation of 4-ethyl-2-formyl-1*H*-pyrrole-3-carboxylic acid derivatives as tyrosine kinase inhibitors. The World Intellectual Property Organization, patent no. WO 2005009957, Feb 03, 2005.

80. Stemp, G.; Johnson, C. N. 5-(2-alkoxyphenyl)pyrroles as dopamine D3 receptor antagonist antipsychotic agents. . US Patent 5637609, Jun 10,1997.